Spring 5-31-2006

Gas chromatography on self assembled single walled carbon nanotubes

Mahesh Kumar Karwa
New Jersey Institute of Technology

Copyright Warning & Restrictions

The copyright law of the United States (Title 17, United States Code) governs the making of photocopies or other reproductions of copyrighted material.

Under certain conditions specified in the law, libraries and archives are authorized to furnish a photocopy or other reproduction. One of these specified conditions is that the photocopy or reproduction is not to be "used for any purpose other than private study, scholarship, or research." If a, user makes a request for, or later uses, a photocopy or reproduction for purposes in excess of "fair use" that user may be liable for copyright infringement,

This institution reserves the right to refuse to accept a copying order if, in its judgment, fulfillment of the order would involve violation of copyright law.

Please Note: The author retains the copyright while the New Jersey Institute of Technology reserves the right to distribute this thesis or dissertation

Printing note: If you do not wish to print this page, then select "Pages from: first page # to: last page #" on the print dialog screen

ABSTRACT

GAS CHROMATOGRAPHY ON SELF ASSEMBLED SINGLE WALLED CARBON NANOTUBES

by
Mahesh Kumar Karwa

Carbon nanotubes (CNTs) are nano-sized carbon-based sorbents, which have high surface area, large aspect ratio, can be self-assembled and are known to be stable at high temperatures. It is therefore conceivable that separation techniques, such as, gas chromatography (GC) can benefit from their unique properties and nano-scale interactions. Self-assembly, in-contrast to packing these materials in a tube, prevents them from agglomeration and thus facilitates in retaining their nano-characteristics. In this research, novel substrates, such as, steel tubings, on a scaled-up level have been explored for the self-assembly process of CNTs, for applications such as gas chromatography, where the CNTs served as stationary phases.

In the first part of this research, the self-assembly of multi-walled carbon nanotubes (MWCNTs) on the inside wall of long stainless steel tubings was studied. The CNTs were deposited by the chemical vapor deposition (CVD) using ethylene as the carbon source and the iron nanostructures in the stainless steel as the catalyst. Variation in uniformity in terms of the thickness and morphology of the deposited film and surface coverage were studied along the length of a tube by scanning electron microscopy (SEM). The effects of process conditions, such as flow rate and deposition time on the coating thickness, were studied. The catalytic effect of the iron nanostructures depended on surface conditioning of the tubing. It was found that the pretreatment temperature influenced the quality of the nanotube coating. The morphology of the CNT deposit

supported the base-growth scheme and VLS (vapor–liquid–solid) growth mechanisms of CNTs. This study served as the basis for the development of CNTs in the larger scale application. Scaled up self-assembly of single-walled carbon nanotubes (SWCNTs) was studied in long tubes and finally they were used as GC columns.

The strategy for selective SWCNT growth required the prevention of iron in the bulk steel from participating in the catalytic CVD process, as the presence of iron always led to MWCNT formation. Consequently, silica lined stainless steel tubings, such as, Silcosteel^{TM} and Sulfinert^{TM} were selected. A SWCNT film with an average thickness of 300 nm was self-assembled by a unique single-step, catalytic CVD process consisting of dissolved cobalt and molybdenum salts in ethanol, where ethanol served as the precursor and cobalt and molybdenum as catalysts. Such large-scale assembly required process and catalyst optimization. A variety of organic compounds with varying polarity were separated at high resolution and the column efficiency demonstrated around 1000 theoretical plates/m, comparable to commercial GC columns. Evaluation of Van't Hoff and Van deemter plots suggested that the CNTs followed classical chromatography behavior. Comparison of capacity factors (k') and isosteric heats of adsorption (ΔH_s) with a packed column containing a commercial sorbent (Carbopack C^{TM}) showed comparable results. This demonstrated high capacity and strong sorbate-sorbent interactions on the SWCNT phase. Evaluation of the McReynolds constants suggested that the SWCNT was a non-polar phase. The high surface area of the SWCNT media allowed separations of gases, and at the same time, its high thermal stability (>425^{o}C) permitted separations of higher molecular weights at higher temperatures, thus extending the range of conventional chromatography on the same column.

GAS CHROMATOGRAPHY ON SELF ASSEMBLED SINGLE WALLED CARBON NANOTUBES

by
Mahesh Kumar Karwa

A Dissertation
Submitted to the Faculty of
New Jersey Institute of Technology
in Partial Fulfillment of the Requirements for the Degree of
Doctor of Philosophy in Chemistry

Department of Chemistry and Environmental Science

May 2006

APPROVAL PAGE

GAS CHROMATOGRAPHY ON SELF ASSEMBLED SINGLE WALLED CARBON NANOTUBES

Mahesh Kumar Karwa

Dr. Somenath Mitra, Dissertation Advisor — Date
Professor of Chemistry and Environmental Science, NJIT

Dr. Zafar Iqbal, Committee Member — Date
Research Professor of Chemistry and Environmental Science, NJIT

Dr. Edgardo T. Farinas, Committee Member — Date
Assistant Professor of Chemistry and Environmental Science, NJIT

Dr. Daniel J. Watts, Committee Member — Date
Professor of Chemistry and Environmental Science, NJIT

Dr. Manish Chhowalla, Committee Member — Date
Assistant Professor of Materials Science and Engineering, Rutgers

---

Dr. Frank J. Owens, Committee Member — Date
US Army, Armament Research Development and Engineering Center, Picatinny

BIOGRAPHICAL SKETCH

Author: Mahesh Kumar Karwa

Degree: Doctor of Philosophy

Date: May 2006

Undergraduate and Graduate Education:

- Doctor of Philosophy in Chemistry,
  New Jersey Institute of Technology, Newark, NJ, 2006
- Master of Technology in Modern Methods of Chemical Analysis,
  Indian Institute of Technology, Delhi, India, 1999
- Master of Science in Chemistry,
  Sri Sathya Sai Institute of Higher Learning, Puttaparthi, India, 1998
- Bachelor of Science (Honors) in Chemistry,
  Sri Sathya Sai Institute of Higher Learning, Bangalore, India, 1996

Major: Chemistry

Presentations and Publications:

Mahesh Karwa and Somenath Mitra

"Techniques for the Extraction, Isolation, and Purification of Nucleic acids", Book Chapter for "Sample Preparation Techniques in Analytical Chemistry." 2003, John Wiley & Sons.

Mahesh Karwa, Dittmar Hahn and Somenath Mitra

"A Sol-gel immobilization of Nano and Micron size sorbents in Poly(dimethylsiloxane) (PDMS) Microchannels for Micro-scale Solid-phase extraction (SPE)." Analytica Chimica Acta, 546, (2005) 22-29.

Mahesh Karwa, Zafar Iqbal and Somenath Mitra

"Self assembly of Carbon Nanotubes Inside Steel Tubing for Chromatography Applications." Preprints of Extended Abstracts, 230th ACS National Meeting, Division of Environmental Chemistry, 45, (2005) 783-786.

Mahesh Karwa, Zafar Iqbal and Somenath Mitra

"Scaled-Up Self-assembly of Carbon Nanotubes inside long steel tubings." Carbon 44, (2006) 1235-1242.

Mahesh Karwa and Somenath Mitra

"Gas Chromatography on Self-Assembled Single Walled Carbon Nanotubes." Analytical Chemistry, 78, (2006) 2064-2070.

Mahesh Karwa and Somenath Mitra

"Extraction, Preconcentration and Purfication of DNA in Poly(dimethylsiloxane) PDMS Based Microfluidic Channels." Preprints of Extended Abstracts, 232nd ACS National Meeting, Division of Polymeric Materials: Science and Engineering, San Francisco, CA, September 10-14, 2006.

Mahesh Karwa, Zafar Iqbal and Somenath Mitra

"Scaled-up, Selective, Single Step Self-assembly of Single Walled Carbon Nanotubes inside a Steel Capillary Tubing." Submitted to Journal of Materials Research.

Mahesh Karwa and Somenath Mitra

"Applications of Carbon Nanotubes in Analytical Chemistry." Review Article in Preparation for Analytical Chemistry-A Pages.

Mahesh Karwa, Mustansar Ahmed, Chutarat Saridara and Somenath Mitra

"Preconcentration on Single and Multi Walled Carbon Nanotubes in a Microtrap." Article in Preparation for Journal of Chromatography A.

Mahesh Karwa and Somenath Mitra

"Sample Preparation in Lab-On-a-Chip." Review Article in Preparation for Journal of Biochemical and Biophysical Methods.

Mahesh Karwa, Zafar Iqbal and Somenath Mitra

"Self Assembly of Single Walled Carbon Nanotubes for Analytical Separations." Poster Presentation, 232nd ACS National Meeting, Division of Inorganic Chemistry, San Francisco, CA, September 10-14, 2006.

Mahesh Karwa and Somenath Mitra

"Extraction, Preconcentration and Purfication of DNA in Poly(dimethylsiloxane) PDMS Based Microfluidic Channels" Invited Oral Presentation, Division of Polymeric Materials: Science and Engineering, 232nd ACS National Meeting, San Francisco, CA, September 10-14, 2006.

Mahesh Karwa, Zafar Iqbal and Somenath Mitra

"Gas Chromatography on Self-Assembled Single Walled Carbon Nanotubes." Oral Presentation, 38th Middle Atlantic Regional Meeting, Hershey, PA, June 4-7, 2006.

Mahesh Karwa, Zafar Iqbal and Somenath Mitra

"Self Assembly of Single Walled Carbon Nanotubes for Analytical Separations." Poster Presentation, ISPE-NJ chapter, April 2006.

Yubing Wang, Mahesh Karwa, Chutarat Saridara, Zafar Iqbal and Somenath Mitra

"Approaches to carbon nanotubes self-assembly: Microwave induced reactions and chemical vapor deposition." Oral Presentation, 231st ACS National Meeting, Atlanta, GA, March 26-30, 2006.

Mahesh Karwa, Zafar Iqbal and Somenath Mitra

"Self assembly of Carbon Nanotubes inside steel tubing for chromatography applications" Oral Presentation, 230 ACS Meeting, Washington, D.C, August 2005.

Mahesh Karwa, Somenath Mitra and Dittmar Hahn

"A Sol-gel immobilization of Nano and Micron size sorbents in Poly(dimethylsiloxane) (PDMS) Microchannels for Microscale Solid-phase extraction (SPE)" Poster presentation, ISPE-NJ chapter, April 2005.

Somenath Mitra, Mahesh Karwa and Zafar Iqbal

"Self-assembly of nano-particles for preconcentration in environmental sensing platforms." Oral Presentation, ACS Meeting, March 2004, Anaheim, CA.

Mahesh Karwa, Somenath Mitra and Dittmar Hahn

"A sol-gel approach for fabrication of μ-SPE on PDMS Microchannels." Oral Presentation, Eastern Analytical Symposium, Nov 2003, Somerset, NJ.

To
" Satyam, Shivam, Sundaram "
Truth, The Absolute and Beauty

ACKNOWLEDGMENT

In this earthly sojourn one cannot discount the value of a guiding hand while treading in the realms of unknown. I feel greatly blessed that I always had one at every turn that my life had taken in the form of parents, siblings, teachers, relations, countless friends, strangers and most importantly, the almighty God. All of them have and will continue to shape my life and add meaning to it. At this juncture, I would like to express my gratitude to all of them for having helped me in approaching to this difficult milestone.

I would like to gratefully acknowledge my deepest appreciation to my dissertation advisor, Dr. Somenath Mitra in giving life to the researcher inside me. I would like to thank him for extending his encouragement and support for the completion of my dissertation. I am grateful for his valuable guidance and patience in the completion of this dissertation. But for his resources and insight it wouldn't have been possible to surmount this milestone.

I would also like to express my appreciation and thanks to Dr. Zafar Iqbal for his guidance, expertise and for offering to do with recording Raman measurements when and as required with cheer. This dissertation wouldn't be complete without my committee offering to give their time and participation. My sincere thanks to Dr. Zafar Iqbal, Dr. Daniel Watts, Dr. Manish Chhowalla, Dr. Edgardo Farinas and Dr. Frank Owens for serving on my committee.

I gratefully acknowledge the funding support received from the government agencies, NJCST and EPA.

My sincere thanks to Mr. Chandrakant Patel, Dr. Dittmar Hahn, Dr. Larrisa Krishtopa, Mr. Yogesh Gandhi, Xueyan Zhang and Donguang Wei for their help and

assistance. I would also like to thank my colleagues and friends, Mahesh Pallerla, Dr. Chutarat Saridara, Dr. Roman Brukh, Dr.Pavan Sarda and countless other friends for their help and for adding cheer in my life.

Lastly I would like to thank my family, my parents and my lovely wife, Jyoti for always being very supportive of me. I would also like to take this opportunity to express my profound gratitude to Bhagawan Sri Sathya Sai Baba without whose grace and blessings this work would not have been possible.

TABLE OF CONTENTS

TABLE OF CONTENTS
(Continued)

TABLE OF CONTENTS
(Continued)

Chapter **Page**

TABLE OF CONTENTS
(Continued)

LIST OF TABLES

LIST OF TABLES
(Continued)

LIST OF FIGURES

LIST OF FIGURES
(Continued)

LIST OF FIGURES
(Continued)

LIST OF FIGURES
(Continued)

LIST OF FIGURES
(Continued)

CHAPTER 1

INTRODUCTION

1.1 Background Information

Separations is a key process for chemical manufacturing and analysis in industries, such as, pharmaceutical and petrochemical where it accounts for a significant portion of production costs. By definition, separation implies the resolution of a mixture into its components. It is also used to test the purity and to characterize the chemical constituents of a matrix. Conventional separation techniques include distillation, absorption, adsorption, extraction, filtration and crystallization. Over the last three decades, chromatography has evolved as a high resolution separation technique and has gained immense popularity for its simplicity, sensitivity, precision and its ability to perform the analysis (sampling, separation and measurement) in a minimum amount of time and in a reproducible manner. Consequently, chromatography today is recognized as a key tool for analytical separations.

The word "chromatography" was coined by the Russian scientist Mikhail Tswett in 1906 while demonstrating the separation of plant pigments into colored zones by percolating extracts through a column packed with an adsorbent. Since then, "Chromatography" has become a generic term for processes where separation occur via differential partitioning between two phases; in most cases one phase is a stationary and the other is mobile. Table 1.1 lists the various types of chromatographic techniques possible between the two phases that are currently in vogue. Chromatographic separations are based on the principles of partition and adsorption.

Table 1.1 Various Types of Chromatographic Techniques Possible Between Two Phases

Mobile phase	Stationary Phase	Type	Equilibrium
Gas	Liquid	Gas Liquid Chromatography (GLC)	Partition
	Solid	Gas Solid Chromatography (GSC)	Adsorption
	Liquid on Solid	Gas Liquid Solid Chromatography	Both
Liquid	Liquid	Liquid Liquid Chromatography	Partition
	Solid	Liquid Solid Chromatography (HPLC),	Adsorption
		Ion exchange	Ion exchange
		Size exclusion	Partition/Sieving

1.2 Development of Gas Chromatography

In gas chromatography (GC) the sample is vaporized and injected into the chromatographic column. Elution is brought about by the flow of an inert gaseous mobile phase whose function is to transport the analyte through the column. The molecules of the components that exhibit higher vapor pressures remain largely in the mobile phase and are swept more rapidly towards the detector. These solutes elute early from the column relative to the ones, which have lower vapor pressures, or which engage in higher interactions with the stationary phase and take longer periods to reach the detector; the separation is thus achieved.

The origin of chromatography can be traced to 1905 when W. Ramsey separated a mixture of gases on adsorbent charcoal [1]. Soon after, Michael Tswett, demonstrated the separation of chloroplast pigments by adsorption liquid chromatography [2]. Tswett later became known as the "father of chromatography". Some work was done with liquid solid chromatography in the following years, but a major step was made in 1941 when two

biochemists, A. J. P. Martin and R. L. M. Synge developed partition chromatography for the separation of amino acids [3]. Martin and Synge won a Nobel Prize in 1952 for their pioneering work in partition chromatography. In 1952, Martin collaborated with A. T. James to introduce gas liquid chromatography (GLC), which they used to separate volatile carboxylic acids and amines [4]. The separation was performed with a gaseous mobile phase and a stationary liquid that had been coated onto an inert support. Another milestone of chromatography occurred when M. J. E. Golay introduced wall coated open tubular (WCOT) capillary gas chromatography columns in 1958 at the International GC symposium held in Amsterdam [5]. The introduction of capillary columns revolutionized chromatography by vastly improving separation efficiency and ever since then the technique has been exploited to solve a range of problems that encompass medical, biological, and environmental sciences, as well as industrial applications.

The limitations of this technique are established primarily by the ability to volatilize the samples, thermal stability of the samples, stationary phases and chromatographic substrates. Generally, one is restricted to an upper temperature of around 250 – 350°C and a molecular weight less than 1000 – 1500 units.

The GC column is a vital component in a gas chromatograph, which holds the stationary phase in the form of an elongated tube. The two extremes in column types are packed columns and open tubular columns [6]. General properties and characteristics of typical gas-chromatographic columns is presented in Table 1.2.

Open tubular, or capillary columns are of two basic types, namely, wall-coated open tubular (WCOT) and support-coated open tubular (SCOT). Wall-coated columns are simply capillary tubes coated with a thin layer of the stationary phase typically

polymeric liquids. Fused-silica based open tubular columns (FSOT) are examples of WCOT columns which have gained immense popularity because of their inherent advantages, such as chemical inertness towards sample components and the ability to draw them into coils and thus fabricate flexible long columns. In FSOT columns the stationary phase, typically polymeric liquid is cross-linked or chemically bonded or both to the surface of the inside wall of the tubes. Generally gas-liquid chromatography (GLC) is performed on FSOT columns. SCOT columns are generally gas-liquid-solid chromatography(GLSC) based columns where the inner surface of the capillary is lined with a thin film (~ 30 μm) of a support material, such as diatomaceous earth onto which the stationary phase is adsorbed. Porous-layer open tubular columns (PLOT) columns are examples of open tubular gas-solid chromatography (GSC) based columns where a thin layer of the adsorbent in the form of molecular sieves or porous polymers is affixed on the inner walls of the capillary. The film thickness of the stationary phase inside the open tubular columns primarily affects the retentive character and the capacity of a column. Thicker films are widely used with highly volatile analytes because such films retain solutes for a longer time, thus providing a greater time for separation to take place.

Packed columns consist of either a solid sorbent or a thin film of liquid over an inert granular support packed in a tube, typically stainless steel. At present times packed columns are used mostly for GSC separations such as gas analysis, and also for preparative applications where high resolution is not required. Permanent gases and very volatile organic compounds can be analyzed by GSC as their volatility lead to low capacity factors in GLC, leading to rapid elution. Surface adsorption is the major retention mechanism in GSC. The common sorbents used in GSC are silica, alumina,

porous polymers such as porapaks (Waters Associates), Chromosorb Century Series (Johns-Manville), HayeSep (Hayes separation) and Molecular sieves referred to as Zeolites and a variety of Carbonaceous materials. The most commonly used support materials are diatomite supports and graphitized carbon.

Table 1.2 General Properties and Characteristics of Typical Gas Chromatographic Columns

Parameters	Type of Column			
	FSOT	**WCOT**	**SCOT**	**Packed**
Length, m	10 – 100	10 – 100	10 – 100	1 – 6
Inside Diameter, mm	0.1-0.53	0.25-0.75	0.5	2-4
Efficiency, Plates/m	2000-4000	1000-4000	600-1200	500-1000
Total Plates	$(20\text{-}400)*10^3$	$(10\text{-}400)*10^3$	$(6\text{-}120)*10^3$	$(1\text{-}10)*10^3$
Sample Size, ng	10-75	10-1000	10-1000	$10\text{-}10^6$
Relative back Pressure	Low	Low	Low	High
Relative Speed	Fast	Fast	Fast	Slow
Chemical Inertness	Best →			Poorest
Flexible	Yes	No	No	No

(Source: Reference [6])

1.3 Carbon Sorbents in Preconcentration and Chromatography

Development and the use of novel carbonaceous sorbents as stationary phases for GSC and for preconcentration of organic compounds has been actively pursued by the scientific community [7]. The main advantage of the carbon-based sorbents is their high chemical inertness, thermal stability, non-polar character and well defined surface properties. Unlike SiO_2 based sorbents, their use is not limited by pH and compared to organic polymer sorbent, they can withstand higher temperatures. Carbon based sorbents

may also serve as a matrix for attaching various functional groups or developing coatings such as in gas liquid/solid chromatography. The development of carbon based sorbents suitable for the enrichment of analytes has generally paralleled the development of chromatographic sorbents. Active carbon sorbents were routinely used in classical liquid chromatography. With the advent of gas chromatography, attention turned to graphitized thermal carbon blacks (GTCB), which were found to be suitable nonpolar sorbents either for GSC or, when coated with a small percentage of liquid phase as a "tailing reducer", for gas-liquid/solid chromatography. Interest in preparation of the novel carbonaceous sorbents have recently increased because of the non-polar characteristics of these materials for HPLC, their applicability over a wide pH range, and better defined surface properties in comparison to activated carbon. This has led to the development of porous carbon packings and porous glassy carbon.

1.3.1 Synthesis of Carbon Based Sorbents

In principal four consecutive stages may be distinguished in the formation of carbons from naturally occurring or synthetic precursors: homogenization, carbonization, volatilization of inorganic impurities, and graphitization [8]. The term "homogenization" covers all operations, which lead to an improved ordering of the structure of any solid or liquid carbonaceous starting material. It usually consists of a thermal treatment of the starting material at 450-700°C in an inert atmosphere. It is well known that the degree of structural order of the carbon precursor essentially determines the extent to which the penultimate material is converted into a graphitic or an amorphous carbon, which represent the two limiting cases.

Carbonization is a process by which solid residues with increasing content of the element carbon are formed from organic material usually by pyrolysis in an inert atmosphere. It typically increases the percentage of carbon content and introduces pores. Frequently used organic precursors include phenolic resin, furan resin, and coal tar pitch. It also covers a number of other processes including coking, charring and reaction with oxidizing gases such as oxygen, carbon dioxide and water vapour. As with all pyrolytic reactions carbonization is a complex process in which many reactions take place concurrently such as dehydrogenation, condensation, hydrogen transfer and isomerization. It differs from coalification in that its reaction rate is faster by many orders of magnitude. The final pyrolysis temperature applied controls the degree of carbonization and the residual content of foreign elements, e.g., at T ~ 1200 K the carbon content of the residue exceeds a mass fraction of 90 wt. %, whereas at T ~ 1600 K more than 99 wt. % carbon is found. The products so formed are termed active carbons and possess a high adsorptive capacity.

Active carbons may still contain inorganic impurities such as sulphur and silica depending upon their origin. These can be removed by volatilization at 1200-1700°C. This process leaves a large number of defect sites in the structure and causes a disordering of the mutual arrangement of layers. Microscopic holes may even be formed within the particles.

Graphitization covers the subsequent heat treatment in an inert atmosphere at 1700- 3000°C. Such heat treatment brings about densification with concurrent removal of structural defects, and forms a three-dimensionally ordered graphitic structure. The degree of graphitization of any carbon brought about by high temperature treatment

depends strongly on its initial structure. Thus treatment of some active carbons at temperatures as low as 1200°C can greatly reduce, or even completely eliminate the porosity of the material, whereas some glassy carbons may not convert to graphite even on heating to 3000°C.

1.3.2 Types of Carbon Sorbents, Classification and Characterization

At present commercially available types of carbon sorbents [8] are: i) Actived Carbon, ii) Graphitized Carbon Black (GCB), iii) Carbon Molecular Sieves (CMS), and iv) Porous Graphitic Carbon (PGC). They are described in detail in Table 1.3. They differ in their physico-chemical characteristics, such as pore size and shape, surface area, size, volume of pores, functionality of surface, and chemical inertness. Their specific surface areas range from 5 to 2000 m2/g. The extent to which these often conflicting characteristics can be achieved depend upon the source of starting material, procedure chosen for preparation of the product, and conditions under which the sorbent is used.

According to the classification scheme of Kiselev [9], there are three classes of sorbents (Table 1.4). Class I adsorbent is an adsorbent which interacts non-specifically with the four groups of adsorbates (groups A, B, C, D), whereas class II and III adsorbents interact both non-specifically (i.e., London forces, Vanderwaals forces) and specifically (i.e., strong dipole-dipole interactions). Only class I interacts non-specifically with all groups of adsorbates (Table 1.5).

Examples of the four groups of adsorbates are: group A molecules-n-alkanes; group B molecules-aromatic hydrocarbons, chlorinated hydrocarbons; group C molecules-organo-metallic compounds; and group D molecules-primary alcohols, organic

Table 1.3 Comparison of the Carbonaceous Sorbents

Type	Sources	Producing Process	Surface Structure
Activated Carbon	Biomass materials such as wood, peat, coconut shell & fruit nuts. Fossilized plant sources such as coals, petroleum coke.	A two-step process of carbonization at 400-500°C to eliminate the bulk of the volatile matter and then activation by partial gasification at 800-1000 °C to develop the porosity & surface area. A mild oxidizing gas such as CO_2 or molten KOH is used in the gasification / activation step.	Highly Porous containing micro / meso / macro pores (pore volumes range from 0.07 – 0.6 cm^3/g & pore size range from 10–30 A°).Contain a wide range of functional groups. Consists of a twisted network of defective hexagonal carbon layer planes, cross linked by aliphatic bridges. Demonstrate high sorption capacity, heterogenous, irreversible sorption and low recovery. (BET Surface area can be as high as 4000 m^2/g, depending on the activation condition).
Carbon Molecular Sieves (CMS)	From Polymeric materials, such as PVDC poly (vinylidenechloride), from coals, such as anthracite. Carbon deposition by coating of the pore mouths of activated carbon by cracking a hydrocarbon.	Various molecular sieving properties are obtained by changing the carbonization temperature (above 700°C). PVDC carbonized at 700°C can adsorb flat molecules such as benzene, naphthalene but not spherical ones such as neopentane.	Uniform pore size ranging from 2 – 6 A° with definite shape. Its the pore size & shape that offers them their molecular sieving properties. Highly porous structure with almost uniform micropores, very small crystallites crosslinked to yield a disordered cavity-aperture structure. CMS 5A has micropore volume of 0.18 cm^3/g for pore size 5A° and a macropore volume of 0.38 cm^3/g for pores of 2.0 μm. CMS 3A is O_2/ N_2 selective & is used for air separation.
Graphitized Carbon Black	Ordinary Carbon Blacks.	Heating carbon blacks to about 3000°C in an inert gas atmosphere. This eliminates volatile, tarry residues It induces the growth of graphite crystallites.	Homogenous surface without micropores, free of functional groups. Contain graphite like array of carbon atoms. Adsorption is mainly on non-polar external surface sites. BET surface area is about 100 m^2/g. They are used in GLC after a surface coating with a liquid modifier to reduce tailing.
Porous Graphitic Carbon (PGC)	Produced by impregnating suitable silica gel or another porous template with a phenol-formaldehyde resin mixture, or Saccharose. Polymers such as styrene & divinylbenzene are also used.	After polymerization within the pores of the template material the polymer is converted to glassy carbon by, heating in an inert atmosphere to about 1000°C. Then removing the template by alkali to give PGC. Finally, firing in an inert atmosphere at 2000°C -2800°C to produce some degree of graphitization	Homogenous hydrophobic surface; surface chemistry is determined by the final heat treatment, and any subsequent chemical treatment. The particle size, shape, porosity and pore size are determined by the choice of template material. It has been used as a HPLC stationary phase. The pore size usually ranges from 200–500 A°. Specific surface areas can rage from 20–120 m^2/g and specific pore volumes can range from 0.3 – 1 cm^3/g.

Table 1.4 Classification of Sorbents

Class	Adsorbent	Surface
Class I	Graphitized Carbon Black	Graphitic carbon
Class II	Activated Silica Gel	Oxides of silica gel
Class III	Activated Charcoal	-Oxides of amorphous carbon
	Carbon Molecular Sieves	-Amorphous carbon (weak Class III, can approach Class I)
	Porous Polymers, e.g. Tenax	-Organic "plastics" (weak-strong Class III)

(Source: Reference [7])

Table 1.5 Classification of Sorbates

Group	Molecules	Adsorbents	
		Class I	Class II & III
A	-Spherically symmetrical shells -σ-bonds	Nonspecific interaction Dispersion forces	
B	-Electron density concentrated on bonds/links -π-bonds	Nonspecific interaction	Nonspecific
C	-(+) -Charge on peripheral links	Nonspecific interaction	+
D	-Concentrated electron densities -(+) -Charge on peripheral links		Specific interaction

(Source: Reference [7])

acids, organic bases. The classification of some typical sorbents assists in determining the adsorbate/adsorbent interactions occurring between the two surfaces.

The graphitized carbon blacks, or graphitized carbons, behave as class I sorbents. The carbon molecular sieves, or amorphous carbons, behave as weak class III adsorbents and may approach a class I classification. Activated charcoal, due to the oxidized carbon present on the sorbent (amorphous carbon) surface, is classified as a class III adsorbent.

The various types of carbon sorbents used for chromatographic and preconcentration purposes are listed in Table 1.6. Sorbents having a higher surface area per mass unit have a higher number of active accumulation sites. The surface area can be increased by a porous structure of the sorbent. The factor of pore size is inversely proportional to the surface area. Particle size and shape influence the hydrodynamic conditions in the bed of a sorbent, and are related to the value of the surface area. Smaller particles have a larger surface area, and columns packed with these particles yield a higher performance.

1.3.3 Choice of the Proper Sorbent

The choice of carbon sorbents depends upon the application, as well as the techniques used. The choice is made by considering the nature and concentration of the chemicals to be sampled, the external conditions (temperature and humidity). One must consider a wide range of physical and chemical properties of both the sorbent and the analytes. In order to get the best adsorption/desorption efficiencies for the analytes, sorbents are selected based on their collection efficiency, and desorption efficiency, i.e., the ability to quickly release the sorbed compounds. The general physico-chemical characteristics taken into account for the evaluation of sorbents are functionality, particle size/shape, surface area, pore size and chemical inertness. Dewulf and Langenhove [10] summarized four criteria for the choice of sorbent. First, breakthrough of the analytes has to be avoided. Second, the sorbent itself should not produce any artifacts. The sorbents must be kept free of contamination before and after sampling. Finally, the retention of water on the sorbent material has to be low, so that negative interferences in GC/MS analysis, and

Table 1.6 Carbon Sorbents Used in Preconcentration and Chromatography

Type	Name	Particle Size (mesh)	Porosity (nm)	Surface Area (m^2/g)	Producer
Activated charcoal			1.8-2.2	500-1200	
Molecular Sieve	Carbosieve B		1-1.2	117	King's Lynn. Norfolk
(Permanent gases application)	Carbosieve S-III	60/80	1.3	1000	Supelco. Inc.
	Carbosieve S-II	60/80	3.9	1000	
	Carboxen 1000	60/80	7	1200	
	Carboxen 1001	60/80		500	
	Carboxen 1002	60/80		1100	
	Carboxen 563	20/45		510	
	Carboxen 564	20/45		400	
	Carboxen 569	20/45		485	
	Purasieve	20/40		1070	Union Carbide.
	Spherocarb	60/80	1.5	1200	Analabs. Inc.
	Sortophase				
	Carbosphere	80/100			Alltech.Assoc.
	Saran Carbon				
	Ambersorb				
Porous Carbon (HPLC stationary phase)	Carb I			1200	Polymers Institute SAS
	Carb II			400	Shandon, Runcorn,
	Hypercarb			150-200	
	TSK-Gel Carbon 500			150-200	
Graphitized Carbon Blk Supports in packed GC columns	Carbopack F	60/80		5	Supelco. Inc.
	Carbotrap F	20/40		5	Supelco. Inc.
	Carbograph 3			6-7	Alltech. Assoc.
	Carbopack C	60/80		12	Supelco. Inc.
	Carbotrap C	20/40		12	Supelco. Inc.
	Carbograph 2			10-12	Alltech. Assoc.
	Carbopack B	60/80		100	Supelco. Inc.
	Carbotrap B	20/40		100	Supelco. Inc.
	Carbograph 1			80-100	Alltech. Assoc.
	Graphtrap			80-100	Alltech. Assoc.
	Graphtrap 5				Alltech. Assoc.
	Graphon. Spheron			80-100	

(Source: Reference [7])

the blockage of the cryogenic traps may be avoided.

1.3.4 Structure of Graphitic Carbon

The term "graphitized carbon" generally means that a particular carbon has been heated to a temperature in the region of 3000°C in a graphitizing furnace. In crystallographic terms, the degree of graphitization of such a carbon may fall within wide limits, supposedly "graphitized" carbons ranging from almost amorphous materials to perfect three-dimensional crystalline graphites. The sp^2-hybridized carbon atoms in graphite form infinite planes composed of regular hexagons. Real graphite bodies contain a certain amount of disordered atoms intercalated in the interlayer space. These atoms can occur in the *sp*-, sp^2-, or sp^3-hybridized states. The ideal structure of graphite is, essentially, an infinite series of mutually parallel layers composed of hexagons formed by carbon atoms.

There are, in fact, three distinct forms of carbon to which the term "graphitized" can reasonably be applied and which have well-defined crystal structures. The Bernal structure of perfect three-dimensional graphite (Figure 1.1) consists of layers of carbon atoms, organized in a hexagonal array and ordered ABABAB.... This form of graphite is termed hexagonal graphite [11]. A rarer form of three-dimensional graphite, the Lipson-Stokes form, also exists, but here the layers are ordered ABCABC. This is termed rhombohedral graphite [12]. In naturally occurring graphites, the content of the rhombohedral form can reach 30%, and in artificial, this form is virtually lacking. In both crystalline forms the layer spacing is 3.35 A, and the atomic spacing within the layers is 1.42 A. Each atom in the layer is connected with three neighboring atoms, and the bond angles are 120°. The bonds involve three of the four valence electrons, and the remaining electrons form a common electron cloud. Perfect graphite is rarely formed

synthetically from amorphous solid carbon, since the bonding between the carbon atoms within the graphitic planes is extremely strong, while the interlayer bonding is weak. Thus graphitization tends to develop by the formation of graphitic sheets, which are initially randomly oriented. The reorganization of these sheets into ordered three-dimensional graphite requires such high activation energy that formation of three-dimensional crystalline graphite is generally impossible below 3000°C. Thus, most synthetic carbons, when heated to about 3000°C, assume the two-dimensional graphite (Warren structure, Figure 1.1) in which graphitic sheets are randomly oriented relative to one another.

In two dimensional graphites the layer spacing is slightly greater than in three-dimensional graphites at 3.40-3.43 A^{o} and the atomic spacing within the layers is slightly less. While three-dimensional graphites rarely arise from heating of amorphous solid carbons, they can nevertheless arise by high temperature pyrolytic deposition from organic vapours in the gas phase. Presumably, properly oriented layers are laid down in the first place, and no reorganization is required. Real bodies contain a multitude of areas comprised of the ordered carbon atoms, which have finite dimensions differing by several orders of magnitude for different samples of carbon bodies with graphite or graphite like structures. The structures of these areas can approach that of the ideal graphite lattice or differ there from owing to intralayer distortions and irregular alternation of the layers.

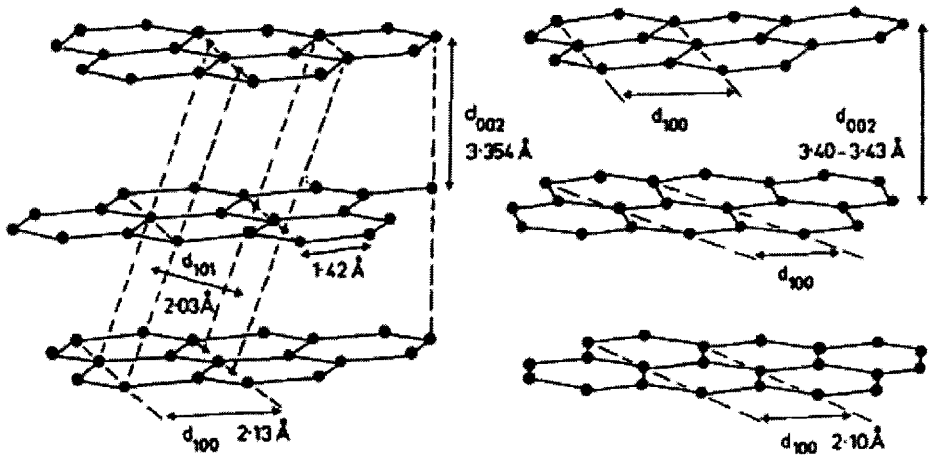

Figure 1.1 Atomic structures of graphite. (Left: Bernal structure of perfect 3-D graphite with ABAB layer registration. Right: Warren structure of 2-D turbostratic graphite with no layer registration.).
(Source: Reference [7])

1.4 Carbon Nanotubes

Carbon exists in four allotropic modifications, namely, diamond, graphite, fullerenes, and linear carbon polymer (karbin / polyyne). Carbon nanotubes are carbon-based nanomaterials with a unique cylinder shaped structure closely related to graphite and fullerenes in their atomic arrangements. The scheme in Figure 1.2 shows the hierarchy of the carbon structures and the place of the carbon nanotubes. Graphite and diamond were discovered as early as in 18th century. Karbin [13], fullerenes and carbon nanotubes were prepared in laboratories recent decades. The physical and chemical properties of the above-mentioned carbon modifications strongly vary with the type of the bonds between the carbon atoms in the molecules of these substances.

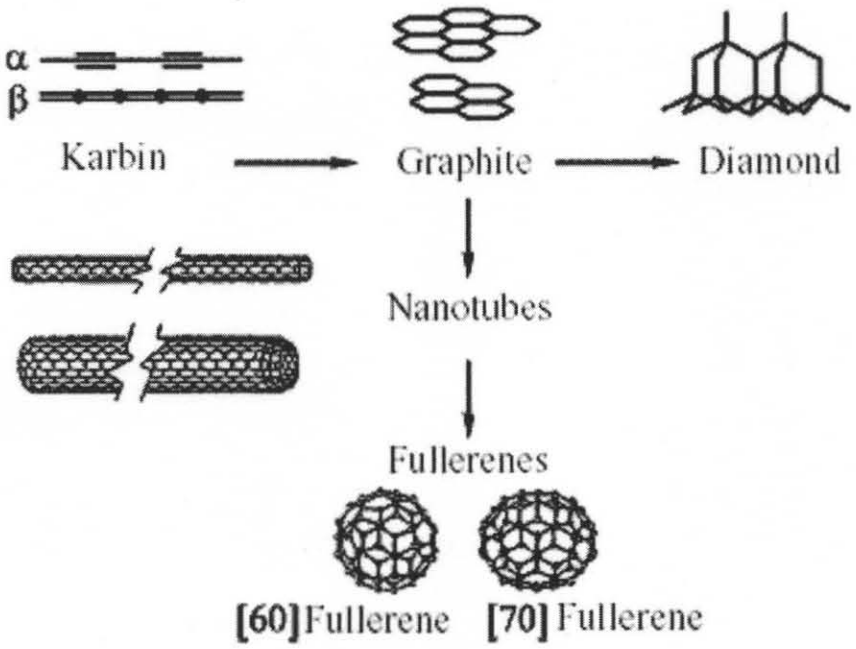

Figure 1.2 Hierarchy of carbon structures.
(Source: Reference [14])

Table 1.7 Properties of the Principal Carbon Modifications

Modification	Hybridization	Bond length, nm	Density, $g.cm^{-3}$	Crystal lattice
Diamond	sp^3	0.148	3.515	Cubic
Graphite	sp^2	0.142(0.335)*	1.848	Hexagonal
Karbin	Sp	α: 0.125/0.149***; β: 0.138	1.917	Hexagonal
Fullerene	sp^2	0.144/0.139**	1.651	Molecular cubic face-centered
Carbon Nanotube	sp^2	0.142(0.34)*	Varies	Hexagonal

(* Interlayer spacing., ** Pentagon-hexagon/hexagon-hexagon, *** Triple/ordinary bonds)
(Source: Reference [14])

1.4.1 Discovery of Carbon Nanotubes

Carbon nanotubes have been synthesized for a long time as products from the action of a catalyst over the gaseous species originating from the thermal decomposition of hydrocarbons. The preparation of vapor-grown carbon fibers had actually been reported as early as more than one century ago [15]. Since then, the interest in carbon nano-filaments / nanotubes has been recurrent, though within a scientific area almost limited to the carbon material scientist community. The review published by Baker et al. [16] gives few references regarding the early works on carbon nanotubes. The worldwide enthusiasm came unexpectedly in 1991, after the catalyst-free formation of nearly perfect concentric multiwall carbon nanotubes (c-MWCNTs) was reported [17] as by-products of the formation of fullerenes by the electric-arc technique. But the real breakthrough occurred two years later, when attempts in situ to fill the nanotubes with various metals led to the discovery – again unexpected of single-wall carbon nanotubes (SWCNTs) simultaneously by Iijima et al. [18] and Bethune et al. [19].

1.4.2 Structure of Carbon Nanotubes

Nanotubes are formed by rolling up of a graphene sheet (a graphene being the same polyaromatic mono-atomic layer made of an hexagonal display of sp^2 hybridized carbon atoms that genuine graphite is built up with) into a cylinder closed at both ends with two fullerene halves. The resulting structure is governed by the orientation angle of the graphite plane along the lattice vectors (m, n) with respect to the nanotube axis. The indices (m, n) determine the diameter and chirality, which are key parameters of a nanotube (Figure 1.3). Depending on the chirality (the chiral angle between hexagons and the tube axis), SWCNTs can be either metals or semiconductors, with bandgaps that are

relatively large (~0.5 eV for typical diameter of 1.5 nm) or small (~10 meV), even if they have nearly identical diameters [20]. For same chirality semiconducting nanotubes, the band gap is inversely proportional to the diameter. Thus, there are infinite possibilities in the type of carbon tube "molecules", and each nanotube could exhibit distinct physical properties. There exist single- and multi-walled, open- and closed-ended nanotubes differing in the length and diameter. Multi Walled Nanotubes (MWCNTs) can be considered as a collection of concentric SWCNTs with different diameters. The length and diameter of these structures differ a lot from those of SWCNTs and, of course, their properties are also very different. The interlayer spacing in MWCNTs is equal to 0.34 nm as opposed to 0.335 nm in genuine graphite. MWCNTS differ from SWCNTs by a greater diversity of shapes and configurations, such as, concentric, herringbone and bamboo [22].

1.4.3 Properties of Carbon Nanotubes

The physical and chemical behavior of SWCNTs are related to their unique structural features. The following are some of the properties of the nanotubes.

Chemical reactivity: The chemical reactivity of a CNT is, compared with a graphene sheet, enhanced as a direct result of the curvature of the CNT surface. Carbon nanotube reactivity is directly related to the pi-orbital mismatch caused by an increased curvature [24]. Therefore, a distinction must be made between the sidewall and the end caps of a nanotube. For the same reason, a smaller nanotube diameter results in increased reactivity. Covalent chemical modification of either sidewalls or end caps has shown to be possible. For example, the solubility of CNTs in different solvents can be controlled

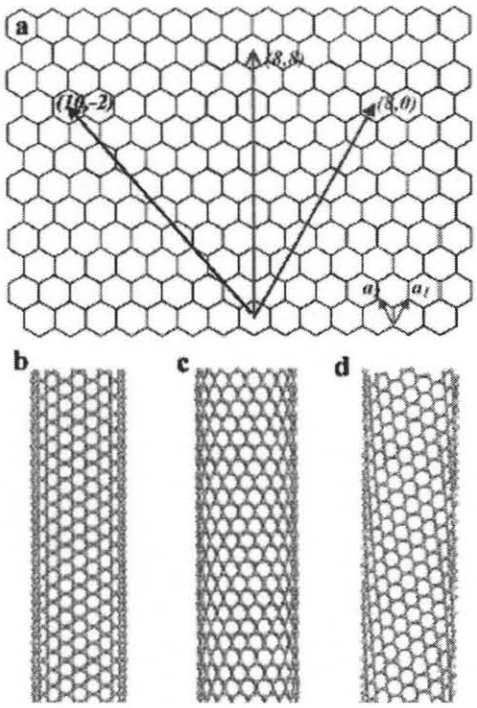

Figure 1.3 (a) Schematic honeycomb structure of a graphene sheet. Single-walled carbon nanotubes can be formed by folding the sheet along lattice vectors. The two basis vectors a1 and a2 are shown. Folding of the (8,8), and (10,-2) vectors lead to armchair (b), zigzag (c), and chiral (d) tubes, respectively.
(Source: Reference [21])

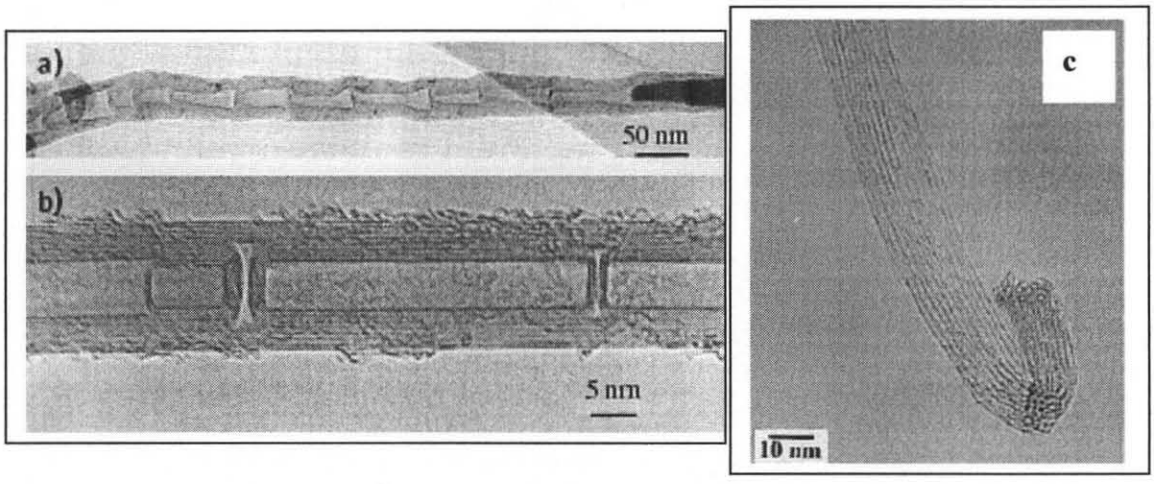

Figure 1.4 TEM images of carbon naotubes. a) low magnification of a bamboo-herringbone MWCNT showing the nearly periodic feature of the texture, b) HRTEM image of bamboo-concentric MWCNT. (Source: Reference [22]), c) TEM image of a bundle of SWCNTs.
(Source: Reference [23])

this way. Though, direct investigation of chemical modifications on nanotube behaviour is difficult as the crude nanotube samples are still not pure enough.

Electrical conductivity: Depending on their chiral vector, carbon nanotubes with a small diameter are either semi-conducting or metallic.

Optical activity: Theoretical studies have revealed that the optical activity of chiral nanotubes disappears if the nanotubes become larger [25]. Therefore, it is expected that other physical properties are influenced by these parameters too. Use of the optical activity might result in optical devices in which CNTs play an important role.

Mechanical strength: Carbon nanotubes have a very large Young modulus in their axial direction. The nanotube as a whole is very flexible because of the great length. Therefore, these compounds are potentially suitable for applications in composite materials that need anisotropic properties.

1.5 Adsorption Properties of Carbon Nanotubes

An interesting feature of SWCNTs is their very high surface area, the highest ever due to the fact that a single graphene sheet is probably the unique example of a material energetically stable in normal conditions while consisting of a single layer of atoms. Ideally, i. e., not considering SWCNTs in bundles but isolated SWCNTs, and provided the SWCNTs have one end opened (by oxidation treatment for instance), the real surface area can be equal to that of a single, flat graphene, i. e., ~ 2,700 m^2g^{-1} (accounting for both sides) [22]. But practically, nanotubes – specifically SWCNTs – are more often associated with many other nanotubes to form bundles, and fibers rather than as a single entity. Such architectures develop various porosity ranges important for determining

adsorption properties. It is thus most appropriate to discuss adsorption on SWCNT-based materials in terms of adsorption on the outer or inner surfaces of such bundles. Furthermore, theoretical calculations have predicted that the molecule adsorption on the surface or inside of the nanotube bundle is stronger than that on an individual tube. A similar situation exists for MWCNTs where adsorption could occur either on or inside the tubes or between aggregated MWCNTs. Additionally, it has been shown that the curvature of the graphene sheets constituting the nanotube walls can result in a lower heat for adsorption with respect to that of a planar graphene.

1.5.1 Accessible CNT Surface Area

Various studies dealing with the adsorption of nitrogen on MWCNTs [26] and SWCNTs [27] have highlighted the porous nature of these two materials. Pores in MWCNTs can be divided mainly into inner hollow cavities of small diameter (narrowly distributed, mainly 3–10 nm) and aggregated pores (widely distributed, 20–40 nm), formed by interaction of isolated MWCNTs. It is also worth noting that the ultra-strong nitrogen capillarity in the aggregated pores contributes to the major part of the total adsorption, showing that the aggregated pores are much more important than the inner cavities of the MWCNTs for adsorption.

Adsorption of N_2 has been studied on as-prepared and acid-treated SWCNTs, and the results obtained point out the microporous nature of SWCNT materials, as opposed to the mesoporous MWCNT materials. Also, as opposed to isolated SWCNTs, surface areas well above 400 m^2g^{-1} have been measured for SWCNT bundle containing materials, with internal surface areas of 300 m^2g^{-1} or higher. The theoretical specific surface area of carbon nanotubes ranges over a broad scale, from 50 to 1,315 m^2g^{-1} depending on the

number of walls, the diameter, or the number of nanotubes in a bundle of SWCNTs [28]. Experimentally, the specific surface area of SWCNTs is often larger than that of MWCNTs. Typically, the total surface area of as-grown SWCNTs ranges between 400 and 900 m^2g^{-1} (micropore volume, 0.15–0.3 cm^3g^{-1}), whereas values ranging between 200 and 400 m^2g^{-1} for as-produced MWCNTs are often reported. In the case of SWCNTs, the diameter of the tubes and the number of tubes in the bundle will affect mainly the BET value. It is worth noting that opening/closing of the central canal noticeably contributes to the adsorption properties of nanotubes. In the case of MWCNTs, chemical treatments such as KOH activation are efficient to develop a microporosity, and surface areas as high as 1,050 m^2g^{-1} have been reported [29]. Thus it appears that opening or cutting as well as chemical treatments (purification step for example) of carbon nanotubes can considerably affect their surface area and pore structure.

1.5.2 Adsorption Sites and Binding Energy of the Sorbates

Adsorption of gases in a SWNT bundle can occur inside the tubes (pore), in the interstitial triangular channels between the tubes, on the outer surface of the bundle, or in a groove formed at the contact between adjacent tubes on the outside of the bundle (Figure1.4). Starting from closed-end SWCNTs, simple molecules can adsorb on the walls of the outer nanotubes of the bundle and preferably on the external grooves. For the more attractive sites, corresponding to the first adsorption stages, it seems that adsorption or condensation in the interstitial channel of SWCNT bundles depends on the size of the molecule (or on the SWCNT diameters) and on their interaction energies [30]. Then, adapted treatments to open the tubes will favour the gas adsorption (e.g., O_2, N_2 in the inner walls [31]). For hydrogen and other small molecules, computational methods have

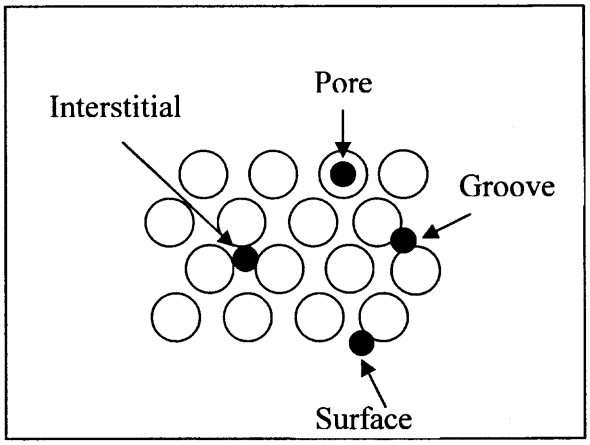

Figure 1.5 Sketch of a SWNT bundle illustrating the four different adsorption sites.

shown that, for open SWCNTs, the pore, interstitial, and groove sites are energetically more favourable than the surface site, with respect to the increasing number of carbon nanotubes interacting with the adsorbed molecules [32].

For MWCNTs, adsorption can occur in the aggregated pores, inside the tube or on the external walls. In the latter case, the presence of defects, as incomplete graphene layers, has to be taken into consideration. Although adsorption between the graphenes (intercalation) has been proposed in the case of hydrogen adsorption in h-MWCNTs or platelet nanofibers [33], it is unlikely for many molecules due to steric effect and should not prevail for small molecules due to long diffusion path.

Few studies deal with adsorption sites in MWCNTs, however it has been shown that butane adsorbs more in the case of MWCNTs with smaller outside diameters, which is consistent with another statement that the strain brought to curved graphene surfaces affects sorption. Most of the butane adsorbs to the external surface of the MWCNTs while only a small fraction of the gas condensed in the pores [34]. Comparative

adsorption of krypton or of ethylene on MWCNTs or on graphite has allowed scientists to determine the dependence of the adsorption and wetting properties on the specific morphology of the nanotubes. Higher condensation pressure and lower heat of adsorption were found on nanotubes with respect to graphite [35]. These differences result mainly from a decrease in the lateral interactions between the adsorbed molecules, related to the curvature of the graphene sheets.

A limited number of theoretical as well as experimental works exist on the values of the binding energies for gases on carbon nanotubes. If most of these studies report low binding energies on SWCNTs, consistent with a physisorption, some experimental results, in particular in the case of hydrogen, are still controversial. Doping nanotubes with alkali may enhance hydrogen adsorption, due to the charge transfer from the alkali metal to the nanotube, which polarizes the H_2 molecule and induces dipole interaction [36].

The observed trends in the binding energies of gases with different Van der waals radii suggest that the groove sites of SWCNTs are the preferred low coverage adsorption sites due to their higher binding energies. Finally, several studies have shown that, at low coverage, the binding energy of the adsorbate on SWCNT is between 25% and 75% higher than the binding energy on a single graphene. This discrepancy can be attributed to an increase of the effective coordination in the binding sites, such as the groove sites, in SWCNTs bundles [37]. Representative results concerning the adsorption properties of SWCNTs and MWCNTs are summarized in Table 1.8.

Table 1.8 Adsorption Properties and Sites of SWCNTs and MWCNTs (Letters in column 5 refer to Figure 1.5)

CNT Type	Porosity (cm^3g^{-1})	Surface Area (m^2/g)	Binding energy of the adsorbate	Adsorption sites	Attactive potential per site (eV)	Surface area per site (m^2/g)
SWNT (bundle)	Microporous 0.15-0.3	400-900	Low, mainly physisorption 25-75% > graphite	Surface (A) Groove (B) Pore (C) Interstitial (D)	0.049 0.089 0.062 0.119	483 22 783 45
MWNT	Mesoporous	200-400	physisorption	Surface Pore Aggregated pores	-	-

(Source: Reference [22])

1.6 Thermal Stability of Carbon Nanotubes

Thermogravimetric analysis (TGA) is a widely used analytical technique for the determination of the thermal stability of carbon nanotubes [38-42]. TGA can also help in estimating the purity of the carbon nanotubes by roughly quantifying the amount of amorphous carbon, metal catalyst and other impurities such as graphitic nanoparticles [38]. A typical TGA experiment makes use of 1-5 mg of material, which is at the level 0.01% of the total amount of as prepared -SWCNT soot produced in a bulk preparation. A TGA graph involves a change in % weight of the sample (due to oxidation) as a function of temperature. The peak position of the mass derivative (dm/dT) graph of the TGA curve is recorded as an indicator of the oxidation temperature, T_o. The oxidation temperature can be defined alternatively as an onset (deflection point) temperature, or as a maximum in the derivative weight curve, also known as DTG (derivative of thermogravimetry) curve. The oxidation temperature, T_o of the sample in TGA serves as

a measure of thermal stability of nanotubes in air. In case of nanotube samples, onset temperature is typically poorly defined, since transitions are rather broad, and initial mass

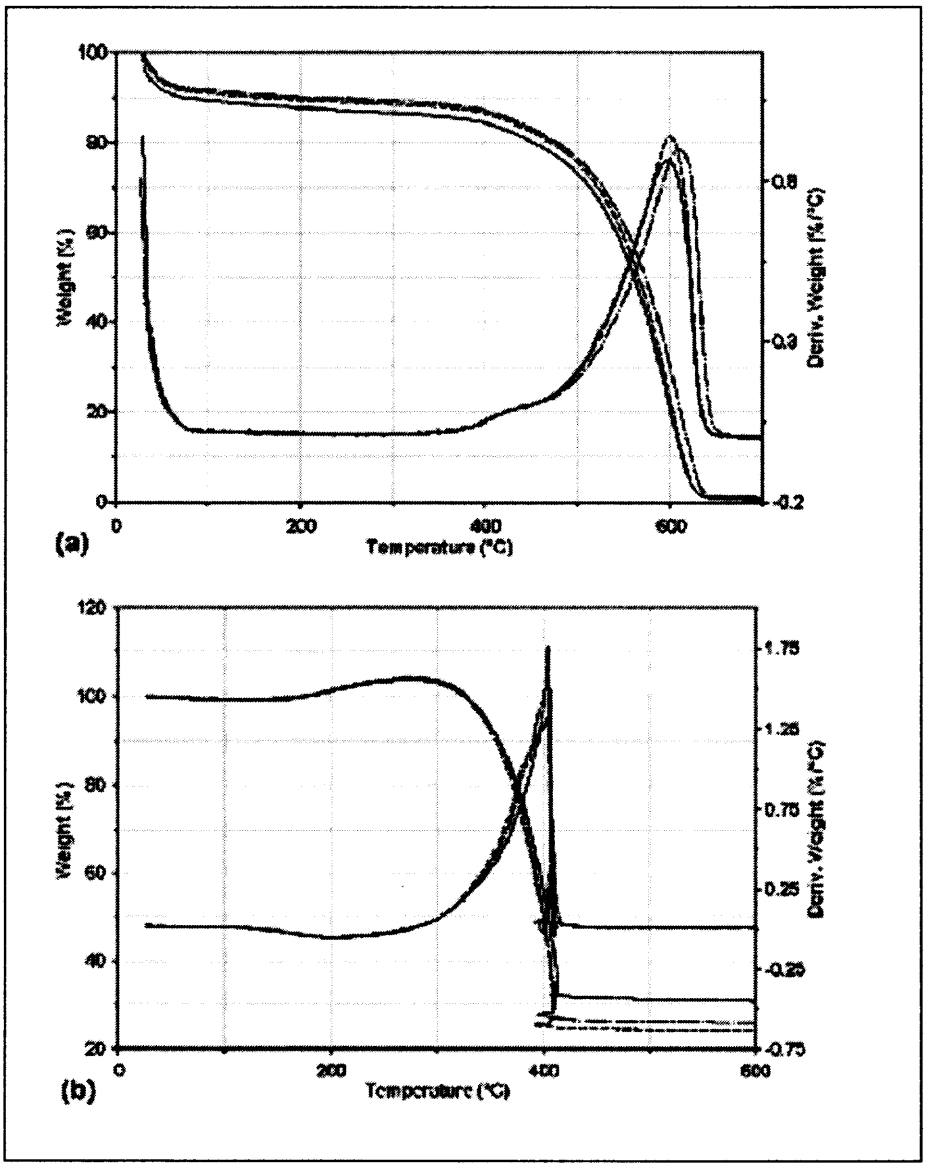

Figure 1.6 TGA mass loss and its derivative for three separate specimens of purified HiPco SWCNT material (a) and corresponding raw nanotubes (b). Note the variability of data due to in-homogeneity of material.
(Source: Reference [38])

loss is attributed to the oxidation of amorphous carbon impurities rather than nanotubes themselves. Maximum in the DTG curve, on the other hand, can be defined and measured precisely, and is associated with burning of nanotubes rather than impurities. Therefore, T_o is defined as a DTG maximum.

The thermal stability of carbon nanotubes depends on a number of parameters [38-42]. For example, smaller diameter nanotubes are believed to oxidize at lower temperature due to higher curvature strain. Defects and derivatization moiety in nanotube walls can also lower the thermal stability. Active metal particles present in the nanotube samples catalyze carbon oxidation, so the amount of metal impurity in the sample can have a considerable influence on the thermal stability. It is difficult to distinguish these contributions, but nevertheless thermal stability is a good measure of the overall quality of nanotube sample. Higher oxidation temperature is always associated with purer, less defective samples as seen in Figure 1.6. The oxidation temperature is also dependent on the heating rate [38]. Higher heating rates can cause nanotube combustion [41], which leads to qualitatively different shape of TGA traces and larger standard deviations of residual mass (M_r) and T_o [39]. It is important to emphasize that in order to be able to compare the T_o values across the board, all TGA measurements have to be performed at the same heating rate. The 5^o C/min heating rate is generally chosen taking into account these effects. Other factors that can influence the thermal stability of carbon nanotubes is the synthesis process, such as the type of catalyst, the precursor, and the CVD temperature. This is due to the fact that the CNTs produced by different catalysts and preparation methods are different in their graphitization degree. Nanotubes with higher degree of graphitization generally have lesser defect sites along the walls and thus have

relatively higher thermal stability [42] as seen from Figure 1.7. For example, the arc preparation of MWCNTs occurs under extremely high-energy conditions and as-obtained arc MWCNTs are highly graphitic [42] and undergo combustion at higher temperatures.

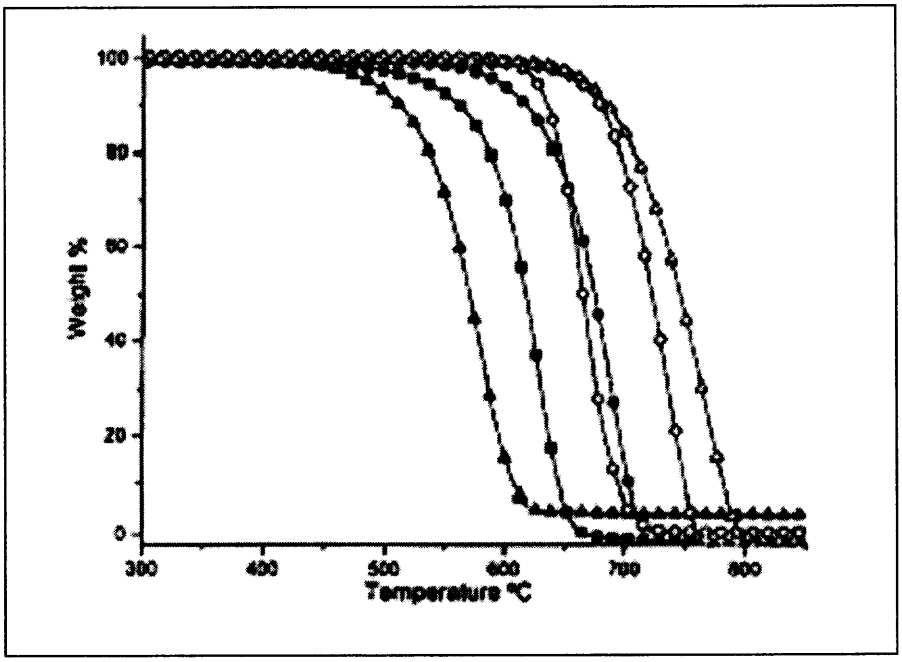

Figure 1.7 Weight loss curves for raw MWCNTs, diamond, annealed diamond, graphite, annealed MWCNTs and annealed graphite: ▲ raw MWCNTs; ■ diamond; O annealed diamond; ● graphite; ◊ annealed MWCNTs; Δ annealed graphite.
(Source: Reference [42])

1.7 Applications of Carbon Nanotubes in Analytical Chemistry

A variety of applications have been demonstrated with carbon nanotubes in analytical chemistry. These applications are based on the novel and/or superior adsorption properties and the unique electronic and chemical properties of nanotubes. The adsorption properties are in-turn a result of their morphological characteristics, such as,

porosity, high surface area, aspect ratio, etc. These characteristics form the basis in using carbon nanotubes as a novel carbon-based sorbent material for specialized applications, such as, chromatography, VOC's preconcentration, extraction and removal of chemical and toxic wastes from water. It is relevant to mention that a part of the first two applications have been explored and developed by our research group by the process of self-assembly of CNTs inside steel tubings. The electronic properties of the nanotubes in conjunction with the property of molecule adsorption have led to their applications in chemical sensors, biosensors and electrochemical sensors. High sensitivity, fast response, good reversibility at room temperature as a gas molecule sensor, rapid electron transfer when used as electrodes in electrochemical reactions and easy protein immobilization with retention of activity when used as potential biosensors are some of the advantages of carbon nanotubes in sensing applications. The ability to functionalize nanotubes with various chemical and biochemical species has further catapulted its role in these sensing mechanisms. This is an emerging field with high potential and a great deal of research is currently underway.

1.7.1 Applications of Carbon Nanotubes in Preconcentration and Chromatography

1.7.1.1 Preconcentration of VOC's. Multi-walled carbon nanotubes were self-assembled as a thin film by chemical vapor deposition (CVD) on the inside wall of stainless steel capillaries which then provided an active surface for adsorption/desorption of organic molecules [43]. The selected application device termed as a microtrap or a nanoconcentrator could be used in chemical sensing, trace monitoring, and gas chromatography (GC). A gaseous stream containing trace (parts per million, ppm) levels of hexane and toluene was generated by diffusing a controlled amount of the analytes

form the diffusion capillary into a flow of N_2. The stream flowed constantly through the microtrap, and the organics were trapped in the self-assembled CNT film. An electrical pulse applied to the metal capillary at predetermined intervals, raised the microtrap temperature to 300-400°C and released the organics as a pulse. This desorption pulse was then detected using a flame ionization detector based gas chromatograph (GC). The CNT film in the capillary showed high adsorption as well as fast desorption of the organic molecules, which is an important feature for adsorption and sensing applications.

Li et al. evaluated purified MWCNTs, graphitized carbon black (Carbopack B) and VOCARB 3000 as an adsorbent for trapping VOC's in a purge and trap GC system [44]. The study indicated that MWCNTs had much higher break through volumes (BTVs) than Carbopack B due to their porous structure. The desorption recoveries of the VOCs were found to be near 100% on the MWCNTs thus demonstrating as a potential useful sorbent for trapping VOCs in air and water.

1.7.1.2 As a Solid-Phase Extraction Sorbent. Long et al. [45] have reported that MWCNTs have stronger adsorption capacity for dioxin than activated carbon which was attributed to the stronger interactions between dioxins and CNTs. This research led to the idea that carbon nanotubes may have great analytical potential as effective adsorbents for solid-phase extraction (SPE). The first report was published by Cai et al. [46] for the SPE of three endocrine disruptors as model compounds from real time environmental water samples. They showed, that MWCNTs were superior to C-18 for the extraction of the more polar analyte bisphenol A and atleast as effective as C-18 for the extraction of 4-n-nonylphenol and 4-tert-octylphenol. Compared to XAD-2 copolymer, MWCNTs

exhibited a better property for the extraction of all three analytes. The same group also demonstrated the SPE of several phthalate esters [47] from water samples.

Peng et al. [48] have shown that as-grown CNTs show higher adsorption of organics, such as, dichlorobenzene (DCB) than graphitized CNTs. Li et al. [49] reported that CNT supported amorphous alumina had higher fluoride adsorption capacity, about 13.5 times higher than AC-300 carbon and four times higher than that of γ-Al_2O_3. After oxidation with nitric acid, CNTs also showed high adsorption efficiency for lead removal from water. This adsorption capability as a result of oxidation is a result of regeneration of surface functional groups, such as, –COOH and –OH. It was found that the Pb^{2+} adsorption capacity of nanotubes increases significantly with the increase in pH value from 3 to 7 as a consequence of cation exchange capability [50]. MWCNTs have also demonstrated the preconcentration of trace metal ions, such as, Cd, Mn and Ni and their adsorption capacity was found to be higher than activated carbon [51]. Ionic dyes were eliminated efficiently by MWCNTs encapsulated in cross-linked alginate (ALG) microvesicles using Ba^{2+} as the bridging ion [52]. Van der Waals interaction occurring between the hexagonally arrayed carbon atoms in the graphite sheet of MWCNTs and the aromatic backbones of the dyes was attributed for the selective partitioning of the ionic dyes onto MWCNTs.

Munoz et al. [53] evaluated the preconcentration capacity of fullerenes, MWCNTs and RP-C_{18} sorbents for the sorption of several organometallic compounds in environmental samples. Their study indicated that there were no significant differences between C_{60} and C_{70} fullerenes and MWCNTs in their sorption capacity towards

organometallic samples. However, they found that these sorbents were superior to graphitized carbon black and RP-C_{18} in their extraction capacity.

1.7.1.3 As a Column Packing Material for Gas Chromatography. Quanlong et al. [54] investigated the gas chromatographic properties of purified-MWCNTs and compared with activated charcoal and graphitized carbon black (Carbopack-b) in a packed column approach. The MWCNTs were purified inorder to clean up the catalyst residual, limit the hydrophilic functional groups on the surface and open the ends of the tubes. PMWCNTs showed stronger retention of compounds, being suitable for the separation of compounds with relatively low boiling points and both hydrophobic and hydrophilic groups. However, they showed smaller theoretical plate numbers about three times lesser than Carbopack-b. This was attributed to their open ends and diffusion into their cavities. Carbopack-b showed asymmetric peaks with hydrophilic compounds such as alcohols and ketones due to the stronger interaction between the polar groups on its surface. Activated charcoal exhibited the strongest affinity and highest capacities for the analytes and was considered unfit for performing chromatography due to asymmetrical peaks. In all PMWCNTs was found to be an attractive alternative adsorbent to activated charcoal and Carbopack B as gas chromatographic column packing material for volatile organic compounds with low boiling points.

1.7.1.4 Gas Chromatography on Open-Tubular Self-Assembled MWCNTs. Carbon nanotubes in a powder form, when used in the packed column approach could agglomerate and form large aggregates, because of which, much of their nanoscale characteristics may be lost. Consequently an open tubular column approach was developed by Saridara et al. [55]. MWCNTs were self-assembled inside long steel

capillary tubings via CVD with ethylene as the carbon source and iron inside steel as the catalyst. They demonstrated the separation of gases such as methane, ethane and acetylene as well as liquids, such as, benzene and toluene. The CNT phase demonstrated classical chromatography behavior. The major advantage was found to be the ease of fabrication of such CNT based columns.

1.7.2 Carbon Nanotubes in Chemical Sensing for Gas and Organic Vapor Detection

Chemical resistive sensors based on single walled carbon nanotubes have recently attracted a great deal of attention. The main advantage of SWCNT resistive sensors is that ppb/sub-ppm levels of analytes can be readily detected at room temperature, where as it requires temperatures higher than 350°C for the conventional metal oxide microfilm sensors. SWNT sensors have been demonstrated for the detection of oxygen [56], nitrogen dioxide [57], ammonia, methane [58], nitrotoluene [59], and dimethyl methylphosphonate (DMMP) [60], a nerve agent stimulant. Nanocomposite materials consisting of MWCNTs and poly (3-methylthiophene) [61], a conducting polymer have been reported recently in sensing chloromethanes.

The property of chemical sensing in nanotubes is attributed to the drastic change in the electrical conductivity of the semiconducting SWCNTs due to the adsorption of the analyte molecules on its surface as shown in Figure 1.8 [62]. At this juncture it is pertinent to remind that carbon nanotubes behave electrically as a metal or semiconductor depending on their structure namely their diameter and helicity (symmetry of the two dimensional carbon lattice). Response time (defined as time duration for resistance change by one order of magnitude) of nanotube sensors was a few seconds. The sorption

results in inducing a charge transfer in the analyte molecules, which have electron-donating or withdrawing groups. This leads to the modulation of the Fermi level in the semiconducting tubes (either intertube or intratube modulation of electronic states) resulting in the change in conductivity [63-64]. It has been shown that modification of the electronic structure of the SWCNTs offers further scope for improving the sensing performance.

Polymer functionalization of nanotubes has been shown to impart high selectivity and sensitivity to the CNT-sensors. Polyethyleneimine coating affords n-type nanotube devices capable of detecting NO_2 at less than 1 ppb (parts-per-billion) concentrations while being insensitive to NH_3. While coating nanotubes with Nafion (a polymeric perfluorinated sulfonic acid ionomer) has been shown to block NO_2 and allows for selective sensing of NH_3 [65]. Functionalization of nanotubes with molecules, such as, poly(m-aminobenzenesulfonic acid) (PABS) has shown to improve sensitivity in gas sensing upto ppb levels of NH_3 [66]. For the detection of molecules, which do not have any electron donating or -withdrawing properties SWCNTs loaded with transition metal particles are used. It has been shown that Pd-loaded SWCNTs are capable of detecting small concentrations of H_2 in air [67] and SnO_2/SWCNTs hybrid material shows an enhanced sensitivity to NO_2 [68]. Recently ab initio studies have predicted that doping of alien atoms (B or N) into SWCNTs will allow the possibility of detecting molecules, which do not bind to a nanotube such as CO and H_2O [69]. This could result in widening of the molecular sensing capacity and the reliability of the SWCNT sensors. A typical sensor device consists of a network of SWCNTs in a transistor/array configuration lying between electrodes. In contrast to the individual SWCNT devices, such devices have

shown to improve device reproducibility and high yield due to statistical averaging of the different local nanotube arrangements such as metallic or semiconducting. However it is found that the sensor needs to be often regenerated by external means due to the irreversible binding of nanotubes to a wide range of analytes or due to the strong binding of the analytes on the nanotubes. Different methods, which have been studied for sensor regeneration are venting under ambient conditions [59], heating to high temperature [59], applying bias to the Si gate [62] or by exposing to UV light [66].

Although most of the reported CNT based chemical sensors operate via change in their electrical resistance, some research has also been reported on CNT based resonant sensors and surface acoustic wave sensors. A resonant ammonia sensor [70] based on single- or multi- wall carbon nanotubes has been proposed for remote chemical sensing, at room temperature, by monitoring the changes in the resonant frequency to detect gases. Penza et al. [71] have reported a surface acoustic wave sensor coated by either single or multi-walled carbon nanotubes for chemical detection of VOC's at room temperature.

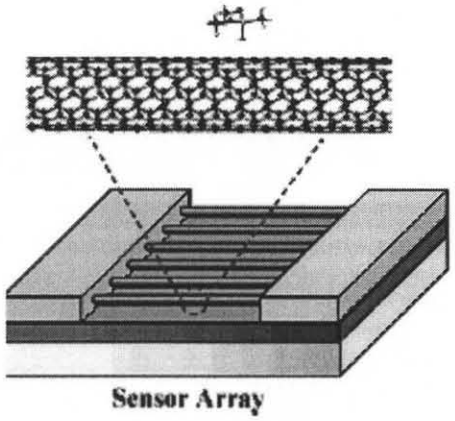

Figure 1.8 Schematic of a typical nanotube gas sensor array.
(Source: Reference [62])

1.7.3 Electrochemical Sensors and Biosensors based on Carbon Nanotubes

The structure-dependant metallic character of carbon nanotubes along with its distinctive electronic properties permit them to promote and mediate rapid electron transfer reactions with electroactive species in solution when used as an electrode material as shown graphically in Figure 1.9 [72]. This characteristic, along with their nano dimensions and high surface area, provides the ground for their role as electrocatalysts in electrochemical and biochemical sensing systems. Since, small surface area leads to constraints concerning the minimum loading or immobilization of biomolecules, such as, enzymes on its surface.

The immobilization of biomolecules and their covalent functionalization with CNTs resulted in a new class of biosensors with improved performances. It has been demonstrated that enzymes, such as, myoglobin and horse radish peroxidase can be covalently attached via amide linkages to the carboxyl groups on the ends of the carbon

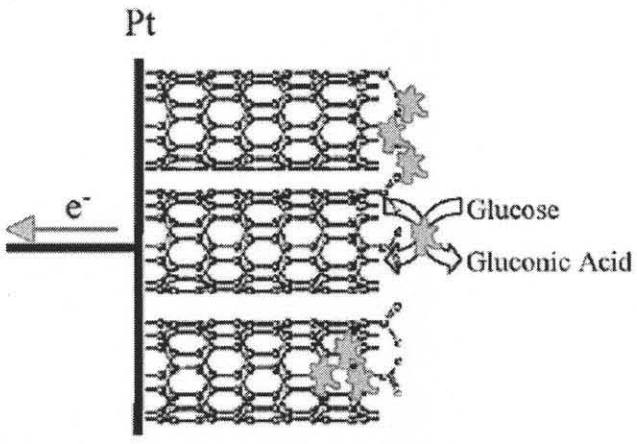

Figure 1.9 Schematic diagram of the carbon nanotube array biosensor. The enzyme immobilization allows for the direct electron transfer from the enzyme to platinum transducer.
(Source: Reference [72])

nanotubes and they can be used to detect concentrations as small as 100 nM H_2O_2 via a quasi reversible Fe^{III}/Fe^{II} voltammetric response. Results suggested that these aligned arrays of functionalized nanotubes behaved electrically similar to a metal, conducting electrons from the external circuit to the redox sites of the enzymes [73]. It has been speculated that the similarity between size scales of these biomolecules and chemically shortened nanoscale diameter CNTs might promote the likelihood of CNTs being able to intimately interact and be within electron tunneling distance of enzyme redox sites.

CNT modified electrodes have shown superior performance when compared with the traditional carbon paste electrodes (CPE) for improving the electrochemical behavior of important analytes including cytochrome c [74], catecholamine neurotransmitters [75], nucleic acids [76], by promoting toward the oxidation/reduction and amplifying the signals leading to an improvement in the sensitivity of their electrochemical detection. The modified CNT electrodes were prepared by casting a dispersion of the SWNTs in *N*,*N*-dimethylformamide (DMF) on a glassy carbon (GC) electrode to form a carbon nanotube film.

Recently Munge et al. have used CNTs as amplification platforms by demonstrating the detection of femtomolar levels of proteins via highly sensitive electrochemical protocol based on covalent functionalization of multiple enzyme tags onto a CNT carrier [77]. The ability of carbon nanotubes to promote the electron-transfer reactions of NADH [78-79] and hydrogen peroxide [80] suggests great promise for dehydrogenase- and oxidase- based amperometric biosensors. Recently, Zhang et al. [81] have demonstrated an amperometric biosensor for quantification of NADH by integrating carbon nanotubes with a redox mediator (azure dye, (AZU)) and polymeric matrix

(chitosan, (CHIT)). The integration of CNT led to a decrease in the overpotential for the redox mediated process by ~30 times and amplified the NADH current by ~35 times and further decreased the response time from ~ 70 s for CHIT-AZU to ~5 s for CHIT-AZU/CNT films. Higher sensitivity and stability has been demonstrated in batch voltammetric analysis. The enhanced sensitivity has been attributed to the electrocatalytic activity of CNT and to interfacial accumulation onto their surfaces, while the improved stability reflects the minimization of surface fouling at the CNT surface. For further study refer to the review article published on electrochemical sensors based on carbon nanotubes in 2002 [82].

One of the limiting steps in the integration of CNTs with biological systems towards fabrication of biosensors is the inherent insolubility of nanotubes in solvents, particularly in water. Different strategies have been employed to achieve dispersion; one of the first was to shorten the SWCNTs down to about 100-300 nm by prolonged and vigorous acid treatment [83]. Dispersion of full-length nanotubes has mostly been achieved by non-covalent wrapping of water-soluble macromolecules on the nanotubes such as, nafion [80], polyvinyl pyrrolidone (PVP) and polystyrene sulfonate (PSS) [84], or through covalent modification with hydrophilic functionalities [85-86]. Recently Wang et al. [87] have reported a microwave-assisted method to prepare highly water dispersible functionalized single walled carbon nanotubes in about 3 min in a mixture of nitric and sulfuric acids. These CNTs may then be used with biological systems in biosensors.

1.7.4 Applications of Carbon Nanotubes as Nanoprobes

Another important application of carbon nanotubes is their use as nano-probes by functioning as tips in scanning and imaging techniques, such as, atomic force microscopy (AFM) and scanning tunneling microscopy (STM) [88]. These applications are a result of their nano diameters (~ 0.5 – 2.0 nm), high aspect ratio, and mechanical flexibility. The high electron conductivity of the CNTs makes it an attractive material for use as the STM tips, which probes tunneling current flowing to or from sample surfaces. CNT scanning probe technology is gaining importance in semiconductor metrology both as a profilometer [89] and in the characterization of thin films and surfaces [90], especially as the critical dimensions of devices approach the nanometer regime. The considerable mechanical flexibility of CNTs-the ability to buckle elastically-allows the tube to buckle without damage and thus retain its structural integrity. Just as important, this buckling limits the maximum force that can be exerted onto the sample, thus preventing damage to delicate samples, especially those of biological origins and also helps in resolution of steep and deep nanoscale features [91]. Furthermore, CNTs can be chemically derivatized and functionalized at their ends for the possibility of molecular recognition and chemically sensitive imaging in chemistry and biology as shown in Figure 1.10 [92]. An AFM tip of carbon nanotube has been used in imaging nanostructure [93], biological molecules such as DNA,amyloid-b-protofibrils (relate to Alzheimers disease) [94]. Carbon nanotube tips can offer higher resolution than the conventional Si or metal tips.

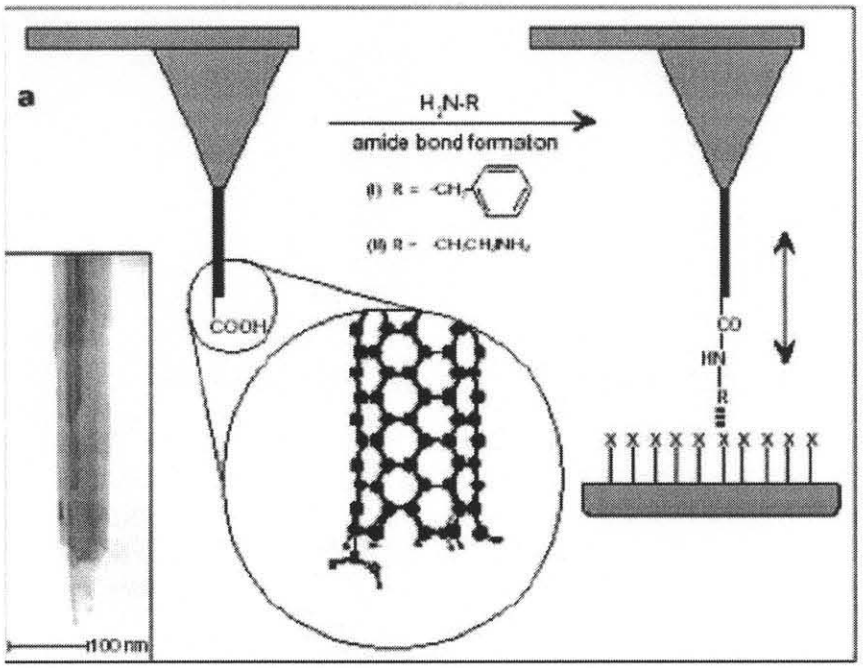

Figure 1.10 Representation of functionalized carbon nanotubes tips. The diagram illustrate the modification of carbon nanotube tips by coupling an amine (RNH_2) to a pendant carboxyl group.
(Source: Reference [92])

1.7.5 Miscellaneous Applications

SWCNT was incorporated into an organic polymer monolith containing vinylbenzyl chloride (VBC) and ethylene dimethacrylate (EDMA) to form a novel monolithic stationary phase for micro-high performance liquid chromatography (μ-HPLC) and capillary electrochromatography (CEC) [95]. The inclusion of SWCNT showed enhanced chromatographic retention of small neutral molecules in HPLC and improved peak efficiency and influenced chromatographic retention during peptide separations by CEC.

Xu et al. [96] investigated carbon nanotubes as Assisted Matrix for Laser Desorption / Ionization Time-of-Flight Mass Spectrometry (MALDI-TOFMS). MALDI has been extensively used in mass spectrometric studies of large polymers and high

molecular weight biomolecules [97]. Characterization of small molecules is found to be obscured and difficult due to matrix ion interference and detector saturation in MALDI-TOFMS. However, carbon nanotubes proved to be an excellent matrix providing a lower laser power threshold for desorption/ionization, higher detection sensitivity and mass resolution of small molecules than the conventional organic matrixes.

CHAPTER 2

RESEARCH OBJECTIVE

Carbon nanotubes (CNTs) are known to have high surface area and high thermal stability and have the potential to be high performance separation media that utilize nanoscale interactions. The objective of this research is to scale-up the self-assembly of carbon nanotubes inside steel and silica lined steel tubings for applications, such as, gas chromatography.

MWCNTs were deposited by the chemical vapor deposition (CVD) using ethylene as the carbon source and the iron nanostructures in the stainless steel as the catalyst. The coating consisted of a layer of CNTs aligned perpendicular to the circumference of the tubes, often with an overcoat of disordered carbonaceous material, which could be selectively oxidized by exposing the CNT layer below to air/O_2 at temperatures near 300°C. Variation in uniformity, thickness of deposition, surface coverage, and diameter of the CVD products, along the length of the tubing were studied along with the process parameters and the oxidative removal of amorphous carbon on the CNT surface.

A variety of catalysts, substrates and precursors were investigated for the self-assemmbly of single walled carbon nanotubes. Finally, a film of SWCNTs was obtained with the aerosol spray of ethanolic solution, consisting of dissolved cobalt and molybdenum as metal catalysts and co-catalysts respectively. The catalyst was generated and activated in-situ inside the interior of the tubing, in parallel with the synthesis of SWCNTs to fabricate open tubular GC columns. Gas chromatographic separation of

various class of compounds was carried out, their chromatographic efficiencies and mass transfer behavior was investigated on this novel stationary phase. Capacity factors and isosteric heats of adsorption (ΔH_s) of few representative samples were calculated and compared with the packed Carbopack C^{TM} column. The polarity of the SWCNT phase was determined from the McReynolds constants.

CHAPTER 3

SCALED-UP SELF-ASSEMBLY OF MULTI-WALLED CARBON NANOTUBES INSIDE LONG STAINLESS STEEL TUBING

3.1 Introduction

Synthesis of carbon nanotubes (CNTs) on bulk metallic surfaces has been attempted by several research groups [98-100]. Yuan et al. [101] synthesized well-aligned multi-walled carbon nanotubes (MWCNTs) on stainless steel grid (type 304) from ethylene-air diffusion flames, Vander Wal et al.. [102] reported CNT synthesis on a stainless steel mesh from benzene – C_2H_2 / CO mixtures. They studied the net effect of different preparative treatments including oxidation, reduction and their combinations, for the generation of catalyst particles suitable for CNT synthesis. Pan et al. [103] also reported synthesis of CNTs and carbon nanofibers (CNFs) on metallic substrates such as Ni containing alloys and steels of various grades from ethanol flames. The rationale behind using bulk metal as substrates is the possibility of generating large amounts of metal nuclei in their nano-scale polycrystalline form on the surface. These centers would then act as catalyst sites for the growth of carbon nanotubes, thus eliminating the need for coating the surface with an additional exterior catalyst layer. In most of the reported cases using bulk metallic substrates resulted in the formation of only multiwall carbon nanotubes (MWCNTs).

Different kinds of growth mechanisms and models have been proposed to explain the formation of carbon nanotubes and carbon nanofibers. The foremost of them is the VLS (Vapor-Liquid-Solid) mechanism [104], which basically consists of three defined steps of adsorption and decomposition of carbon containing species at the catalyst

surface, dissolution and diffusion of these species into the molten catalyst, and finally precipitation of carbon as solid whiskers. Several researchers have also proposed tip growth [105-106] and base type [107] growth schemes as growth mechanisms based on their observations of encapsulated catalyst metal particles either at the tip, or at the base of the nanotubes. The 'tip-growth' model proposes that a nanotube lengthens while carrying away a metal catalyst particle at its end. The carried-along particle supplies the carbon feedstock for the growth. The 'base-growth' model proposes that a nanotube lengthens with a particle-free closed end, and carbon feedstock is supplied from the base where the other end of the nanotube interfaces with the catalyst material. The tip growth scheme has been observed with large catalyst particles and with MWCNT formation and the base growth scheme with the small nano particles and with SWCNT formation. To account for the metallic catalyst particles at both the ends of a CNT, Chen et al. [108] proposed that, the metal particles are in the liquid state and the stretching force causes them to elongate and finally break into two parts. The bottom part remains attached to the substrate, while the upper part remains encapsulated inside the CNTs.

CNTs are expected to find applications in chemical processing and separation [109-110] as high performance materials, such as, the adsorption of gases [111-112] and organics [113-114]. Since most chemical processing and separations are carried out in a flow system, it is important to study the self-assembly of CNTs in tubular, and larger structures. The objective of this research was to self-assemble CNTs on the inside wall of stainless steel tubings (type 316) using C_2H_4 as the carbon source during direct CVD. Variation in uniformity, thickness of deposition, surface coverage, and diameter of the

CVD products, along the length of the tubing are important parameters along with the process parameters and the oxidative removal of amorphous carbon on the CNT surface.

3.2 Experimental

Type 316 grade Stainless steel tubing (0.6 m long, 1.59 mm OD and 1.27 mm ID) was used as substrate for CNT deposition. The tubing was coiled and placed in a quartz tube (Kontes-CGS, Vineland, NJ) located in a 40 cm long horizontal CVD furnace. Though a total length of 0.6 m tubing was used for the CVD, an effective length, which was subjected to the high temperatures, was only about 40 cm long. One end of the tubing was connected to the gas flow. The flow rate of the precursor inside the metal tubing was controlled by flow meters, which were placed before the metal tubing.

The entire self-assembly process consisted of three steps. First the surface of tubing was oxidized at 500°C or 700°C for 45 min by flowing air at 65 standard cubic centimeters per minute (sccm). Then the surface was reduced with hydrogen at 500°C or 700°C for 45 min at the same flow rate. The third step was the CVD at an ethylene flow rate of 5 to 20 sccm at pressures of 275 kPag. The deposition was done at 700°C for 1 – 60 min. The tubing was allowed to cool to room temperature under argon to prevent oxidation during this time, or to the specific temperatures used during the oxidative thermal annealing to burn the overcoat of amorphous carbon in the presence of oxygen at a flow rate of 50 sccm.

Six samples 1 cm in length were cut out from different locations at equal distances from the tubing inlet. The first sample was about 1-2 cm from the front of the tubing, which is subjected to CVD in the hot zone of furnace. The subsequent five

samples were about 10 cm away from each other. Then the samples were cut open to expose the inside surface and analyzed by Leo 1530 VP (Carl Zeiss SMT AG Company, Oberkochen, Germany) field emission-scanning electron microscope. Selected samples were also examined by transmission electron micrsocopy (TEM) using a Leo 922 Omega EF-TEM.

3.3 Results and Discussion

The CVD process resulted in the CNTs firmly anchored to the inner surface of the tubing. The SEM images revealed a layer of CNTs, which was densely packed and aligned, often growing perpendicularly from the inside circumference of the tubing. Figures 3.1a and 3.1b show a cross section of the tubing containing the self assembled CNTs. Figure 3.2 shows TEM images of the CNTs collected from inside the steel tubing. The images reveal the relatively high degree of order of the graphitic structure along the CNT walls, varying inner and outer diameters of CNTs, and an inner hollow core characteristic of somewhat wavy MWCNTs that are typically formed in low temperature CVD conditions. The catalyst particle enclosed inside the CNT tip is also revealed at higher magnifications.

Conditioning of the metallic surface [115] prior to the CVD process was important for two reasons. First, surface conditioning resulted in enhancing / toning the metal surface for its latent catalytic activity by forming nano-scale granular structures. Secondly, the surface became structurally (microscopically) more homogenous, which was important for the uniform growth of nanotubes. The surface conditioning was performed in two stages, oxidation of the metallic surface by airflow at elevated

temperatures followed by its subsequent reduction by the flow of hydrogen [102]. Oxidation by a flow of air resulted in the breakup of the metallic surface to form fine granular structures as seen in the SEM images in Figures 3a. and 3b. This increased the surface area, and then the granular structures acted as catalyst sites. Activation of these catalyst point by a further reduction by H_2 prior to CVD was necessary for enhanced catalytic activity. The efficacy of the oxidation-reduction pretreatment prior to CVD growth of CNT has also been discussed by Vander Wal et al. [102].

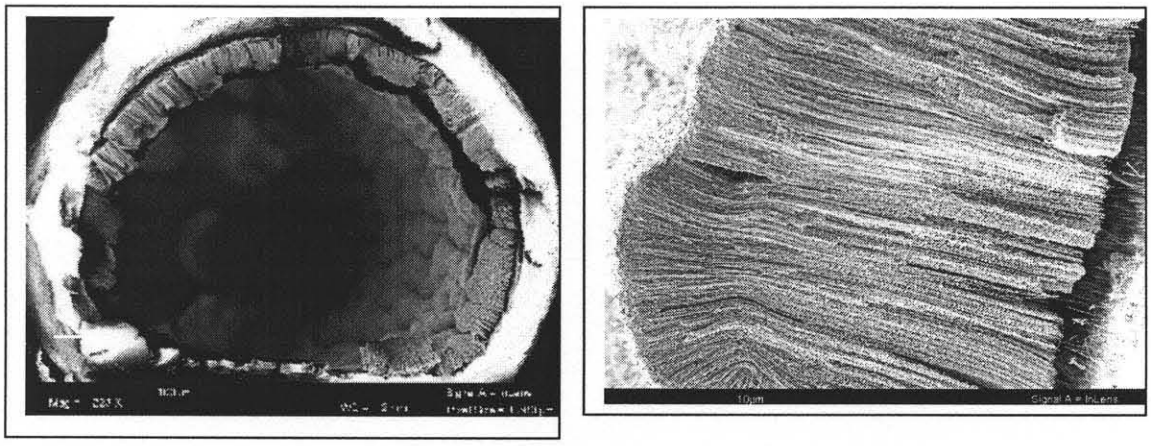

a b

Figure 3.1 SEM image a) of the cross section of the stainless steel tubing showing a layer of the CNT coating inside b) showing perpendicularly aligned CNTs on the steel tubing surface.

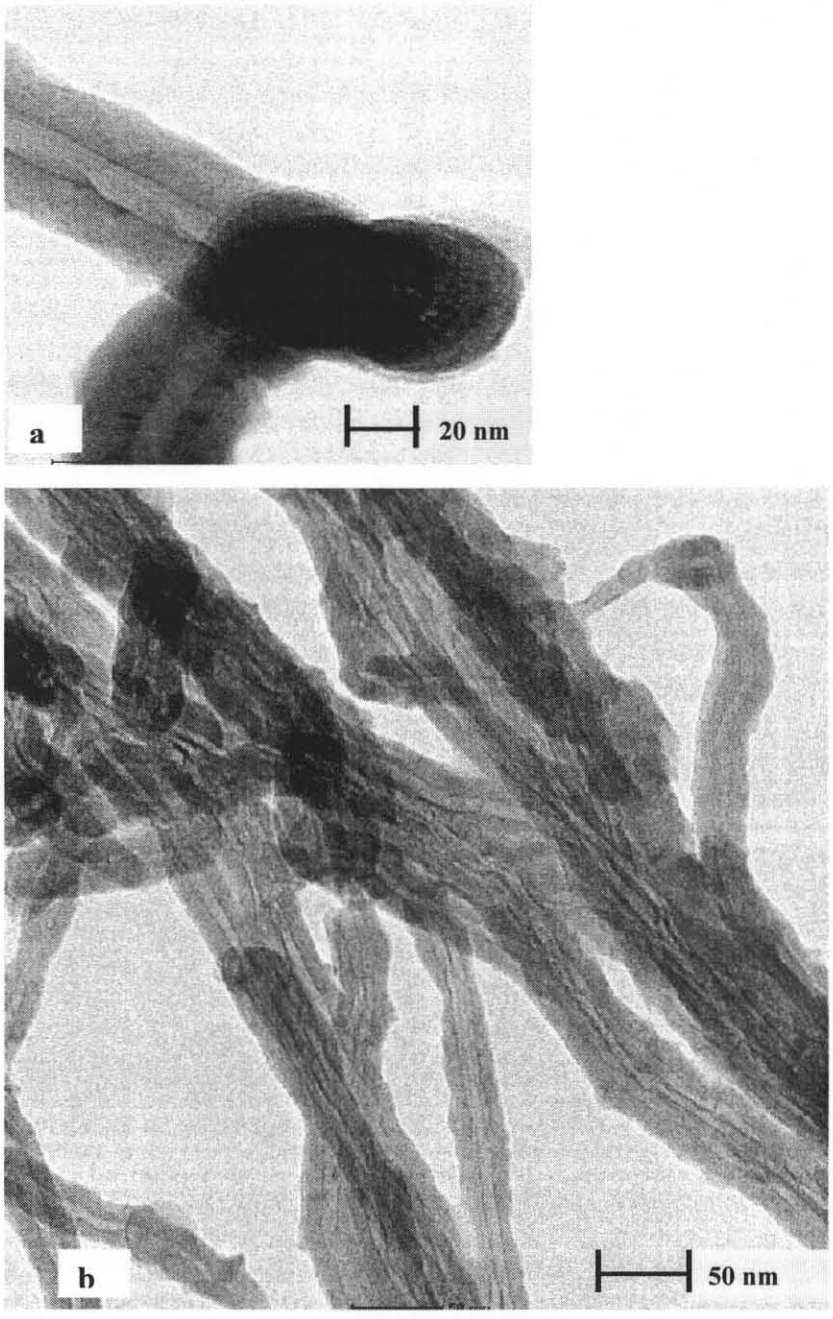

Figure 3.2 TEM images of the CNTs removed from inside the steel tubing. a) The end section of the individual CNTs reveal the inner width of the CNT and the encapsulated catalyst particles at the tip. b) The inner and outer diameters of the CNTs are not uniform along the length.

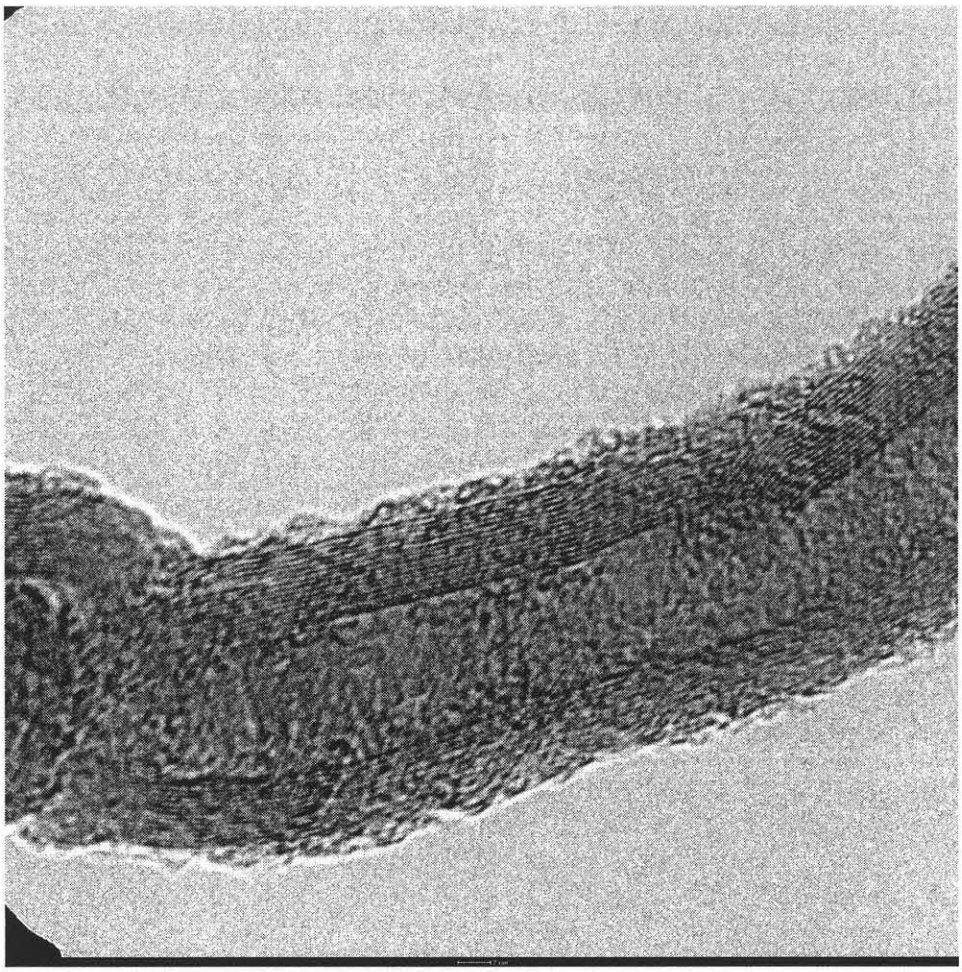

Figure 3.2 c) TEM image of the CNTs removed from inside the steel tubing showing the multiple walls of the carbon nanotubes.

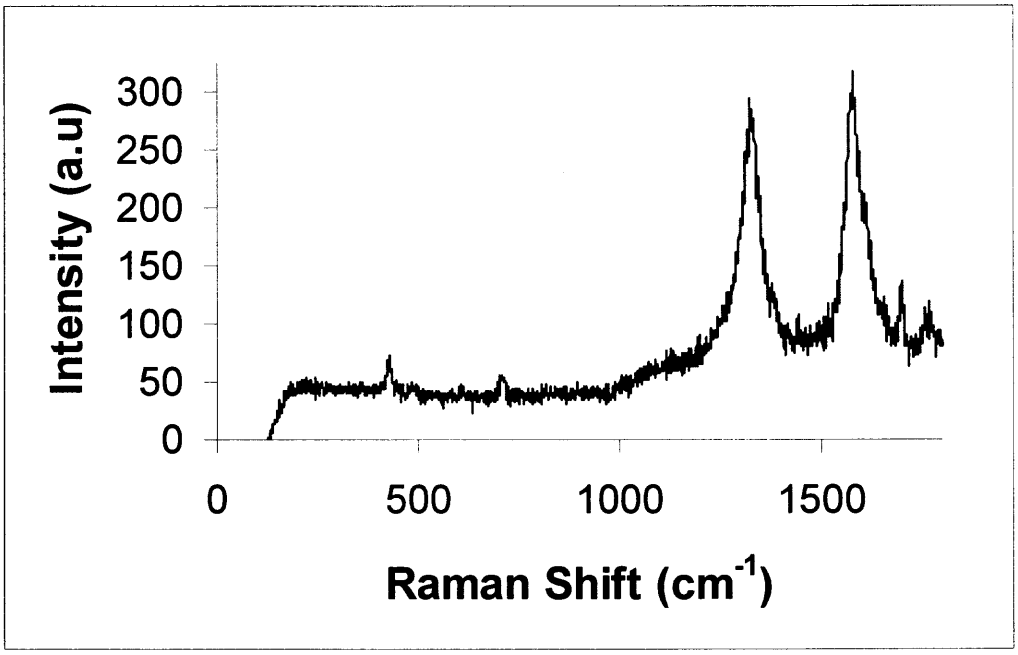

Figure 3.3 Typical Raman spectrum obtained from the stainless steel tubings confirming the presence of multiwalled carbon nanotubes.

Temperature played an important role in the surface conditioning process. Two temperatures namely 500°C and 700°C were evaluated here. When the surface was treated at 500°C for 90 min, a smooth surface was formed with scattered 100 – 300 nm island-like structures as shown in Figure 3.4a. At 700 °C, an apparently smoother surface resulted with finer granular structures as shown in Figure 3.4b. It has been reported previously [116-118], that the diameters of CNTs depend upon the size of the catalyst granules on the substrate. In this study, the average diameter of CNTs varied from 40 – 80 nm (with a few as large as 80 – 120 nm) when the surface was treated at 500 °C. In contrast, the CNTs were 10 – 40 nm in diameter (with few in the range of 50 – 80 nm) when the surface was treated at 700 °C. The SEM image shown in Figure 3.4c reveals decreased CNT density when the substrate was treated at 500 °C. On surfaces pretreated at 500°C, the CNTs were interspersed with larger amounts of amorphous carbon with high percentages of CNTs found only along a small length at the entrance end of the tubing. The surfaces pretreated at 700°C revealed more complete surface coverage of CNTs as shown in Figure 3.4d along the entire length even during a 1 min deposition time. The thickness of the CVD coating at 500°C pretreatment temperature was about two to three times less than what was observed at 700°C.

The variation in the morphology of deposit at about 20 and 40 cm away from the entrance of the tube is illustrated in Figure 3.5. SEM images 3.5a and 3.5b correspond to the surface conditioned at 500°C, and CVD duration of 5 min. As shown in the image 3.5a, the carbonaceous products consist entirely of CNTs interspersed with only very small amounts of amorphous carbon. In contrast, image 3.5b consists of amorphous carbon structures interspersed with fewer CNTs, thus showing significant variations in

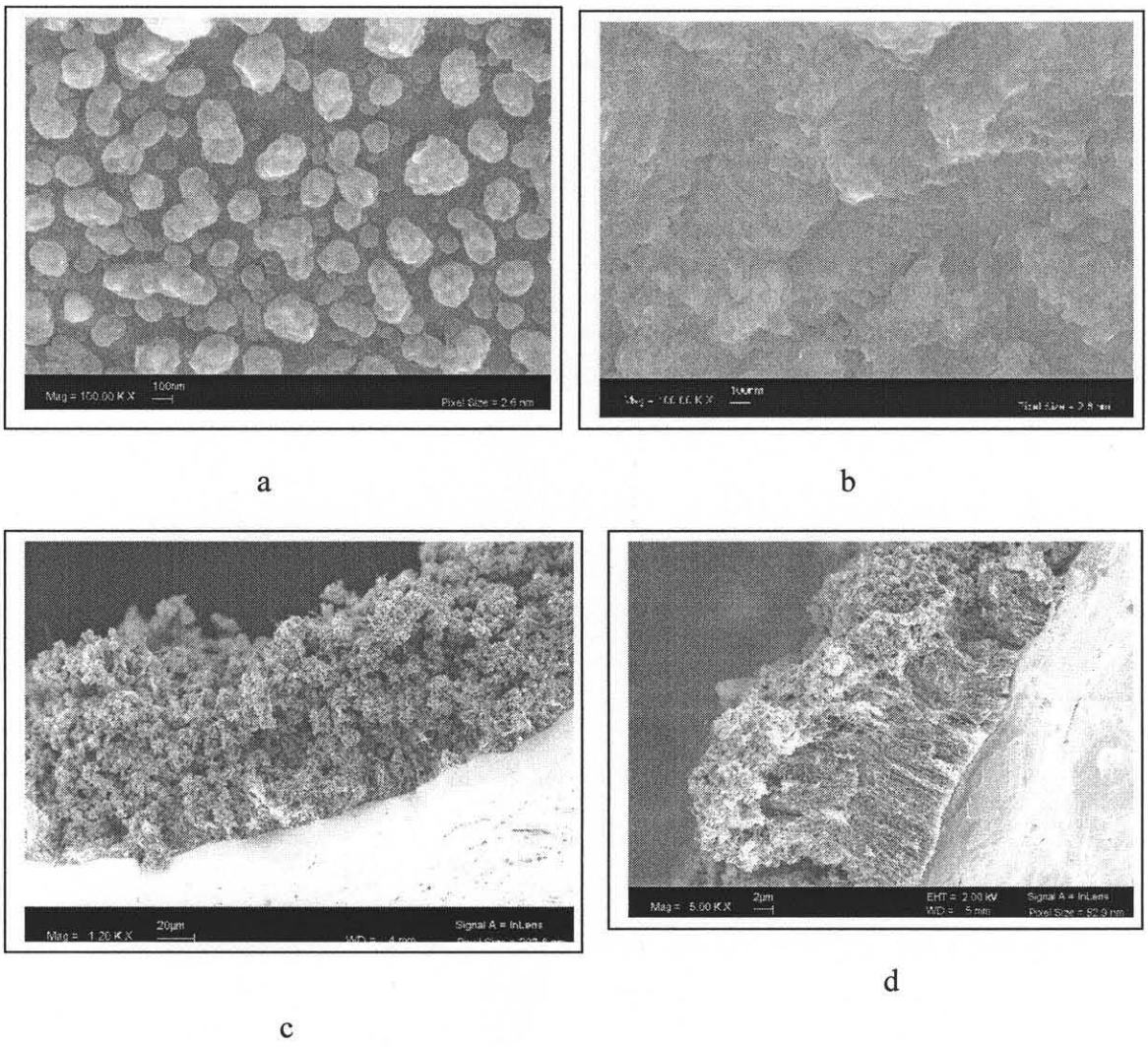

Figure 3.4 SEM images of the stainless steel surface showing granular structures resulting from surface conditioning. a) Steel surface conditioned at 500°C. b) Steel surface conditioned at 700°C. c) SEM image showing typical CNT growth on surface conditioned at 500°C. d) SEM image showing typical CNT growth on surface conditioned at 700°C.

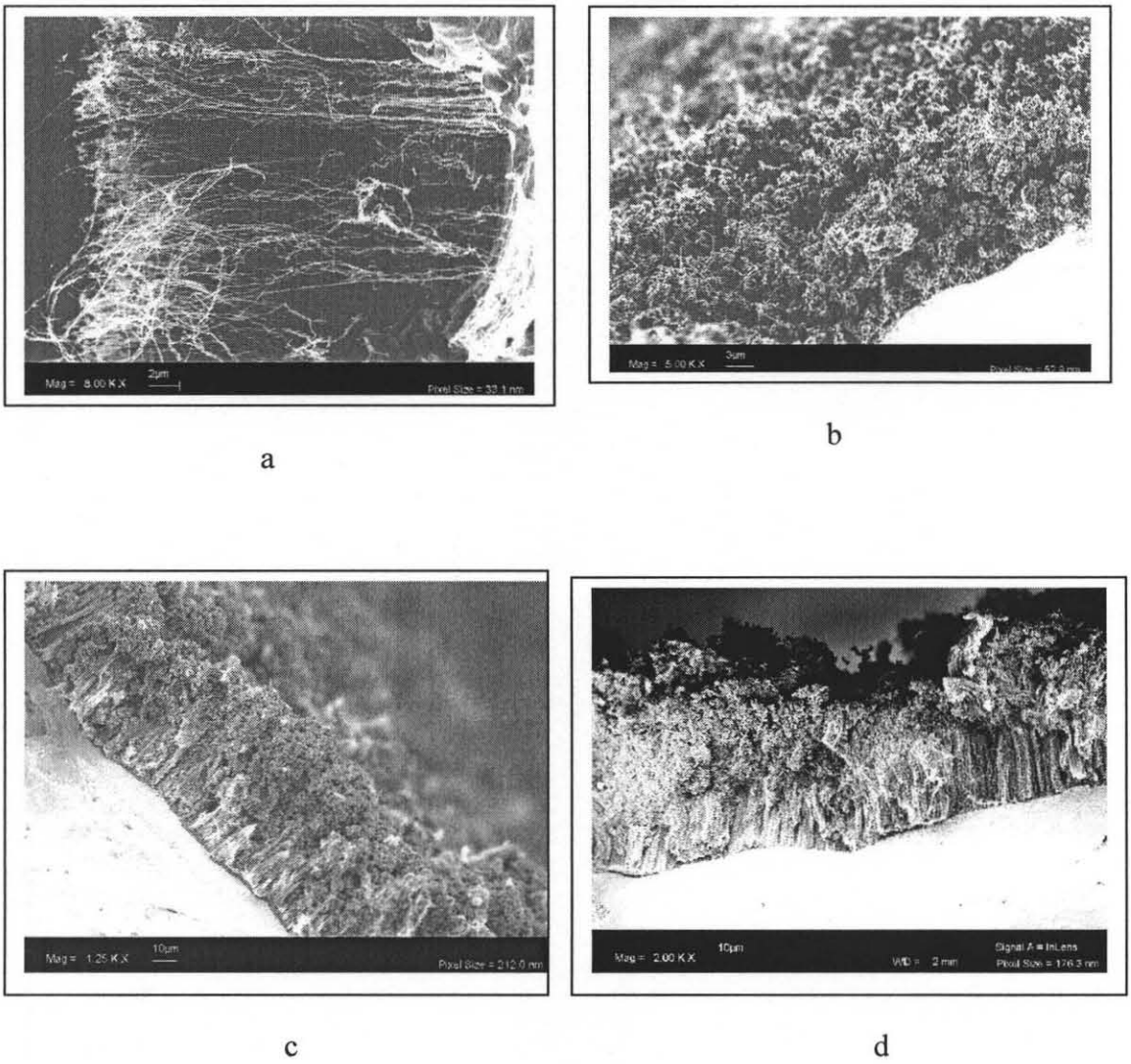

Figure 3.5 SEM images illustrating the variation in uniformity of CVD coating, along the length of the steel tubing at 500°C and 700°C. a) CVD coating at about 20 cm away from the beginning of the steel tubing conditioned at 500°C. b) about 40 cm away from the beginning of the steel tubing. c) CVD coating at about 20 cm away from the beginning of the steel tubing pretreated at 700°C. d) about 40 cm away from the beginning of the steel tubing.

uniformity of deposition. The SEM images 3.5c and 3.5d correspond to the surface pretreated at 700°C and with same CVD duration. The images suggest that the surface coverage of CNTs was more or less uniform. The CNT coating contained an overcoat of amorphous carbon, whose thickness was somewhat higher in the section of the tubing that was further down from the entrance.

The results and observations from the SEM images provided few insights supporting the existing growth mechanisms based on the VLS model for the formation of CNTs. They also went a step further and accounted for the formation of carbonaceous materials on top of the CNTs. The diffusion mechanism in the growth of CNTs was clearly suggested from the thickness of the CVD coating, where lower pretreatment temperatures resulted in lower coating thickness at a given flow rate and CVD time. Finer grain structures at the higher temperature facilitated higher diffusion of carbon into the metal surface. When the solubility of the carbon reached a critical point, the excess carbon began to precipitate, lifting the metal particle at its tip. Finally, the precipitated carbon continued to grow into a tubular structure with or without the metal particle at its tip. The size of the catalytic metal structure also determined the width or diameter of the CNTs as discussed in the earlier section. Several other researchers have documented the growth mechanism until this step. There is no further discussion of the mechanism once the CNTs have formed while the CVD was continued. The observation of amorphous overcoat over the CNT layer was as expected. Once the entire bulk metallic surface wascovered with dense CNTs, the carbon had no access to the catalyst and it began to precipitate as non-tubular amorphous carbon.

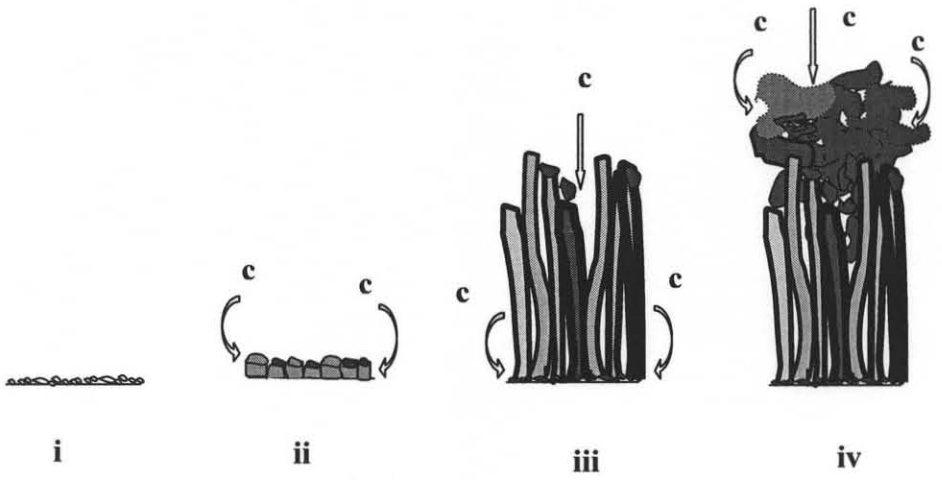

Figure 3.6 A schematic of the growth mechanism of the carbonaceous products formed during the CVD of ethylene as precursor.

i) Diffusion of carbon into the granular metal surface
ii) Precipitation of carbon to form tubules with or without the catalyst metal particles at their tips
iii) Growth of (hollow) MWCNTs and solid CNFs from the tubules.
iv) Formation of amorphous carbon structures at the tips of the CNT's due to the lack of accessibility of the bulk metal surface.

An important inference drawn from the formation of the amorphous carbon over the CNT layer is that the carbon feed for the CNT growth was supplied at the surface/root (as in the base-growth model) rather than at the top (as in the tip-growth model). If the carbon supply were at the top as in the tip growth model then it should have led to relatively longer CNTs until the force of its weight would cause it to bend over and lose its radial alignment. This, however, was not observed. The non-tubular amorphous overcoat started to form once the carbon feed stock failed to access the surface after the CNT grew to a specific length, thus supporting the base-growth model. This is shown pictorially in Figure 3.6.

Table 3.1 summarizes the average thickness ± standard deviation (SD) of the CVD coating and the CNT layer respectively, measured by SEM at 1, 3.5, 5, 15, and 30 min duration of CVD by flowing ethylene at 20 sccm, and also 5 and 15 min duration at 5 and 10 sccm each. The tubing was pretreated at 700°C, and five samples were analyzed along the length of the tubing. Figure 3.7 shows the trend of average thickness of the CNT layer with the non-tubular overcoat at 1, 5, 15 min deposition times. Results from other CVD times showed similar results, and have not been presented for brevity. The figure suggests that the thickness of the CNT layer and the amorphous carbon layer increased with increase in deposition times. The thickness of the deposited film was not uniform and passed through a maximum. The thickness coating does not vary significantly at short CVD times, but the variation was considerable at longer deposition times. With increase in CVD time from 1 min to 15 min, the thickness of the CNT layer increased, along with that of the non-tubular overcoat and formed two layers. At 1 min CVD time, the thickness of the carbon layer was between 1 to 2 μm, which increased

Table 3.1 Thickness (μms) (Avg ± SD) of the CVD Coating Which Includes the CNT and C Along the Length in the Inside of Stainless Steel Tubing at Various CVD Durations at 5, 10 and 20 sccm Flow of Ethylene

Flow rate (sccm)	CVD Duration (min)	Thickness of CVD coating (μm) along the length (cm) in the inside of Stainless Steel tubing at various CVD durations									
		(cm) 10		20		30		35		40	
		CNT+C	CNT	CNT+C	CNT	CNT+C	CNT	CNT+C	CNT	CNT+C	CNT
5	5	42.5 ± 2.5	***40 ±1***	0	***0***	0	***0***	0	***0***	0	***0***
	15	105 ± 5	***100 ±2***	2 ± 1	***1.5 ±0.25***	0	***0***	0	***0***	0	***0***
10	5	70 ± 5	***67 ±3***	2 ± 1	***1.5 ±0.25***	0	***0***	0	***0***	0	***0***
	15	110 ± 10	***80 ±5***	190 ± 10	***55 ±10***	160 ± 10	***50 ±10***	60 ± 7	***32 ±7***	17 ± 5	***10 ±3***
20	1	4 ± 1	***4 ±1***	13 ± 4	***13 ±4***	15 ± 4	***13 ±4***	15 ± 4	***13 ±4***	7 ± 4	***6 ±3***
	3.5	33 ± 4	***16 ±3***	50 ± 7	***25 ±7***	50 ± 7	***25 ±7***	17 ± 4	***15 ±4***	8 ± 3	***5 ±2***
	5	55 ± 7	***25 ±7***	65 ± 7	***30 ±7***	65 ± 7	***40 ±7***	40 ± 7	***38 ±4***	35 ± 7	***25 ±7***
	15	100 ± 7	***35 ±7***	135 ± 14	***40 ±7***	175 ± 14	***60 ±14***	115 ± 14	***50 ±7***	65 ± 7	***50 ±7***
	30	30 ± 7	***13 ±4***	55 ± 7	***28 ±4***	213 ± 17	***55 ±14***	213 ± 17	***55 ±7***	213 ± 17	***55 ±7***

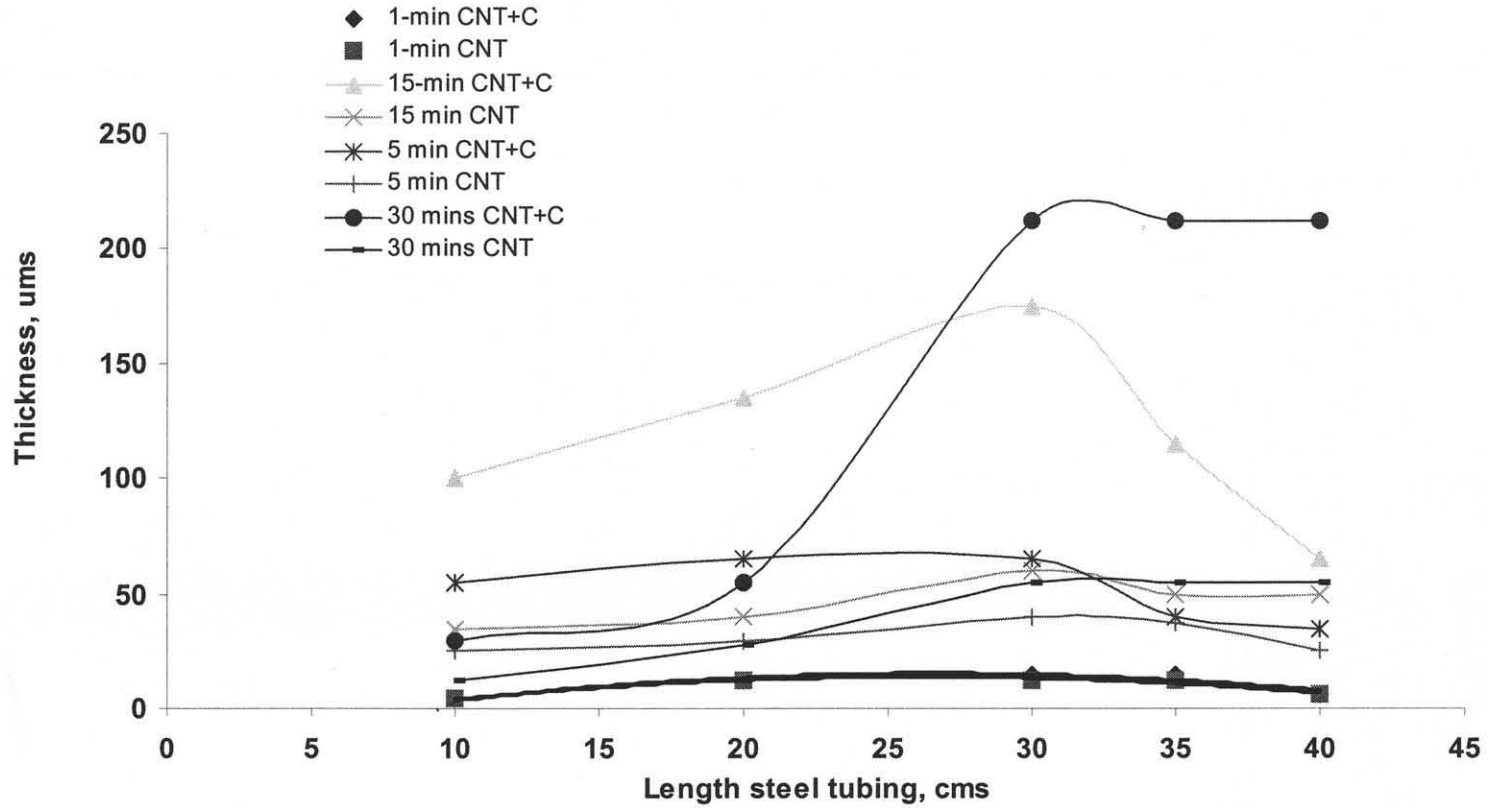

Figure 3.7 Graph Showing the segmentation in CVD thickness consisting of C (carbon) and CNT+C (carbon nanotube + carbon = CVD) along the length of the capillary tube at various CVD durations at 20 sccm flow rate of precursor.

to about 60 μm for 15 min CVD. The temperature inside the furnace was calibrated and was found to be uniform, consequently its influence on the variation of thickness of the CVD coating can be ruled out.

Figure 3.8 summarizes the effect of flow rate of ethylene on thickness of the CVD coating, and surface coverage along the length of the tubing. It shows the average coating thickness at 5, 10, and 20 sccm of flow of ethylene and at 15 min CVD time. The tubing was pretreated at 700°C. Six samples were analyzed along the length of the tubing. At CVD times of 5 min, and flow rates of 5 sccm and 10 sccm of ethylene, surface coverage was seen only in the first half of the tubing while the other half was practically unocoated. At flow rates of 10 sccm, and higher CVD times, such as, 15 min, the coating was obtained along the entire length of the tubing. At flow rates of 20 sccm, the entire length of the tubing showed a CVD coating with surface coverage after just 1 min of deposition time. The plot shows that the coating thickness peaked at different locations at different flow rates, although at higher flow rates it tended to be more uniform. It appears that higher flow rates of the carbon precursor at shorter CVD times could result in a near uniform thickness CVD coating over the entire tube length.

The thickness of the CNT coating at a given CVD time mainly depended on the flow rate. The flow rate affected the residence time and the number of active molecules available for decomposition per unit time. Lowering the flow rate decreased the number of gas molecules, undergoing decomposition per unit time, and also increased the residence time, which was defined as the time that a gas molecule spent in the tube:

$$\tau = (\pi.d^2/4.L) / F \qquad 3.1$$

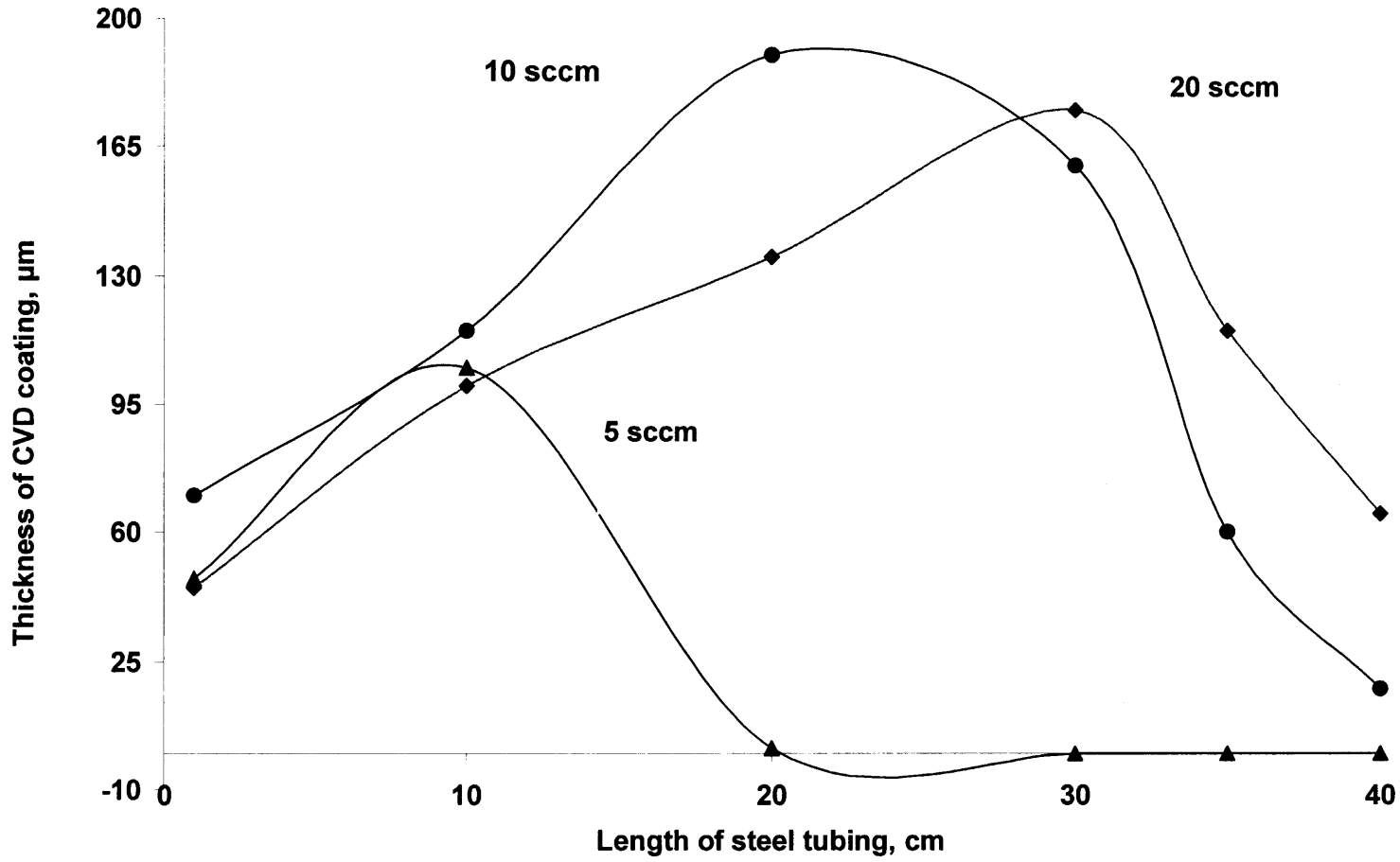

Figure 3.8 Plot showing the thickness of the CVD coating along the length of the steel tubing at flow rates such as 5, 10 and 20 sccm of ethylene precursor at 15 min CVD time.

Where τ is the residence time of the gas molecule, d is the internal diameter of the circular metallic tubing and L is the length of the tubing subjected to high temperature, and F is the flow rate of the gas.

At high temperatures, the longer residence time facilitated rapid and higher decomposition of the molecules to form the carbonaceous products before they could travel further. This explained the absence of any coatings at lower flow rates in the later section of the tubing (Figure 3.8). At higher flow rates, the number of available precursor molecules was higher, thus subjecting more molecules to decomposition at a given time. At the same time, higher flow rates allowed the molecules to travel further before they decomposed. This explained the higher thickness and increased surface coverage at higher flow rates as shown in Figure 3.8. The thickness of the CVD coating is plotted against the precursor gas residence time along the length of the capillary tube at various CVD durations and at various flow rates of the precursor as shown in Figure 3.9.

It has been demonstrated by several researchers [119-120] that heating in the presence of oxygen or air at relatively low temperatures can selectively burn off the non-tubular, carbonaceous material. An optimization of the burn off temperature revealed that heating in the presence of pure oxygen at 375°C did little damage to the CNTs, but effectively burnt off the non-tubular carbon overcoat. The thick overcoat of amorphous carbon which was formed during 5 min CVD over a 0.6 m long tubing is shown in Figure 3.10a. It took 24 hr to burnoff and expose the lower CNT layer as seen in Figure 3.10b. A higher burnoff time may be required for samples deposited with CVD times longer than 5 min in which case the thickness of the amorphous carbon overcoat could be higher. At some locations where the thickness of the amorphous carbon was lower, the burnoff

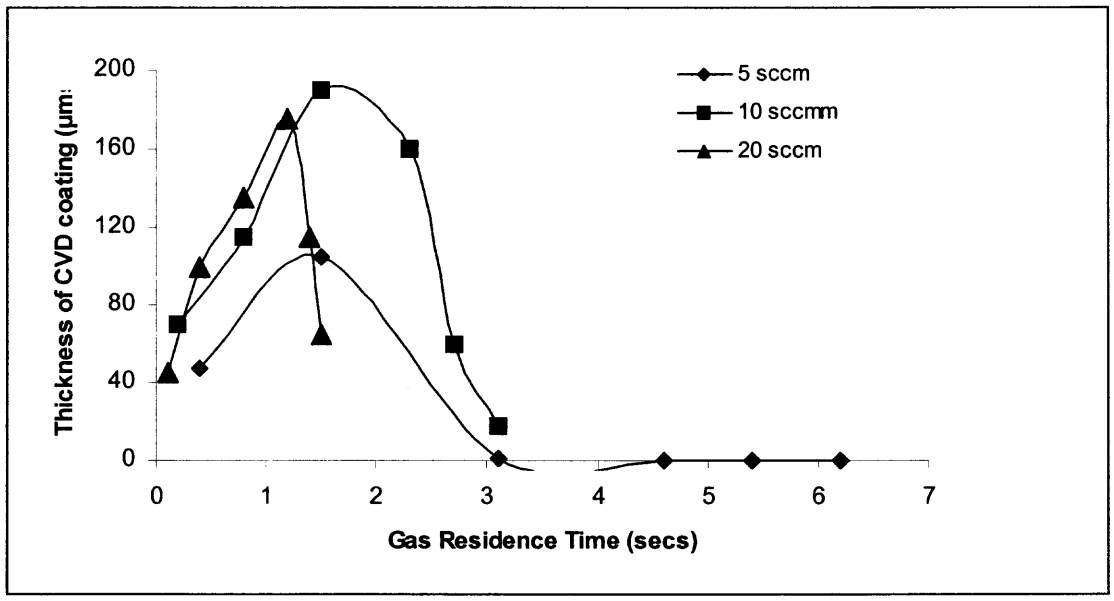

Figure 3.9 Thickness of the CVD coating Vs the precursor gas residence time along the length of the capillary tube at various CVD durations at various flow rates of the precursor.

damaged the CNTs. At temperatures higher than 500 °C, both the CNTs and the carbon products were burnt off in 4 hr. Oxidation in the presence of air however seemed to take a longer time to burn the non-tubular overcoat. The burnoff period therefore needs to be carefully optimized, if damage to the CNT layer is to be prevented.

Figure 3.11 shows a thermogravimetry plot obtained from the oxidation of MWCNTs present as a coating on a tiny section of the stainless steel tubing. The second plot in the figure is from a blank piece of tubing consisting of no coating. The oxidation

program consisted of a hold time of 1 min at 100°C followed by a 5°C / min heating rate until 1100°C. The coating consisted of about 0.18 wt% of the steel tubing piece. The oxidation temperature of the MWCNTs obtained from the peak position of the derivative plot was found to be 558°C. The presence of a single mass derivative peak in the curve indicates a pure or homogenous sample of carbon nanotubes with very little percentage of amorphous carbon.

During the CVD, the gas was collected from the other end of the capillary tubing into a gas sampling device. Later about 100 ul of this sample was injected into GC-MS. The sample was separated into about 14 analytes. Based on the library, the mass spectra of the individual components matched to the following: ethene, ethylene, 1,3-butadiene, cyclopentene, 3-penten-1-yne, 1-pentene, 1,4-pentadiene, 2-hexene, hexane, 3-methyl cyclopentene, benzene, 5-methyl 1,3-cyclopentadiene, 1,3-cyclohexadiene, cyclohexene.

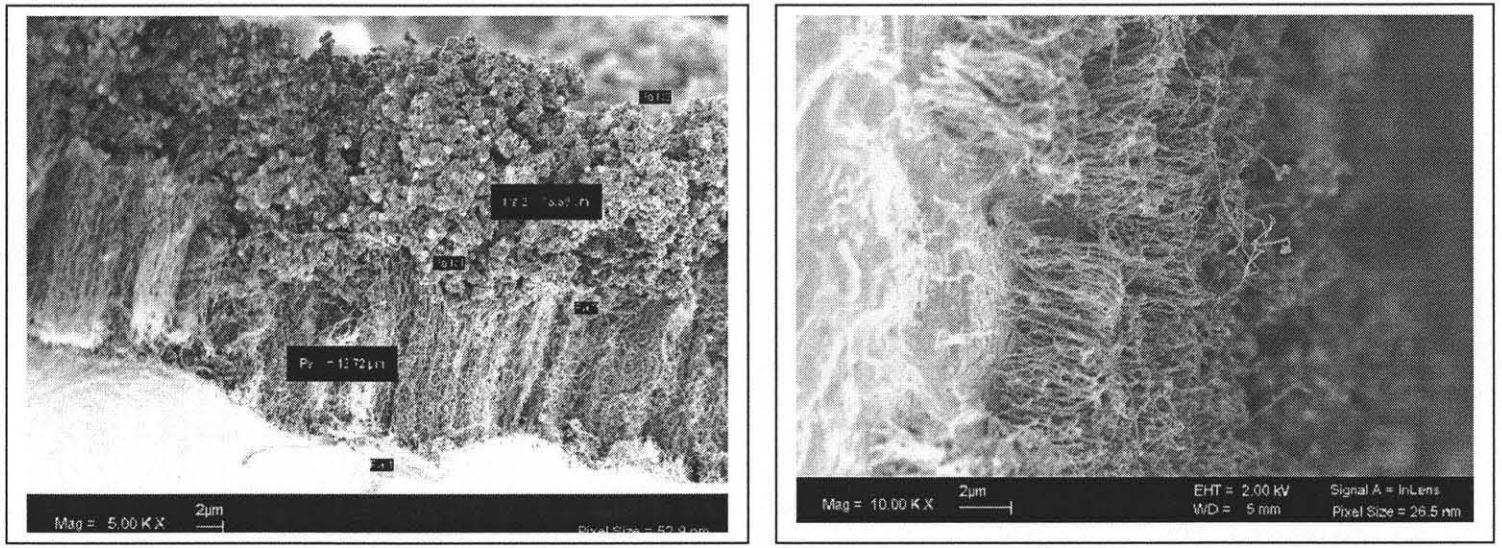

a **b**

Figure 3.10 SEM images of the CVD coating subjected to oxidation by heating in the presence of pure oxygen at 375°C to selectively burn off the amorphous carbon layer. a) SEM image of the CVD coating before the oxidation containing a CNT layer and an overcoat of amorphous carbon layer b) SEM image showing the exposed CNT layer after complete oxidation of the amorphous carbon.

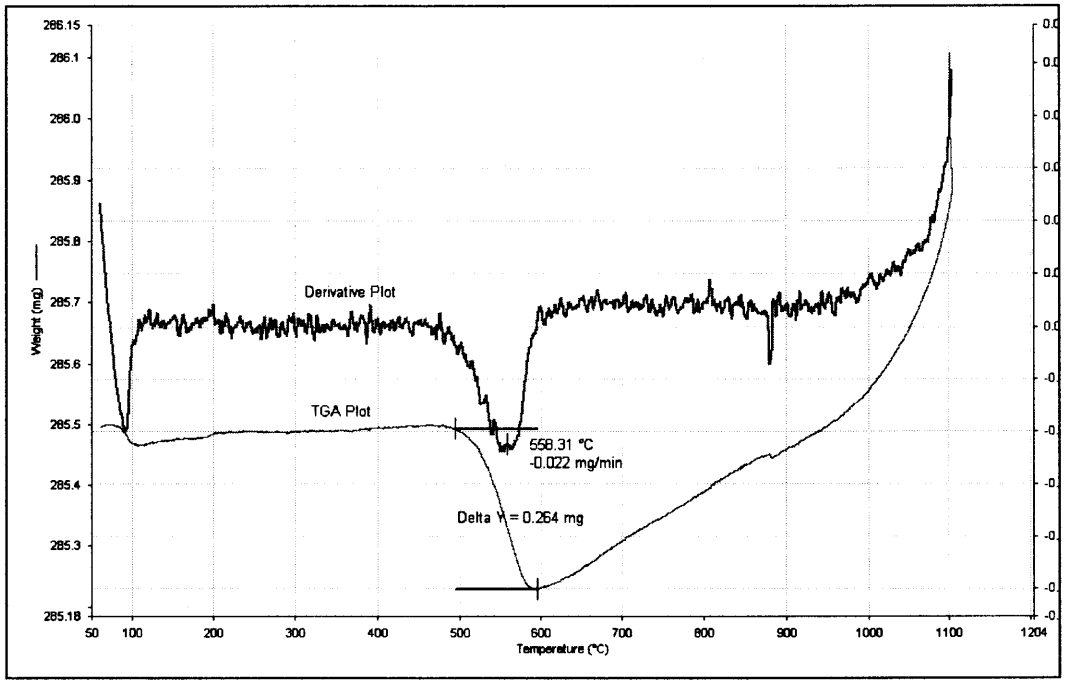

a

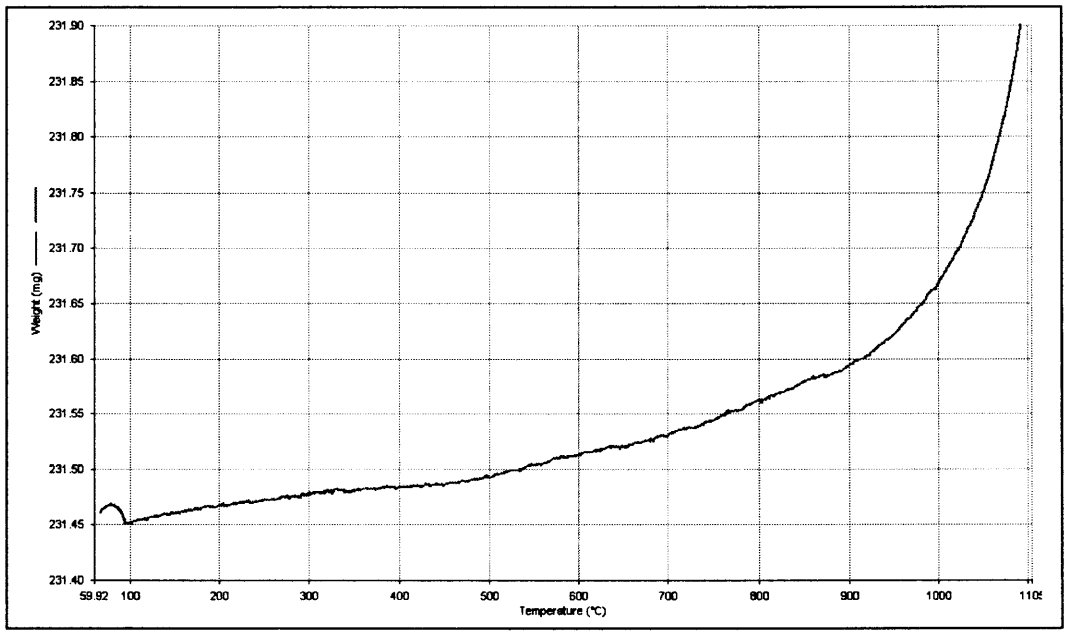

b

Figure 3.11 Thermogravimetry plot obtained from a section of stainless steel tubing a) consisting of MWNT coating b) blank / no coating.

3.4 Conclusions

Carbon nanotubes were self-assembled from the CVD of ethylene on the inside wall of stainless steel tubings. The self-assembly process resulted in a coating of densely packed and aligned CNTs. TEM images indicated that the CNTs deposited are multiwalled. Surface conditioning of the metal surface was performed prior to the self-assembly process to generate nano granular catalyst particles. Higher temperatures generated relatively finer granular catalyst structures, which were found to be important for obtaining a higher and uniform surface coverage of CNTs interspersed with less non-tubular carbon. The alignment, and length of the CNTs, and the formation of the amorphous carbon overcoated on the CNT layer supports a base growth model for CNT formation.

The CVD coating consisted of a CNT layer often with an overcoat of non-nanotubular carbonaceous material. The SEM studies showed that the thickness of the amorphous carbon overcoat and the CNT layer was not uniform along the length of the tubing and the variation in thickness increased with the duration of the CVD process. It was shown that thermal annealing in the presence of oxygen could selectively oxidize the non-tubular carbon overcoat leaving the CNT layer intact.

The flow rate of the carbon precursor inside the tubing affected the residence time of the precursor molecules, which in turn influenced the surface coverage and thickness of the CVD coating, with higher flow rates leading to higher coverage and higher thicknesses. It was predicted that higher flow rates and pressures and shorter CVD duration could lead to more uniform CVD coating over the entire length of the tubing.

CHAPTER 4

SELF-ASSEMBLY OF CARBON NANOTUBES ON OTHER POTENTIAL SUBSTRATES AND PRECURSORS

4.1 Introduction

It has been shown that [133] substrate characteristics like porosity, crystallinity, surface roughness, in addition to CVD conditions, such as, the choice of precursor, deposition time, temperature, pressure, and the catalyst influences the growth, density, morphology and surface coverage of carbon nanotubes. Optimizing so many variables is a challenging task, and limited understanding of these effects has undermined the efforts to fabricate large-scale real world devices.

The scaling up of the self-assembly process of carbon nanotubes on larger structures, such as, long metal tubing is a complex process. Several challenges face such an operation; these include the generation of or the laying down of an uniform nano-sized catalyst, controlling the kinetics of the growth process, to selectively growing CNTs while avoiding the growth of amorphous carbon. Also, CNT synthesis is a substrate and precursor specific process which means the methods need to be tested and optimized if substrates or precursors are different.

The main objective of this research was to self-assemble single walled carbon nanotubes (SWCNTs) inside the capillary metal tubing. Since there is very little published data on this topic, a variety of substrates and precursors needed to be tested to evaluate the CNT growth. This chapter reports the trial and effort investigation to optimize the formation of CNTs of different morphology, density and surface coverage.

4.2 Experimental

About 0.5 m long tubes made of different materials such as, type 316 grade Stainless steel, (1/16" OD and 1.27 mm ID), 304 grade stainless steel, (1/16" OD and 1.27 mm ID), pure Nickel, (1/16" OD, 1.20 mm ID) (Alltech, Deerfield, PA) inconel, (1/16" OD, 1.02 mm ID) and silica lined stainless steel (1/16" OD and 1.10mm ID) (Restek, Bellefonte, PA) were tested as substrates for growing CNT's. Among the precursors tested were ethylene, CO, ethanol and mixtures of CO and ethanol.

Prior to CVD, the tubes were washed with ethanol and allowed to dry. The tubing was coiled and placed in a quartz tube (Kontes-CGS, Vineland, NJ) located in a 40 cm long horizontal CVD furnace. Though a total length of 0.6 m tubing was used for the CVD, the effective length subjected to the high temperature was only about 40 cm long. One end of the tubing was connected to the incoming gas flow. The flow rate of the precursor inside the metal tubing was controlled by flow meters, which were placed before the metal tubing.

The entire self-assembly process consisted of three steps. First the tube surface was oxidized at 500°C or 700°C for 45 min by flowing air at 65 standard cubic centimeters per minute (sccm). Then the surface was reduced with hydrogen at 500°C or 700°C for 45 min at the same flow rate. The third step was the CVD at the precursor flow rate of 5 to 20 sccm at pressures of 275 kPag. The deposition was done at 700°C for 1 – 60 min.

Five 1 cm long samples were cut from different locations at equal distances from the tubing inlet. The first sample was about 1-2 cm from the front of the tubing, which was subjected to CVD in the hot zone of furnace. The subsequent samples were about 10

cm away from each other. Then the samples were cut open to expose the inside surface and analyzed by Leo 1530 VP (Carl Zeiss SMT AG Company, Oberkochen, Germany) field emission-scanning electron microscope. Selected samples were also examined by transmission electron micrsocopy (TEM) using a Leo 922 Omega EF-TEM.

4.3 Results and Discussion

4.3.1 Stainless Steel Tubings

4.3.1.1 Ethylene. The bulk metal (iron) appeared to provide the dominant catalytic activity leading to MWNTs and amorphous carbon formation. The differences in the composition of 304 and 316 stainless steel and CVD morphology obtained is presented in detail in chapter 5. 304 stainless steel tube resulted in only patches of MWNTs after a 30 min CVD. However, after a 1 hr CVD the entire tube was covered with a film of CNTs of about 4 – 8 μm thickness and with diameters ranging from 30 -80 nm, interspersed with large amounts of amorphous carbon. On the other hand, 316 steel tube exhibited profuse surface coverage of MWNTs and amorphous carbon at a mere 1 min CVD duration. The thickness of the CNT coating was between 4 – 8 μm. In contrast to SS 304, the amorphous carbon in 316 steel tube occured as an overcoat rather than on the surface. The diameters of the nanotubes varied widely from 30 – 100 nm. The difference in the thickness of the MWNT coating and morphology on these two types of steel tubings may be attributed to the difference in their chemical composition, their physical characteristics and their grain boundaries. Type 316 stainless steel is known to contain higher molybdenum and nickel and lower concentrations of chromium than 304 steel. Larger

diameters and growth density of the CNTs in 316 stainless steel may also be attributed to the higher rate of diffusion of carbon into its soft body.

4.3.1.2 CO . When CO was used as the CVD precursor for 316 steel tubings, the surface as shown by the SEM image in Figure 4.1 revealed nanotubes with diameters ranging from 50 to 180 μm. The nanotubes showed nodes over its entire surface unlike the relatively smoother surface of the CNT obtained with ethylene. The surface coverage and the thickness of the CVD coating as measured from the SEM images is shown in Table 4.1. The CVD thickness decreases along the length of tubing and was about ten

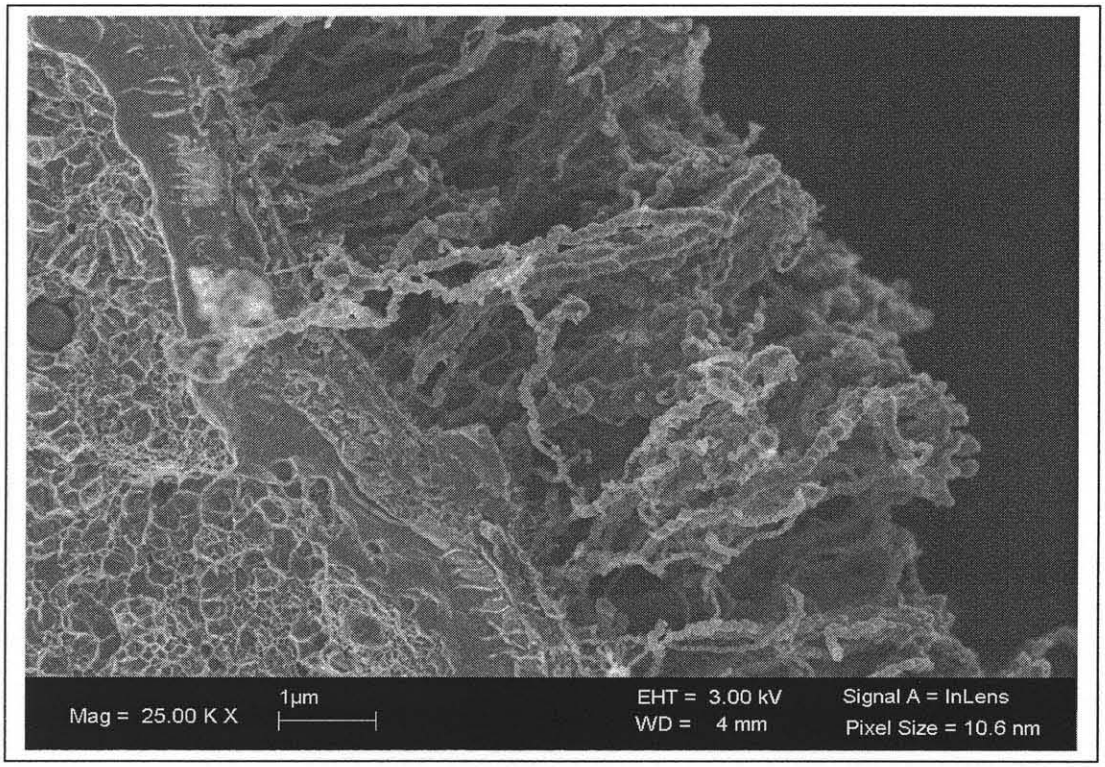

Figure 4.1 SEM image of the CNTs with nodes over its surface obtained with CO as CVD precursor on 316 stainless steel tubing. CVD conditions: surface conditioning at 700°C, CVD at 800°C for 30 min at 20 sccm flow.

Table 4.1 Thickness of the CVD Coating at 5, 30 and 60 min Durations Obtained with CO as Precursor at 20 sccm Flowrate, 800°C and Surface Conditioning at 700°C Inside 316 Steel Tubing

CVD-Time (mins)	CVD Precursor	Thickness (cm) of CO CVD coating along the length in the inside of Stainless Steel tubing (μm)				
		5	12.5	25	35	45
5	CO	0	0	0	0	0
30	CO	4 - 5	1 - 2	6 - 7	2 - 3	1 - 2
60	CO	25 – 30	10 – 15	8 – 12	2 – 4	1 - 2

times less compared to what was obtained with ethylene. The decrease in thickness and surface coverage could be due to the presence of a single carbon atom in the carbonmonoxide molecule relative to the two carbon atoms in the ethylene molecule available during decomposition. The CNT layer did not have a thick overcoat of amorphous carbon as obtained with ethylene. The density of the CNT's was higher in the first half of the metal tubing relative to the second half.

4.3.1.3 Ethanol. Figure 4.2 shows the SEM images obtained with ethanol as the carbon source during the CVD process. The morphology of the CVD products revealed nanotubes interspersed with higher amount of amorphous carbon relative to ethylene and CO. The density of CNTs were similar to that obtained with ethylene as precursor. This could be due to the presence of same number of carbon atoms available in ethylene and ethanol. Based on Raman spectroscopy the CNTs mostly appeared to be multi-walled. However, at higher magnification the CVD coating revealed some CNT's of 1-10 nm diameter as an overcoat over the rest. There is a possibility that these small diameter CNTs are single walled, but did not show up in Raman spectroscopy. This could be due

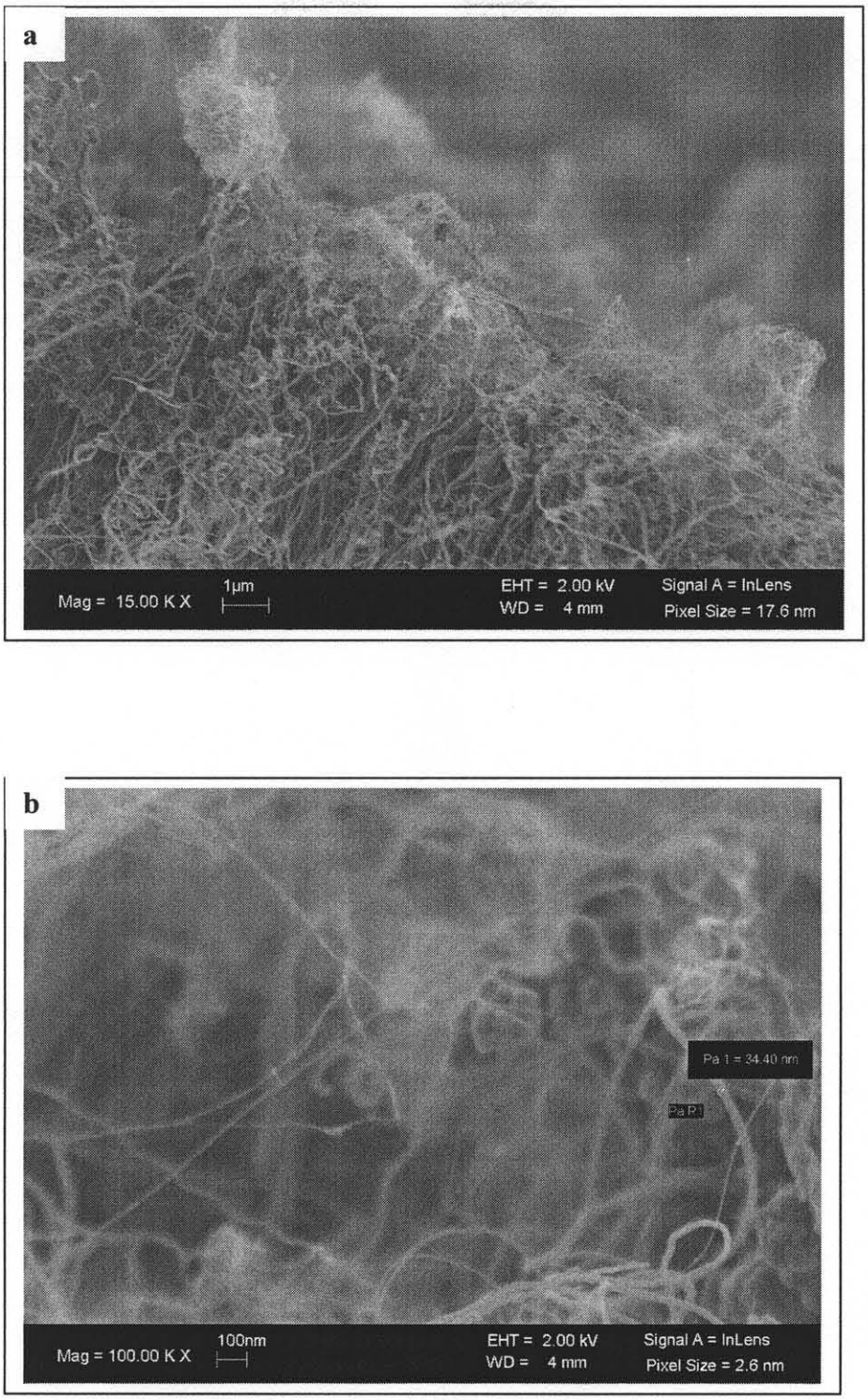

Figure 4.2 SEM images of the CVD coating with Ethanol as CVD precursor. a) Overcoat of low diameter CNTs over the CVD coating b) the same image at high magnification.

Table 4.2 Thickness of the CVD Coating at 5, 15 and 30 min Durations Obtained by Bubbling Argon into Ethanol. Conditions: 20 sccm Flow Rate, 800°C and Surface Conditioning at 700°C

CVD-Time (min)	CVD Precursor	Thickness (cm) of Ethanol CVD coating along the length in the inside of Stainless Steel tubing (μm)				
		5	12.5	25	35	45
5	EtOH	20 - 30	5 - 10	0	0	0
15	EtOH	100 - 120	3 - 5	0	0	0
30	EtOH	200 – 220	65 – 85	15 – 20	2 – 4	1 - 2

to their presence in very small percentages, or the failure to scan the Raman probe over its exact spot. Table 4.2 shows the thickness and the surface coverage of the CVD coating at 5, 15 and 30 min CVD duration.

4.3.2 Silica Lined Stainless Steel Tubing

4.3.2.1 Ethylene. When ethylene was used as the CVD precursor, at 35 min CVD duration, the slices of the silicosteel tubing revealed small specks of black coating over its surface. The SEM images from the slices did not show the presence of any nanotubes. The images revealed a sparse surface coverage of amorphous carbon structures.

4.3.2.2 Bubbling CO into Ethanol. When mixtures of CO and ethanol were used as CVD precursors (by bubbling CO into ethanol), a single layer of nanotube like structures of about 30 – 40 nm in diameter at the base, which taper slightly at the apex to about 10 nm diameter, were self-assembled as seen in the SEM images in Figure 4.3. The SEM images along the length of the tube revealed that these structures were present

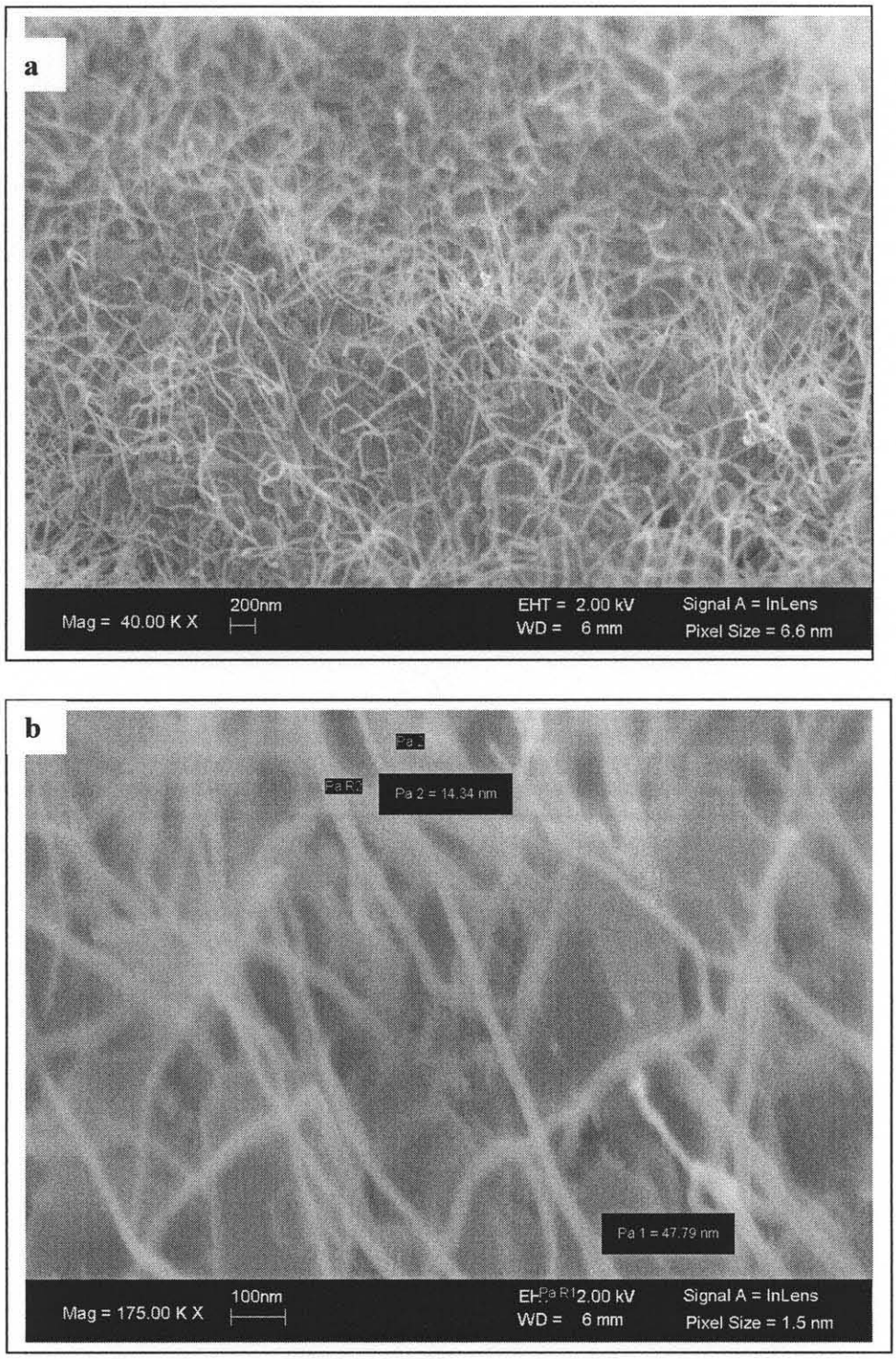

Figure 4.3 SEM images showing the a) morphology of the CVD coating obtained by bubbling CO into ethanol onto silcosteel substrate b) the same image at high magnification.

vertically aligned only towards the middle or end sections of the tubing. The length of the section that they would be seen could be as long as about 25 cm. In the other sections of the tubing these structures were interspersed with some amorphous carbon and lacked any preferential direction of growth.

The presence of a silica layer on the steel restricted the formation of any active sites and prevented any direct interaction of the metal with the carbon generated during the CVD process. This explains the lack of CNT's during the CVD of ethylene. However some nanotubes were visible on the silcosteel surface when either ethanol or ethanol/CO mixture was used as the carbon source. However, the surface coverage was not dense. At present it is not clear as to what catalyzed the formation of nanotubes in this case. There could be an interplay of various intermediates and kinetics of decomposition of the precursor along with some kind of surface interaction with the substrate. Also, it is not possible to rule out any diffusion of metal through the silica coating at the high temperatures during the CVD process.

4.3.3 Nickel Tubing

When ethylene was used as a precursor during the CVD inside the nickel tubing, no products were formed at 5 min CVD duration as observed from the SEM images. After a 45 min CVD, black carbon deposits were seen on the surface of the first two sections of the tubing with naked eye and a sparse coverage was seen on the third section under SEM. The thickness of the deposit varied over the length. The density and growth of the nanotubes appeared sporadic as shown in the Figure 4.4a. The SEM image as shown in Figure 4.4b reveals bulb like structures, scattered on the tube surface. The thick exterior

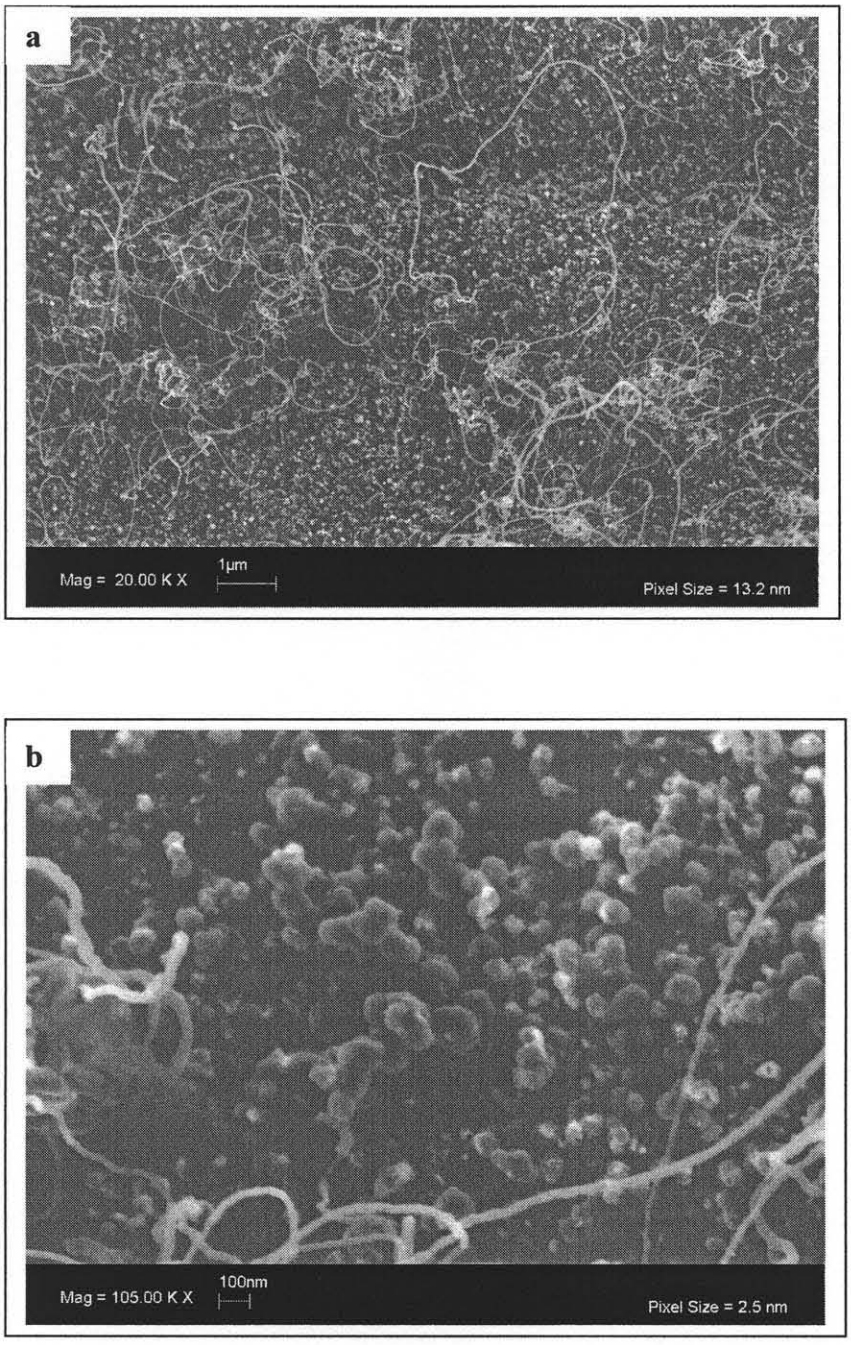

Figure 4.4 SEM images of the CVD coating with ethylene as CVD precursor on nickel tubing showing the a) sparse coverage of nanotubes b) bulb like structures on the surface.

of the cross sections of the tubing prevented in estimating the thickness of the CVD coating on the surface of the nickel tubing under SEM.

Catalysis is an important phenomena and the rate of catalysis varies with different catalysts. The evidence of a good coating of nanotube film just at 1 min CVD time with stainless steel supports the fact that Fe acts as a good catalyzer and accelerates the graphitic product formation thus exhibiting high affinity for carbon. The sparse surface coverage of carbon on nickel tubing even until 1hour of CVD time suggests that the rate of catalysis by Ni substrates is relatively very less and it has weak affinity for carbon.

4.3.4 Inconel Tubing

Inconel is an alloy of nickel containing about 66% nickel, 20% chromium, 8% molybdenum and 1-2% of other metals such as, cobalt, iron, etc. When subjected to the CVD process, this tubing showed higher percentages of CNT's from ethylene relative to the nickel tubing shown in Figure 4.5. After 45 min CVD, at about 12 sccm flow of ethylene a 2 – 3 μm thick CNT film was formed. The density and surface coverage of nanotubes obtained here is almost comparable to when ethylene was used as CVD precursor on 316 stainless steel substrates. Although the rate of catalysis is still lesser, relative to iron in steel.

When ethanol was used as a carbon source, the surface revealed circular hollow tube like structures as shown in the SEM image at high magnification in Figure 4.5b.

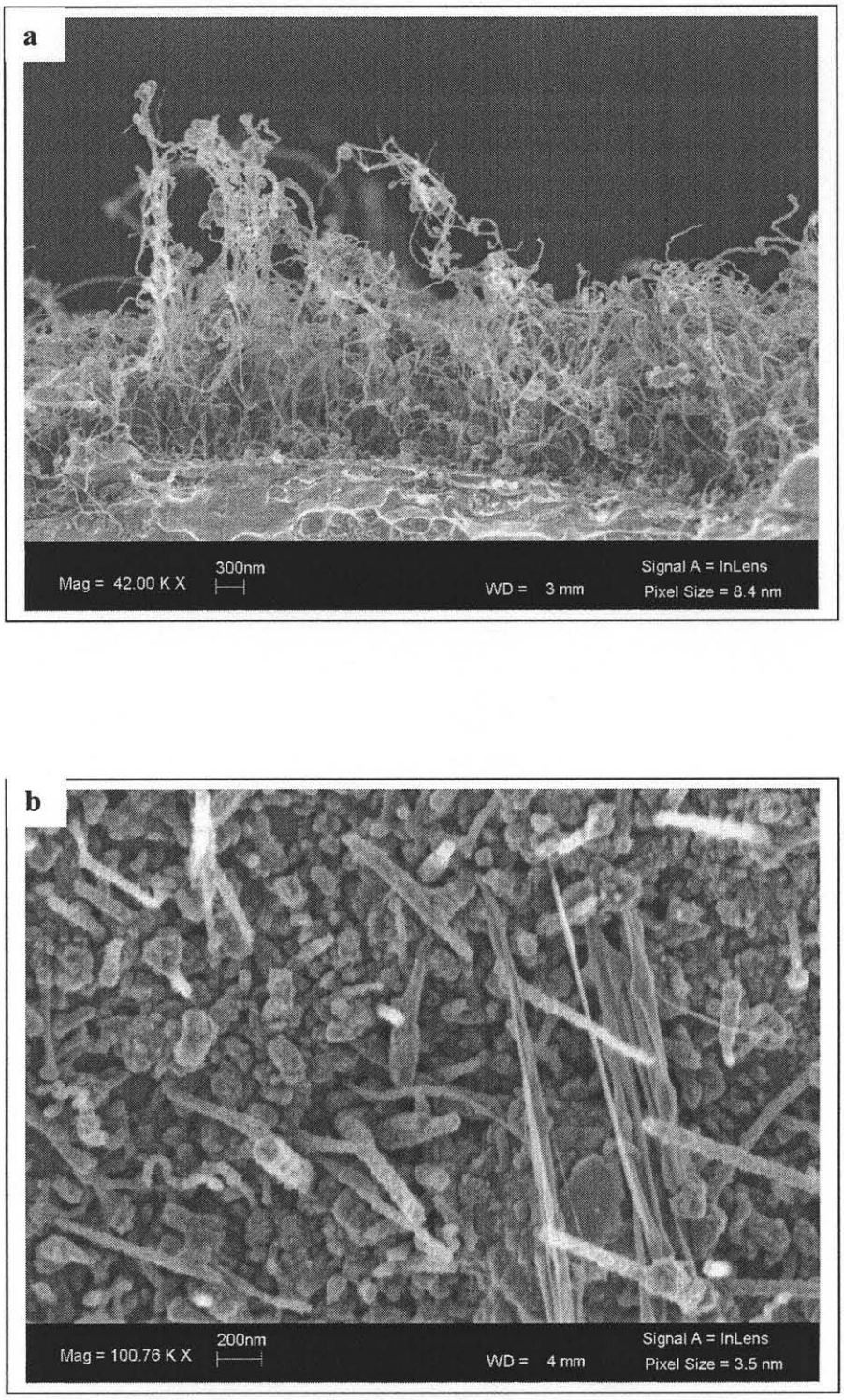

Figure 4.5 SEM images of the CVD coating on inconel tubing obtained with a) ethylene as carbon source and b) ethanol as carbon source.

4.3.5 Use of an External Catalyst

In the above mentioned CVD approaches, the catalyst for the CVD process was generated from the tube substrate. Stainless steel tubings provide iron as the catalyst, nickel tubings provided nickel and inconel tubings contained nickel, chromium and molybdenum chiefly. Active sites were generated during the surface conditioning, which catalyzed the formation of carbon nanotubes during the CVD process.

Apart from the above catalytic CVD approaches, several other methods were attempted, where the catalyst was supplied externally in the inside of steel and silica lined steel tubings. These include, aerosol spray of ferrocene or iron pentacarbonyl, electrodeposition of cobalt, vapor deposition or dip coating of aqueous solutions containing salts of cobalt and molybdenum aqueous solutions, dip coating and aerosol spray of cobalt and molybdenum salts impregnated with poly vinylalcohol (PVA) based polymer.

The stainless steel tubings were coated in the inside by an aerosol spray of certain organometallic catalysts, such as, ethanolic solution of ferrocene (2% weight), or iron pentacarbonyl ($Fe(CO)_5$). The catalysts, about 50 µl volume was injected 2 - 3 times through a T device into the capillary tubing at 700°C. After which, the CVD was performed with CO at a pressure of 115 psi for 30 min at the same temperature. The SEM images of the steel tubings from ferrocene did not reveal any carbon nanotubes. The morphology of the CVD product is presented in Figure 4.6a and is suspected to be of some kind of metallic carbide. The steel tubings from $Fe(CO)_5$ did reveal a sparse coverage of nanotubes as shown in Figure 4.6b interspersed with little amorphous carbon but with catalyst particles of defined shape and features.

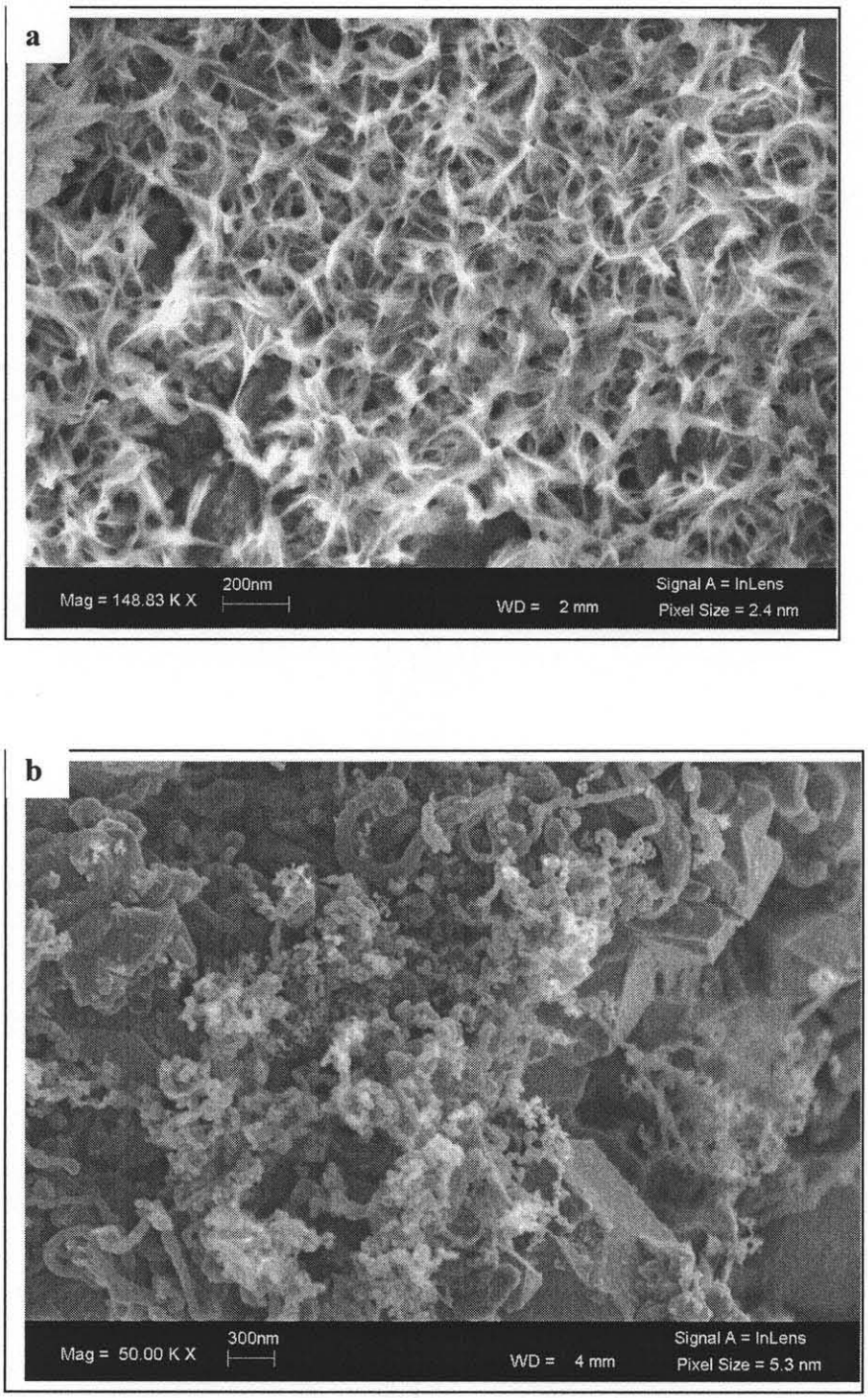

Figure 4.6 SEM images of the morphology of the CVD coating from a) ethanolic solution of ferrocene (2% weight) b) iron pentacarbonyl ($Fe(CO)_5$.

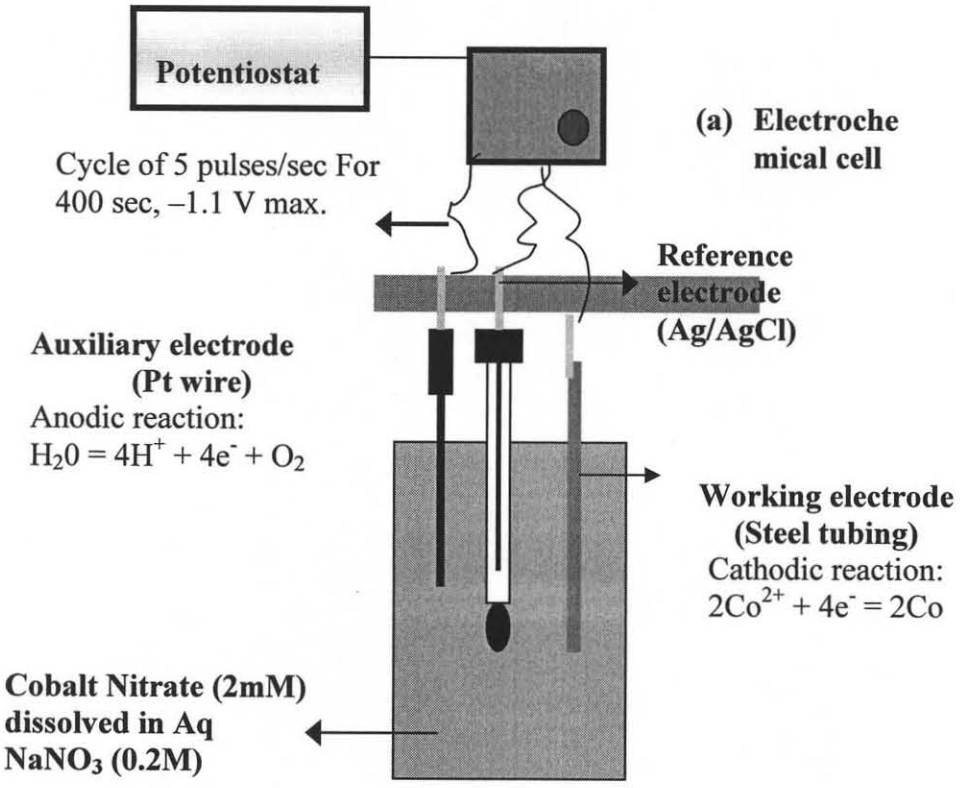

Figure 4.7 Set up of the electrochemical deposition scheme.

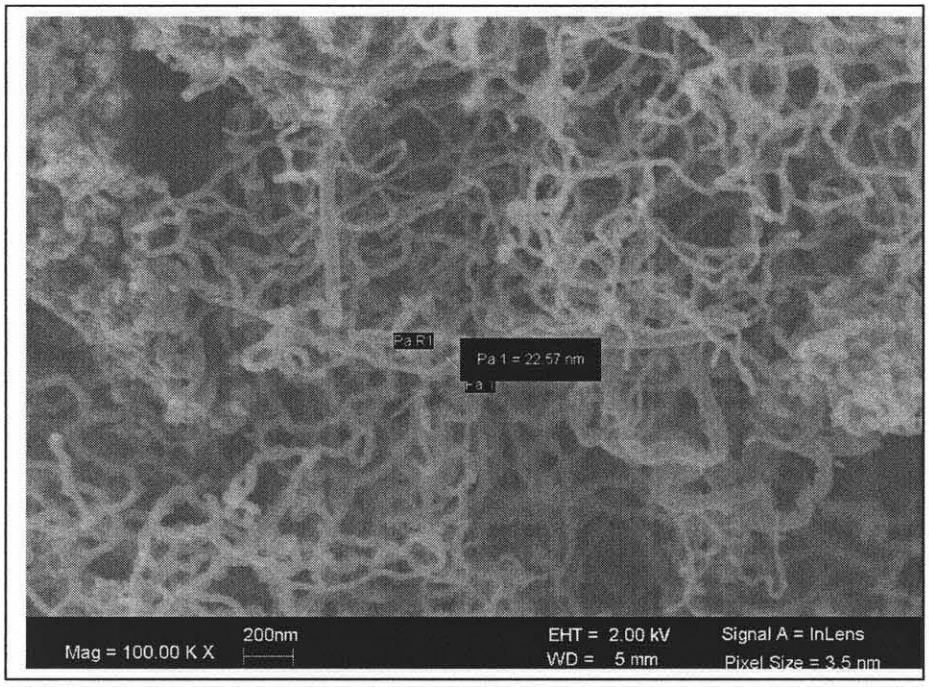

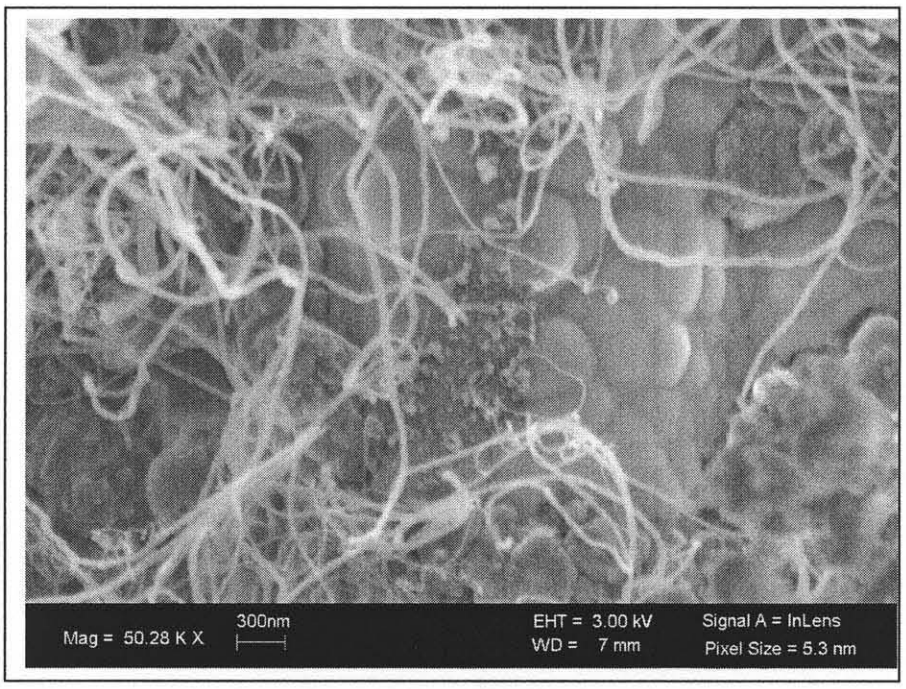

Figure 4.8 SEM images of the carbon nanotubes obtained from the ethanolic polymer solution (poly vinyalchohol) containing cobalt and molybdenum salts.

Among the several approaches mentioned above, the electrodeposition, the dip coating and the vapor deposition of cobalt and molybdenum salts did not affect the morphology of the CVD products significantly as seen from the SEM images. A schematic of the electrodeposition setup used for coating cobalt catalyst is presented in Figure 4.7.

Silica lined steel capillary tubings were dip-coated overnight with 0.9% of ethanolic PVA solution containing 4% cobalt nitrate and 2% ammonium molybdate. The tubing was then subjected to surface conditioning so that the polymer would be oxidized leaving the metal particles behind. The metal was then activated by reduction in the presence of hydrogen. The above solution was diluted to 10% and injected through the "T" connector at a flow rate of 0.1 ml / min for 15 min and was used a CVD precursor. SEM images revealed a non-uniform surface coating of carbon nanotubes consisting predominantly of about 20 - 30 diameter as shown in Figure 4.8. The thickness of the coating varied from 6 μm at few sections to about 250 nm.

4.4 Conclusions

On assessment of the SEM images, the percentage, surface coverage, and uniformity of the carbon nanotubes obtained with ethylene, as a CVD precursor was more than that obtained with ethanol and CO. Ethylene yielded complete surface coverage of CNT's over the entire length of the 316 steel tubing at just 1 min CVD time while CO and ethanol required 30mins for the same. In general, compared to the stainless steel tubings, the Nickel tubings required relatively higher CVD time to grow nanotubes on its surface. The quality of the CVD products as seen from the SEM images was not as good as that

obtained with stainless steel substrates. Among the 316 and 304 stainless steel substrates that were tried, the 316 stainless steel exhibited profuse coverage of nanotubes in just 1 min CVD duration. While, the 304 steel tubing required about 1 hr for the same. The SEM images have shown that, the silicosteel tubing showed complete absence of CNT's when ethylene was used as a carbon source. However the surface coverage was better when mixtures of ethanol and CO were used as precursors. Although the density of CNT's was relatively less than that found on stainless steel substrates.

The surface coverage and morphology of the CVD coating with diverse substrates, precursors and catalysts is presented in the table below. None of the approaches led to the growth of SWCNTs.

Table 4.3 Compilation of the Surface Coverage with Various Substrates, Precursors and Catalysts

Catalyst / Substrate	Precursor	Comment
316 Stainless Steel (Fe)	Ethylene	MWNTs, Good coverage and density in short duration
	Ethanol	MWNTs interspersed with higher amount of carbon
	CO	MWNTs with nodes, requires relatively long time for coverage, diameter of CNTs wide
304 Stainless Steel (Fe)		Same morphology as above but requires more time for CVD for any surface coverage to be seen
Silica lined Steel	Ethylene	No surface coverage at all
	CO+Ethanol	MWNTs, Sparse coverage, diameter of CNTs smaller
Nickel	Ethylene	Sparse coverage, bulb like structures, requires long time
Inconel	Ethylene	MWNTs, good coverage & density.
	Ethanol	Circular hollow tube like structures, density less
Ferrocene	CO	No CNTs
$Fe(CO_5)$	CO	MWNTs, wide diameter, Not uniform coverage
Electrodeposited Cobalt	Ethylene	No significant variation in growth
Ethanolic PVA + Co+Mo	Ethanol	MWNTs, 20-30 nm diameter, non uniform coverage

CHAPTER 5

SCALED-UP, ONE STEP SELECTIVE SELF-ASSEMBLY OF SINGLE WALLED CARBON NANOTUBES IN A STEEL CAPILLARY TUBE

5.1 Introduction

Ever since their discovery, single walled carbon nanotubes (SWCNTs) have attracted the attention of the scientific community since they possess unique physical, chemical, and, electronic properties [122-124]. The SWCNTs are generally synthesized by arc discharge [125], laser ablation [126] or chemical vapor deposition (CVD). However, CVD is the method of choice when it comes to the self-assembly of CNTs over micro or macro structures [127-130]. Typical catalytic CVD involves the thermal pyrolysis of a precursor in the presence of transition metal nanoparticles, such as, Fe, Ni, and Co, which are known to act as catalysts [128] in the synthesis of SWCNTs. An important requirement for the growth of SWCNTs is the nano-structuring of the catalyst because the diameter of the CNTs is commensurate with the diameters of the catalyst nanoparticles [131]. A wide range of precursors such as CO, hydrocarbons, alcohols, and ketones have been used to grow SWCNTs. Alcohols have shown some selectivity towards SWCNT formation and it has been hypothesized [132] that the OH radical formed at high temperatures oxidizes and therefore etches away the amorphous carbon impurity phase formed during nanotube growth.

It has been shown that substrate characteristics [133], such as porosity, crystallinity, and surface roughness, in addition to the choice of precursor, CVD conditions, and the catalyst influences the growth of single and multiple walled nanotubes. Optimizing so many variables is a challenging task, and limited understanding

of these effects has undermined efforts to fabricate larger scale real world nanotube-based devices. However, for chromatographic applications, which would benefit from the high surface area and nanoscale adsorption properties of SWCNTs, large area self- assembly of the type investigated here would be required.

SWCNT synthesis via CVD is typically a two-step process. The first step involves the coating of the substrate (typically Si or quartz) with a catalyst, or the metal impregnation of a catalyst support, e.g., silica, MgO, zeolites, and aerogels [128]. Subsequent heat treatment leads to the formation of metal nano-particles. Catalyst coatings have been deposited by spin coating [134], dip coating [135], sputtering [136], and sol-gel techniques [137] or by merely placing the supported catalyst particles in a ceramic or quartz boat. Ago et al. [138] have reported gas phase catalytic synthesis of SWCNTs using a reverse micelle solution containing Co-Mo nanoparticles. After catalyst deposition, the CVD synthesis of CNTs is carried out; thus involving two distinct processes. However, from the stand-point of process scale up, a single step process that combines catalyst deposition / preparation and CVD synthesis is preferred. Single step processes have, however, been less commonly used. One such method is the floating catalyst [139] based CVD method, where a volatile organometallic precursor, such as ferrocene is typically used to generate the catalyst particles during SWCNT growth.

Self-assembly of SWCNTs has been limited to substrates such as, silicon, quartz, aerogels of silica or alumina of relatively small dimensions mainly used as field emitting devices [140], tips for scanning probe microscopy SPM) [141], and as gas sensing devices [142]. Self-assembly of MWCNTs has been reported on a stainless steel mesh [143]. Recently the self-assembly of MWCNTs inside steel tubings for preconcentration

[129] and gas chromatography [144] has been reported. The scaling up of the self-assembly process on larger structures, such as a long metal capillary tubing is relatively more complex, especially for SWCNTs. Several challenges face such an operation; these include the deposition of an uniform nano-sized catalyst, controlling the kinetics of the growth process, and selectively growing SWCNTs while avoiding the growth of MWCNTs and amorphous carbon. Also, SWCNT synthesis is a substrate specific process [133], which means the methods need to be tested and optimized if substrates are different. High pressure carbon monoxide (HiPCO) [145] and floating catalyst based CVD methods, which have succeeded in selectively synthesizing SWCNTs require temperatures above 1000°C which are likely to melt metal substrates. This paper reports the development of a one-step process for the self-assembly of SWCNTs in a long capillary tube, which can be then used for chromatographic separation applications. It involves the aerosol spraying of an ethanolic solution (where ethanol is the carbon precursor) containing cobalt and molybdenum salts as metal catalyst and co-catalyst precursors, respectively. The catalyst and co-catalyst metal particles are generated and activated in-situ, along with the synthesis of the SWCNTs. Thus, the separate coating of the substrate with catalyst prior to SWCNT synthesis is not required. The entire operation takes about 15 minutes for completion, is easy to scale up, and is economical.

5.2 Experimental

Cobalt nitrate hexahydrate, $Co(NO_3)_2.6H_2O$ and Molybdenum acetate, $(CH_3COOH)_2Mo$ were dissolved in ethanol at 0.2 wt% and 0.05 wt% concentrations respectively. The dissolution process was assisted by sonication. The CVD system is shown in Figure 5.1.

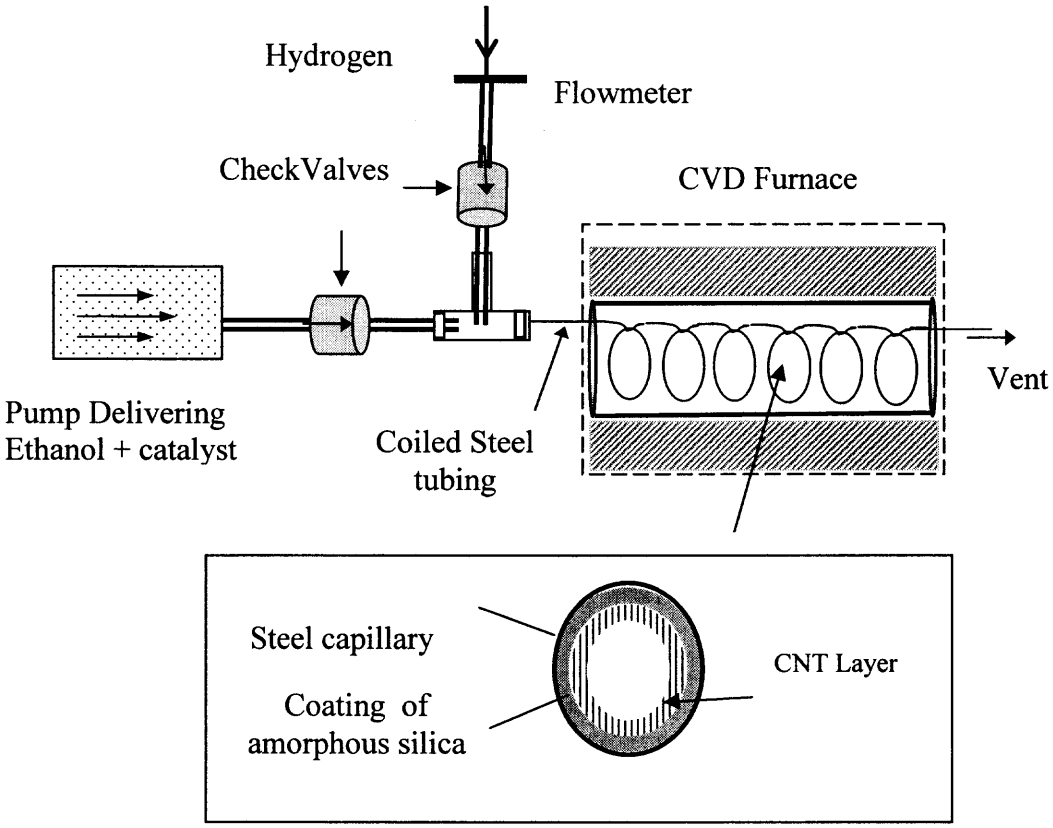

Figure 5.1 Setup of the Vapor Phase Catalytic Synthesis of SWCNTs. The figure inset shows the inside of the steel tubing.

The ethanol solution containing the dissolved catalyst acetate precursors was injected into the capillary metal tubing using a HPLC pump (Waters, Model 501). Typical flow rate of the solution was 100 μl/min. Hydrogen was simultaneously introduced into the steel tubing through a three way connector. The typical hydrogen flow rate was 40 cm^3/min. Check valves (R.S.Crum & Co. Mountainside, NJ) were placed on both lines to restrict back-flow. The CVD was performed typically for about 10 min. Since the substrate plays an important role, different tubing materials including 304, 316 stainless steel (Alltech, Deerfield, IL) and silica lined tubings, such as, Silcosteel™, and Sulfinert™ (Restek, Bellefonte, PA) were tested. The tubes were 1 meter long, with a 0.53 mm ID. Prior to CVD, the tubes were washed with ethanol and allowed to dry.

To study the CNT formation, one cm long segments were cut from the steel tube at five equidistant locations. The samples were cut open to expose the inside surface, and were analyzed by Leo 1530 VP (Carl Zeiss SMT AG Company, Oberkochen, Germany) field emission-scanning electron microscope. The distribution, surface coverage, and the thickness of the SWNT coating were studied based on the SEM images. Selected samples were also examined by transmission electron microscopy (TEM) using a Leo 922 Omega EF-TEM. The presence of SWNTs was confirmed by Raman Spectroscopy performed at 632.8 nm excitation using a Jubin-Yvon / Horiba confocal micro-Raman system.

5.3 Results and Discussion

Nanostructured iron was generated in-situ on the steel tubing by oxidation with O_2 followed by reduction with H_2. This process has been described in detail in previous publications [130, 144]. However the process generated only MWCNTs, no SWCNTs

could be detected by Raman measurements. While ethylene as carbon precursor resulted in excellent MWCNT growth and good surface coverage, similar growth of SWCNTs was not achieved with ethanol, which showed large amounts of amorphous carbon as shown in Figure 5.2a. In the absence of surface conditioning, the nanotubes were interspersed with larger amounts of amorphous carbon.

Co and Mo salts dissolved in ethanol were aerosolized in the presence of H_2 in the steel tubing. It was expected that nano-scale Co and Mo would result in SWCNT formation. When CNT formation inside the tube was observed by SEM, some nanotubes had small enough diameters (7–10 nm) that SWCNT formation was suspected. However, none could be detected by Raman spectroscopy. The bulk metal (iron) appeared to provide the dominant catalytic activity leading to MWCNTs and amorphous carbon formation. Type 304 stainless steel tube resulted in only patches of MWCNTs after a 10 min CVD as shown in Figure 5.2b. However, after a 45 min CVD the entire tube was covered with CNTs with diameters ranging from 10-30 nm, interspersed with large amounts of amorphous carbon. On the other hand, 316 steel tubing exhibited profuse surface coverage of MWNTs and amorphous carbon even after 10 minutes of CVD as shown in Figure 5.2c. The diameters of the nanotubes varied widely from 20 – 120 nm. The difference in MWNT formation and morphology on these two types of steel tubings may be attributed to the difference in their chemical composition, their physical characteristics and their grain boundaries. Type 316 stainless steel is known to contain higher molybdenum and nickel and lower concentrations of chromium than 304 steel. Larger diameters and growth density of the CNTs in 316 stainless steel may also be due to the higher rate of diffusion of carbon into its soft body.

a

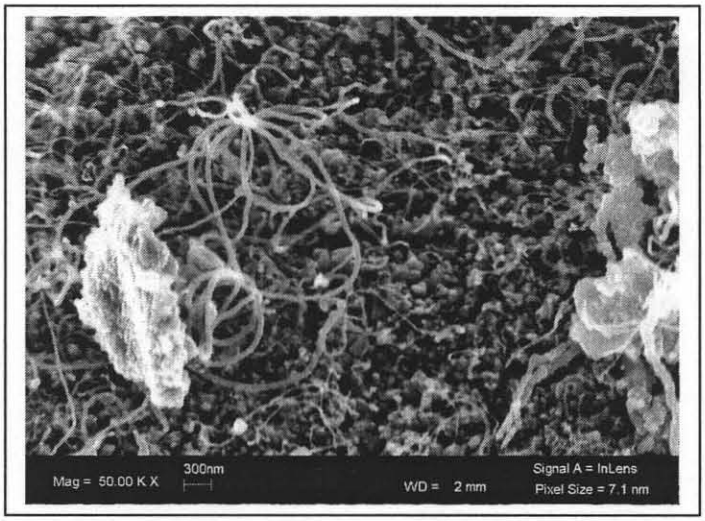

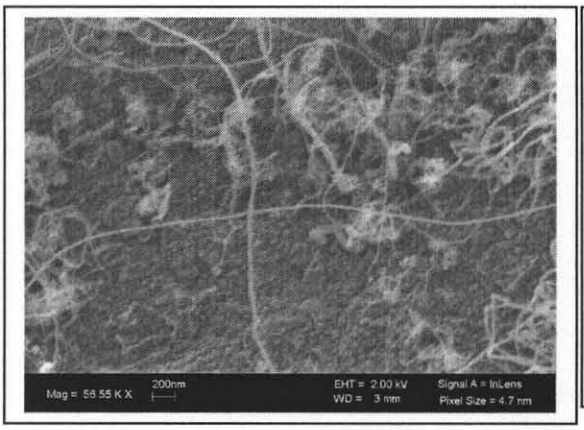

b

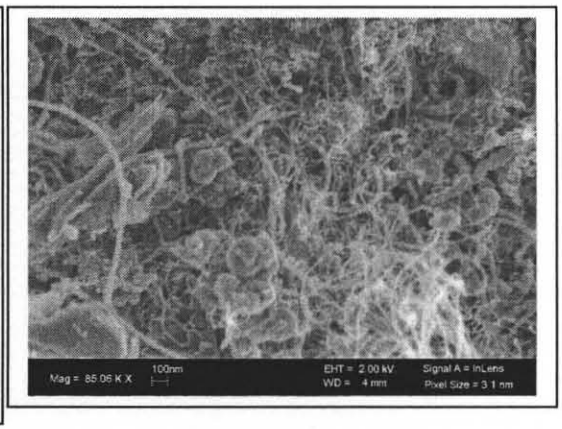

c

Figure 5.2 SEM images a) CVD morphology (30 mins) with Fe inside bulk steel (304) as catalyst b) typical 10 min CVD growth on 304 steel surface with Co & Mo catalysts, c) typical 10 min CVD growth on 316 steel surface with Co & Mo catalysts.

The strategy for selective SWCNT growth required the prevention of iron from catalyzing MWCNT growth. Although the HiPCO process, which is carried out at temperatures above 1000°C, uses iron as catalyst to form SWCNTs, it is possible that at 725 °C iron results in the formation of MWCNTs [128]. Consequently silica lined stainless steel tubings, such as silcosteel™ and sulfinert™ were selected. These tubular substrates contained 1.0 – 1.4 μm thick amorphous silica coating on the metal surface which would provide a barrier to interaction of the carbon with iron during the CVD process. Catalyst for the SWCNT growth therefore needed and was dispersed uniformly along the length of the tubing. The SEM images showed that during high temperature CVD, the silica coating develops small cracks, thus increasing the surface area and roughness. These appear to provide sites for catalyst deposition. The nano-structured metal catalyst was generated in-situ during the CVD process. The metal salt catalyst precursors were dissolved in ethanol. The pumped solution in conjunction with flowing hydrogen created an ethanol-catalyst precursor aerosol inside the tube. At high temperature (725 °C), the solution vaporized and distributed the catalyst along the whole length. The Co-nitrate precursor broke down to form Co nano-particles that were activated in the reducing H_2 environment. The metal then catalyzed SWCNT growth with ethanol serving as the carbon source. In order to study the morphology of the catalyst particles formed on the surface of the substrates, an aqueous catalyst solution was sprayed into the steel tubing in the presence of argon, while the other CVD conditions remained unchanged. It was difficult to see the dispersed catalyst on the rough surface of the silica-lined steel tube, consequently the steel tube was used in this study. Figure 5.3a shows an SEM image of the catalyst deposition on the steel tube substrate. The images

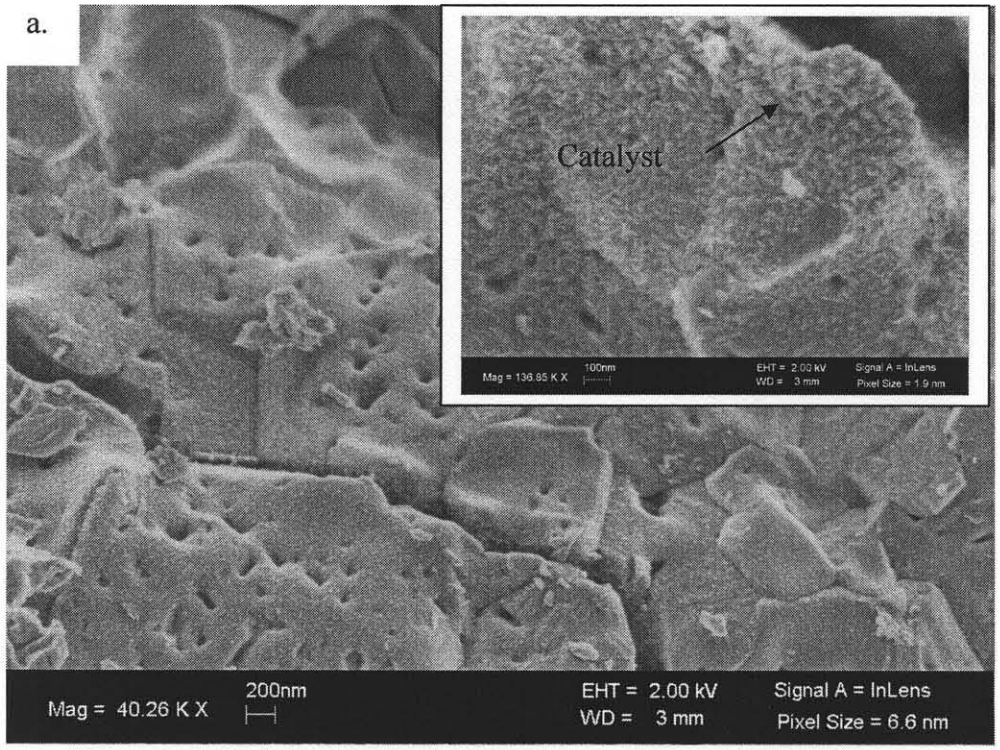

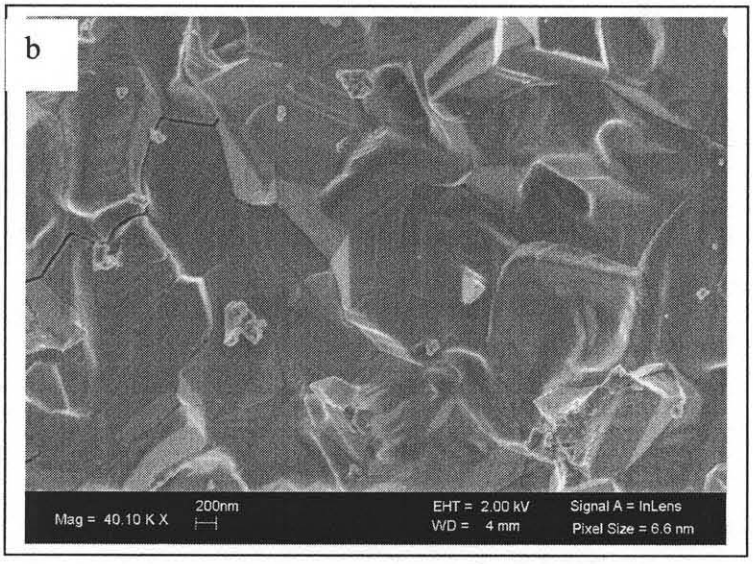

Figure 5.3 SEM images showing a) the dispersed catalyst layer on the steel surface. The image in the inset shows a magnified view of the catalyst. b) the surface of steel without any catalyst.

indicate that the catalyst layer was finely dispersed with a typical particle size around 1 nm, with some as large as 10 – 15 nm. The SEM images indicated that the latter half of the tubing had a slightly denser catalyst layer. An SEM image of the steel surface pretreated at the same temperature with only water (without the catalyst) is also presented in Figure 5.3b which provides a baseline for studying catalyst deposition.

The SEM images of the silica lined tube sections along the length of the tube revealed a randomly distributed, layer of thin SWCNT film on the inside wall as shown in Figure 5.4. The surface coverage along the length varied, with the mid-section having a higher density of nanotubes and a thicker film. This trend could be due to the ends of the tube being relatively cooler than the midsections or due to the kinetics of nanotube formation. The variation in film thickness is presented in Table5.1.

The catalytic metal particles on the substrate and on the SWCNTs were detected using energy dispersive X-ray (EDX) analysis operated at 7 kV and at a scan time of 1000 sec. The EDX profile as shown in Figure 5.5a indicates the presence of cobalt and molybdenum catalyst. The signal intensity for molybdenum was significantly lower than for cobalt in line with their concentrations in the solution. The presence of SWCNTs was confirmed by Raman spectroscopy on all the sections of the tubing. Multiple tubes were analyzed to check reproducibility. The Raman spectrum is shown in Figure 5.5b, it showed the presence of the radial breathing mode (RBM) which is a characteristic of the SWCNTs.

Based on the characteristic peaks at wave numbers of190, 217, 221, 248 and 287 cm^{-1} the SWCNT diameters were computed as $d = 248 / \omega_{RBM}$, [146] where d is diameter and ω_{RBM} is Raman shift [147]. The diameters of the SWCNTs were found to be between

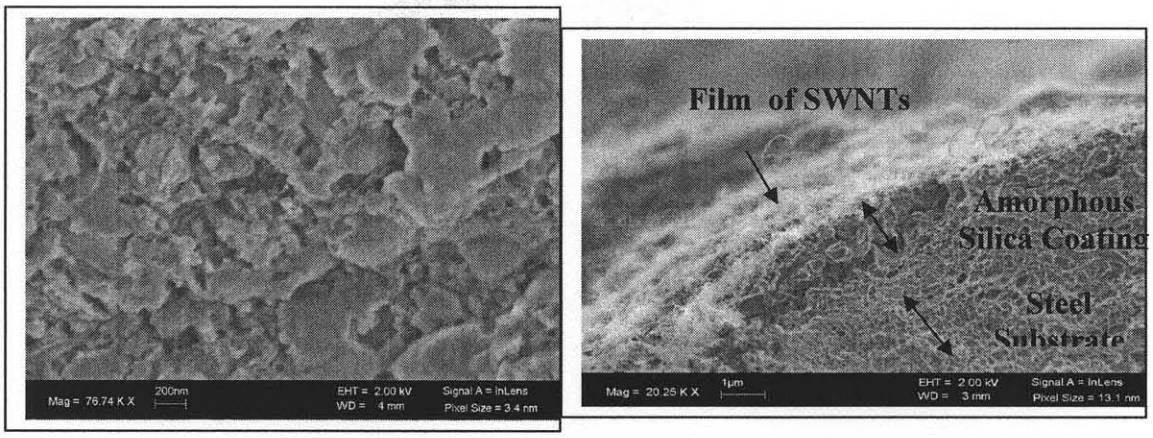

a. b

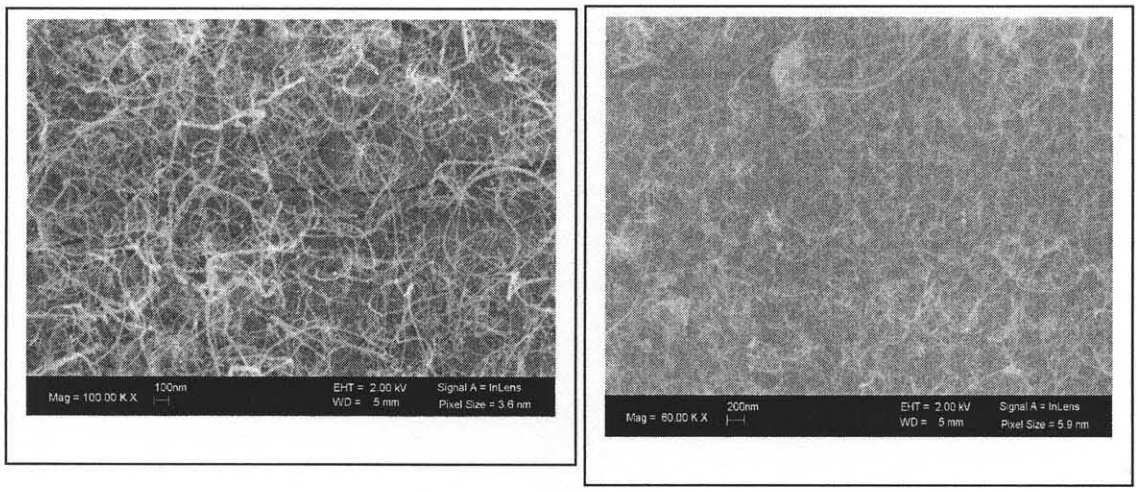

c d

Figure 5.4 SEM images showing a) the rough surface of the silcosteel™ b) the SWCNT film upon the silica lined steel substrate, c) & d) the randomly aligned SWCNTs.

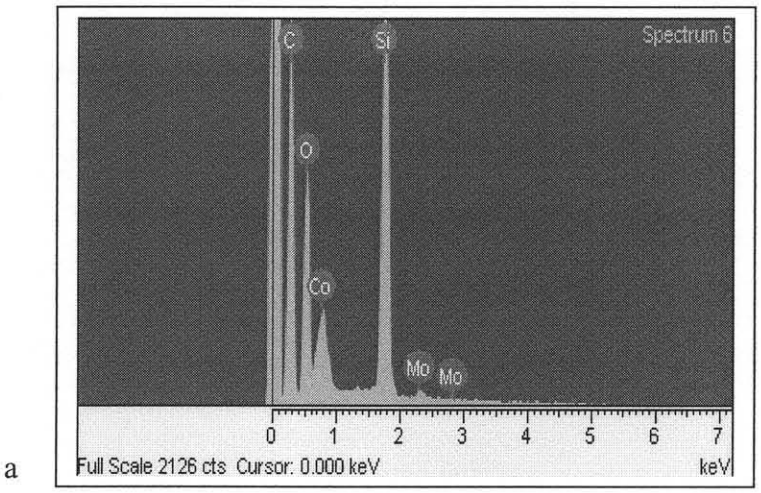

a

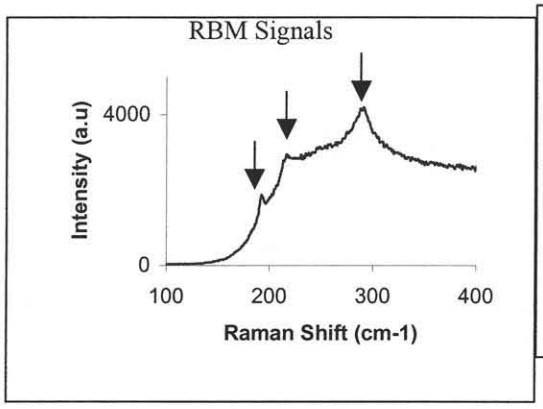

b.

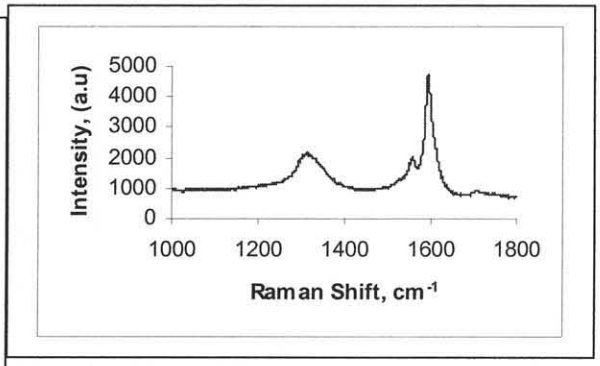

c

Figure 5.5 a) EDX Profile of the SWCNT coating inside the capillary tubing. The profile is marked with the important peaks which are expected and correspond to C(K), O(K), Si(K), Co(L), Mo(L) peaks respectively, b) The Raman spectrum showing the RBM signals characteristic of the SWNT growth, c) The Raman spectrum showing the D & G signals.

Table 5.1 Thickness (μm) Distribution of the SWCNT Coating Measured Along the 1 m Long Sulfinert Capillary Metal Tubing Subjected to Uniform Temperatures

Tubing Length (cm)	**2.5**	**12.5**	**25**	**37.5**	**50**	**62.5**	**75**
SWCNT coating Thickness (μm)	0.025 - 0.05	0.2 – 0.3	0.2 - 0.4	0.2 – 0.4	0.2 - 0.4	0.2 -0.3	0.025 - 0.05

0.87 and 1.3 nm. At higher wave numbers, all spectra showed two Raman bands at ~ 1320 cm^{-1} (D band) and ~ 1590 cm^{-1} (G band). The ratio of intensities of G band to D band over various sections along the length of the silica lined tubing varied form 1.85 to 0.75 suggesting the presence of CNTs with higher degree of crystallinity in some areas, and higher degree of disorder and defects at few other areas.

5.4 Conclusions

SWCNTs were self-assembled on the inside wall of a long silica coated stainless steel capillary tubing using a single step catalytic CVD process that is economical in time, effort and cost. To the best of our knowledge it is also for the first time that SWCNT self-assembly has been reported at such a scaled up level inside a capillary tube. The silica lining was critical to the formation of SWCNTs, while uncoated, plain stainless steel tubings mainly formed MWCNTs. The use of these tubular substrates in the growth of SWCNTs represents a novel idea because it demonstrates the use of traditional metal platforms for fabricating SWCNT based devices for a real-world application, such as gas chromatographic separation using carbon nanotubes.

CHAPTER 6

GAS CHROMATOGRAPHY ON SELF-ASSEMBLED SINGLE WALLED CARBON NANOTUBES

6.1 Introduction

In recent years, Carbon nanotubes (CNTs), have been the subject of intense research because of their unique electrical, mechanical, and chemical properties [148]. Carbon nanotubes are formed by rolling up layers of graphene sheets into hollow seamless cylinders of nano-scale diameters. They can be open or closed ended with several concentric shells as in multi-walled carbon nanotubes (MWCNTs) or single shelled as in single walled carbon nanotubes (SWCNTs). Due to their superior adsorption properties, CNTs have received special attention in specialized applications, such as, gas storage [149] and have recently been used in VOC's preconcentration [150], removal of chemical and toxic wastes from water [151], and gas chromatography [152]. The inner hollow cavity of CNTs, the outside surface, and the interstitial spaces between the nanotube bundles have been cited as possible sites that facilitate adsorption [153]. This provides unique opportunities for the development of higher performance separation techniques that utilize the nano-scale interactions on a material known to have high thermal and mechanical stability. The CNTs thus have the potential to extend the applicability of carbon-based sorbents in gas-solid chromatography (GSC) as a novel stationary phase.

GSC has evolved as a powerful analytical tool in the separation-analysis of gases and low boiling analytes. GSC columns utilize the sorption of the solute on a solid stationary phase as opposed to the partitioning in gas-liquid chromatography (GLC) as the dominant mechanism. The use of a solid sorbent film in place of a liquid stationary

phase may allow the magnitude of the mass transfer term to be reduced and there by allow high efficiency in gas-solid columns. Typical solid phases for gas chromatography (GC) include porous polymers (e.g. Porapak), silica, molecular sieves, and activated carbons. Their microporosity and large surface area (500 – 3000 m^2/g) are mainly responsible for the enhanced sorption capacity. Traditionally these solid phases are packed into a tube as in a packed column, although open tubular phases (PLOT columns) are also available. Many of these sorbents have an upper limit in operation temperatures of about 250 - 350°C, above which they begin to bleed.

Varied affinity and selectivity for a wide range of analytes may be possible with CNTs based upon their size, diameter, form (SWCNTs or MWCNTs), functionalization and film thickness. Two aspects of CNTs are important for chromatography, namely adsorption and fast desorption to achieve separation with in a reasonable time and at high resolutions. The physical / chemical affinity between the sorbate and the sorbent needs to be optimum for this to occur. Recent studies have evaluated MWCNTs as gas chromatographic stationary phase where they were packed into a tube [154], or self-assembled into a steel capillary in an open tubular format [152]. When packed as a powder, some of the nano-characteristics may be lost due to agglomeration, while in-situ self-assembly retains these features.

SWCNTs are extremely attractive as chromatography stationary phase because of large aspect ratio and higher surface area, as much higher chromatographic efficiencies may be realized. They are significantly smaller in diameter than MWCNTs and are known to possess properties that are quite different [155]. SWCNTs are generally synthesized by either laser ablation [156], catalytic arc discharge [157] and chemical

vapor deposition (CVD) [158-160]. However, CVD is most suited for direct deposition and the self-assembly on micro/macro structures. Recently we have reported the scaling up of MWNT self-assembly [161]. It is well known that SWCNT synthesis is significantly more complex [162-163], as MWCNTs and amorphous carbon tend to grow preferentially during such a process. Selective growth of SWCNTs requires precise preparation and laying down of transition metal catalyst such as, Ni, Co or Mo [164]. An additional requirement for the SWCNT growth is the presence of these catalyst particles in angstrom size [165].

The objective of this research was to scale-up SWCNT self-assembly via catalytic CVD to fabricate open tubular GC columns. Such large-scale assembly is being reported for the first time and required process and catalyst optimization. Gas chromatographic separation of various class of compounds was carried out, their chromatographic efficiencies and mass transfer behavior was investigated on this novel stationary phase. Capacity factors and isosteric heats of adsorption (ΔH_s) of few representative samples were calculated and compared with the packed Carbopack C^{TM} column. The polarity of the SWNT phase was determined from the McReynolds constants.

6.2 Experimental

6.2.1 Materials

Cobalt nitrate hexahydrate, Molybdenum acetate, ethanol, benzene, toluene, ethylbenzene, O-xylene, methylenechloride, carbontetrachloride, trichloroethylene, Methanol, ethanol, 2-propanol, 2-pentanone, methyl ethyl ketone, acetone, iso butyl butyrate, 95% n-hexane, heptane, octane, nonane, and decane were purchased from

Aldrich (Milwaukee, WI). The PAH mixture was obtained from Ultra scientific (North Kingstown, RI). All gases were zero grade and obtained from Matheson Tri-Gas (Montgomeryville, PA). The standard hydrocarbon mixture consisting of methane, ethane, propane, butane, pentane and hexane and the branched hydrocarbon standard mixture containing isobutane, 2,2-dimethylpropane, 2-methylbutane, 2,2-dimethylbutane, 2-methylpentane, 3-methylpentane were purchased from Scott speciality gases (Plumsteadville, PA).

6.2.2 Column Preparation

Cobalt nitrate hexahydrate, $Co(NO_3)_2.6H_2O$ and Molybdenum acetate, $(CH3COOH)_2Mo$ were dissolved in ethanol at 0.2 wt% and 0.05 wt% concentrations respectively. The dissolution process was assisted by sonication. The CVD system is shown in Figure 6.1a and was located in a fume hood. The ethanolic solution containing the catalyst in the dissolved form was injected into the capillary metal tubing using a HPLC pump (Waters, Model 501). Typical flow rate was 100 μl/min. Hydrogen was simultaneously introduced into the tubing through a three way connector. The typical hydrogen flow rate was 40 cm^3/min. Check valves (R.S.Crum & Co. Mountainside, NJ) were placed on both lines to restrict back-flow. The CVD was performed typically for about 12 min. Considering the high temperature and the flow of hydrogen gas used during the experiment, adequate safety precautions were taken. Various substrates, such as, 304 and 316 type stainless steel capillary tubing (Alltech, Deerfield, IL), silica lined metal capillary tubings, such as, Silcosteel™, and Sulfinert™ (Restek, Bellefonte, PA) were tested for the self-assembly of SWNTs. Prior to CVD, the tubes were washed with ethanol to remove any particles / impurities. The tubes were 1 meter long, with 0.53 mm ID. Though a meter long tube was

used for the CVD, few centimeters extended out of the furnace. The total length used in GC separation was just 0.75 m. After the CVD process, prior to their use in gas chromatography, the columns were treated at 200°C in air for 1 hr to oxidize amorphous carbon and other impurities generated during the CVD process. Later the column was heated in argon atmosphere at 425°C for 1 hr to remove any low boiling impurities in the column.

The SWCNT film was characterized by Raman spectroscopy performed at 632.8 nm excitation using a Jubin-Yuon / Horiba Confocal micro raman. To study the CNT formation, one cm long segments were cut from the steel tube at five equidistant locations. The samples were cut open to expose the inside surface, and were analyzed by Leo 1530 VP (Carl Zeiss SMT AG Company, Oberkochen, Germany) field emission-scanning electron microscope. The distribution, surface coverage, and the thickness of the SWNT coating were studied based on the SEM images.

6.2.3 Gas Chromatography

A Hewlett-Packard (HP) model 5870 series II gas chromatograph with a flame ionization detector (FID), interfaced with HP 3365 chemstation data acquisition and processing software was used to study the analyte separations. Gas samples were injected using a electronically controlled Valco 10 port sampling valve with injector and detector temperatures at 250°C. Liquid injections were made manually using an injection port with injector and detector temperatures at 280°C. Helium was used as the carrier gas.

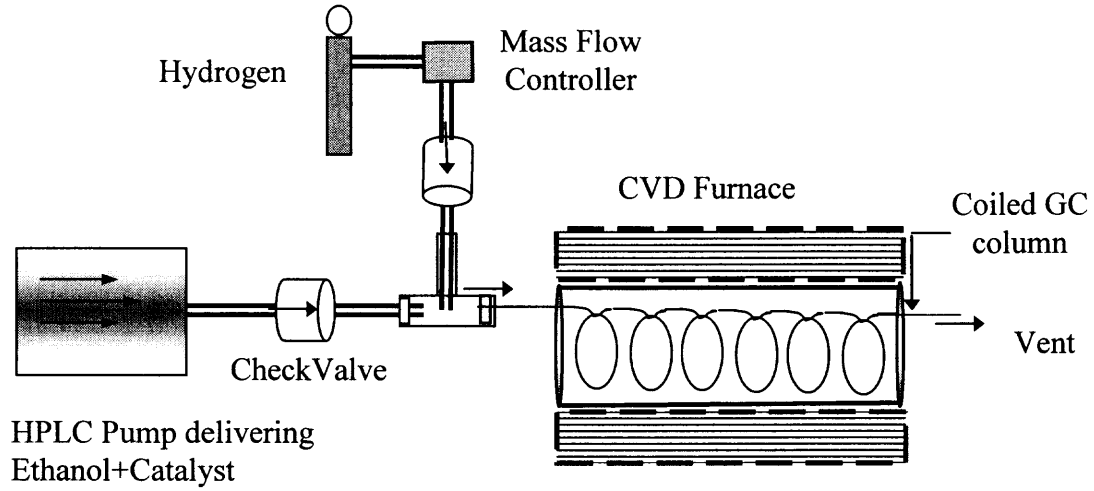

(a)

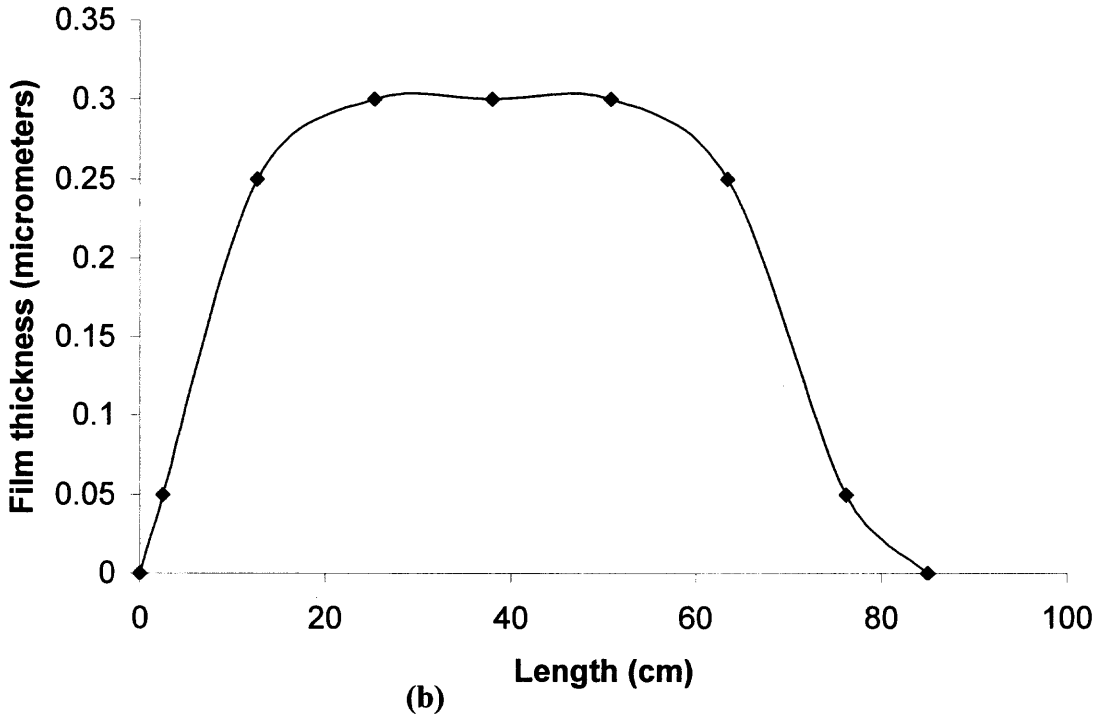

(b)

Figure 6.1 a) Setup of the vapor phase catalytic synthesis of SWCNTs inside the metal capillary tubing. b) Variation in SWCNT film thickness as a function of column length.

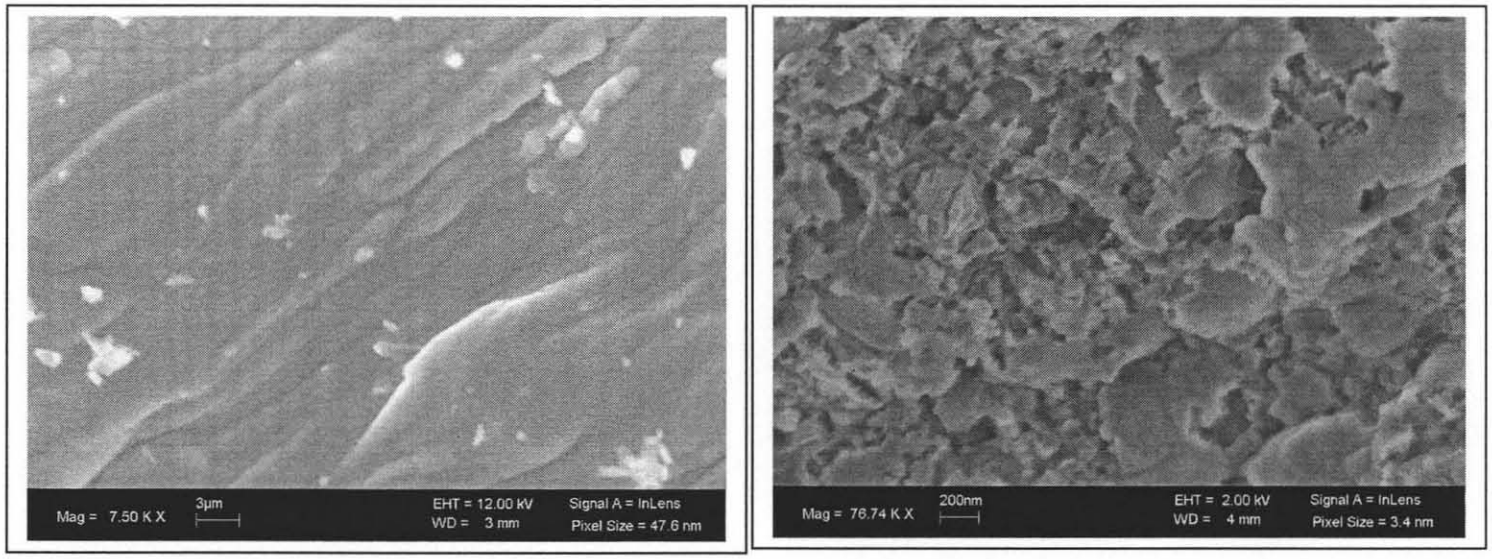

(a) (b)

Figure 6.2 SEM images of the surface of the silica lined tubing a) SEM image of the surface AS-IS without subjected to any pretreatment. b) SEM image of the surface silica lined tubing with water sprayed at 725°C showing the microscale cracks.

altering CVD conditions. The presence of SWCNTs was confirmed by Raman spectroscopy on all the sections of the tubing. Multiple tubes were analyzed to check reproducibility. The Raman spectrum is shown in Figure 6.3a and 6.3b, it showed the presence of the radial breathing mode (RBM) which is a characteristic of the SWCNTs. Based on the characteristic peaks at wave numbers of 190, 217, 221, 248 and 287 cm^{-1} the SWCNT diameters [166] were calculated to be between 0.87 and 1.3 nm.

The SWCNT film was morphologically different from the MWCNT films reported before [152]. The MWCNTs were vertically aligned with the tubes forming forest-like structure. The density could be quite high based on the CVD conditions. In the case of the SWCNTs, the tubes did not have any preferential alignment and formed noodle-like structures. The tube density was significantly smaller than the MWCNTs as shown in Figure 6.3d. Thus, these two stationary phases are expected to be functionally different.

A wide range of organic compounds could be separated on these columns. Separation of the low molecular weights C_1-C_6 alkanes is shown in Figure 6.4a, while larger molecular weights, such as, C_6-C_{14}, and the polyaromatic hydrocarbon (PAH) mixture are shown in Figure 6.4b and 6.4c respectively. Normally, the former would be carried out in a packed GC column, while an open tubular column would be suitable for the latter. The SWCNT allowed both these separation to be carried out in an open tubular format at high resolution. Although methane and ethane could not be separated on a 0.75 m column it is anticipated that longer length column or sub ambient cooling could be used to separate them. The ability of the SWCNT phase in the separation of analytes with

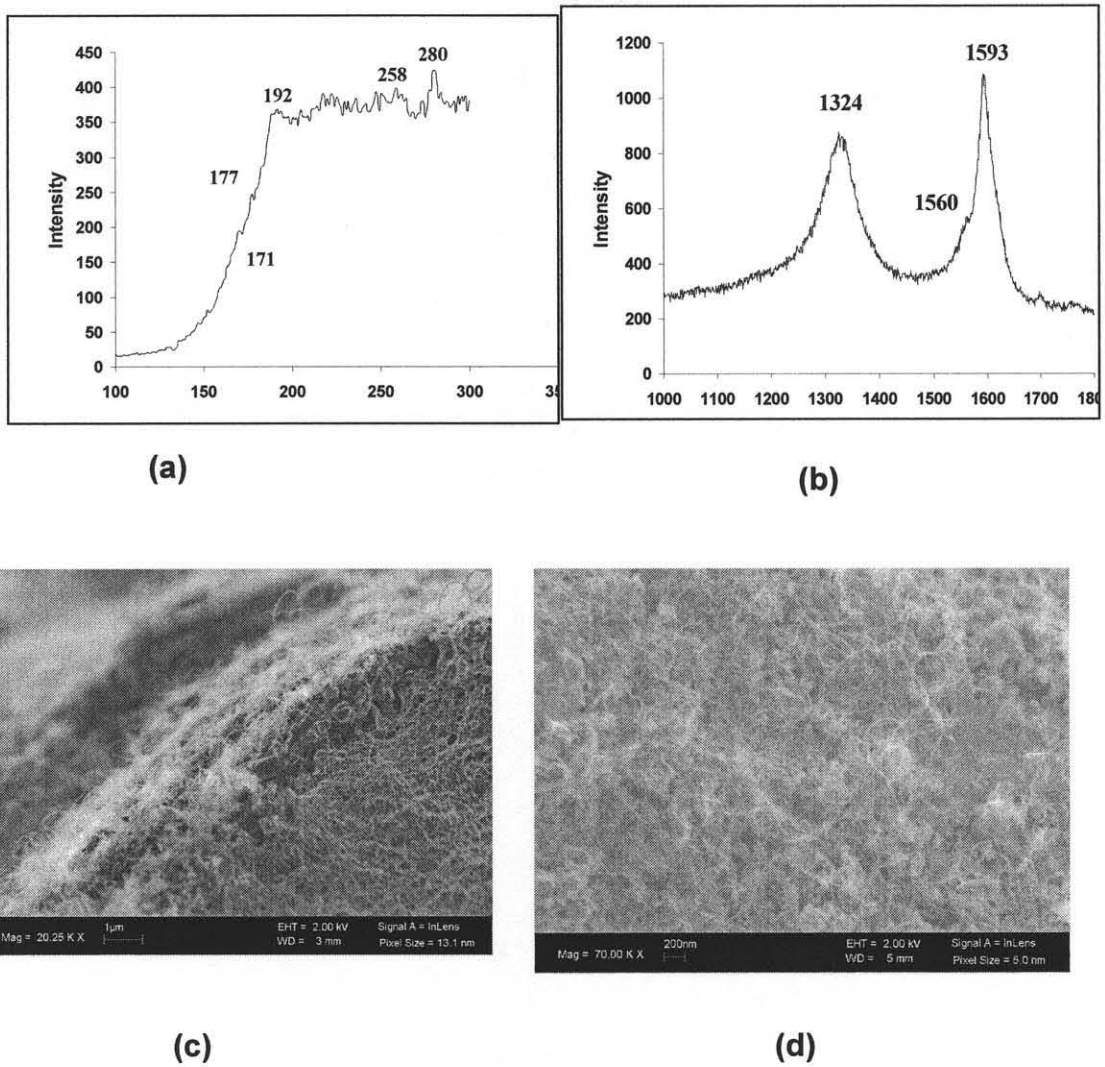

Figure 6.3 a) RBM spectra of the SWCNTs synthesized at 725°C. b) Raman Spectra showing the D and G signals of the SWCNTs. c) & d) SEM images showing the SWCNT film on the metal capillary tubing.

a wide range of boiling points and volatility is quite exciting from the standpoint of gas chromatography.

This was possible due to the stability of the SWCNT phase at high temperatures. This column was also used for a variety of other separations, such as, halo-hydrocarbons, aromatics, alcohols, ketones and alkane isomers of varying polarity as shown in figure 6.4. The baseline from heating the column to 425°C is shown in Figure 6.4d. It is evident that there was no column bleed or other instability at higher temperatures. It is pertinent to note that the analytes, chrysene and perylene in the PAH mixture, as well as, dodecane and tetradecane in the n-alkanes mixture (Figures 6.4b, 6.4c) eluted at temperatures around 425°C with near symmetrical peaks. Typical reproducibility in retention time measured as percentage relative standard deviation (%RSD) are presented in Table 6.1 and 6.2 for the n-alkane and PAH mixture. These RSD's are comparable to those from commercial GC columns.

The band broadening and column efficiency were obtained from the plate theory of chromatography [167]. Typical chromatographic efficiencies on this column are presented in Table 6.3. The number of theoretical plates (N) obtained on the SWCNT film for a 0.75 m length were comparable to the conventional open tubular columns. They were obtained using the following formula:

$$N = 5.54 \, (t_R / W_{1/2})^2 \qquad (6.1)$$

Where N is the number of theoretical plates and is a measure of the column efficiency, t_R is the retention time of the analyte and $W_{1/2}$ is the width of the peak at half its maximum height. The values for t_R and $W_{1/2}$ are obtained directly from the chromatogram. Higher the number of theoretical plates, higher is the column efficiency.

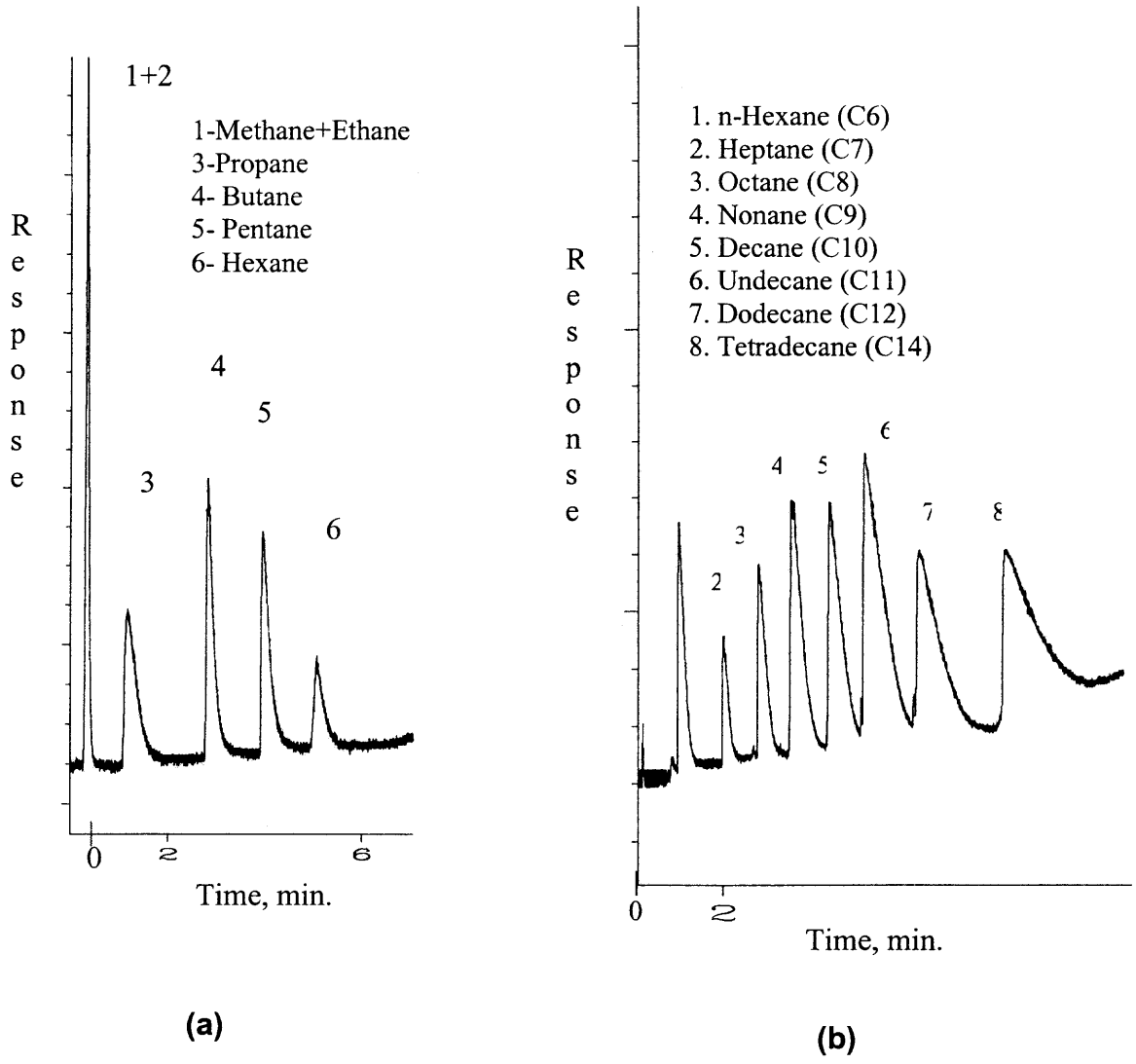

Figure 6.4 Typical chromatograms generated from the SWNT column showing the separation of a) ppm level of alkanes standard, conditions: 30°C, 0.5min, at 40°C/min. to 250°C, flow rate of carrier gas was 1.5 ml/min, 20 µl injection. b) high molecular weight n-alkanes, conditions: 120°C, 0.1min, at 40°C/min. to 425°C, 5 min; flow rate of carrier gas was 5.0 ml/min.

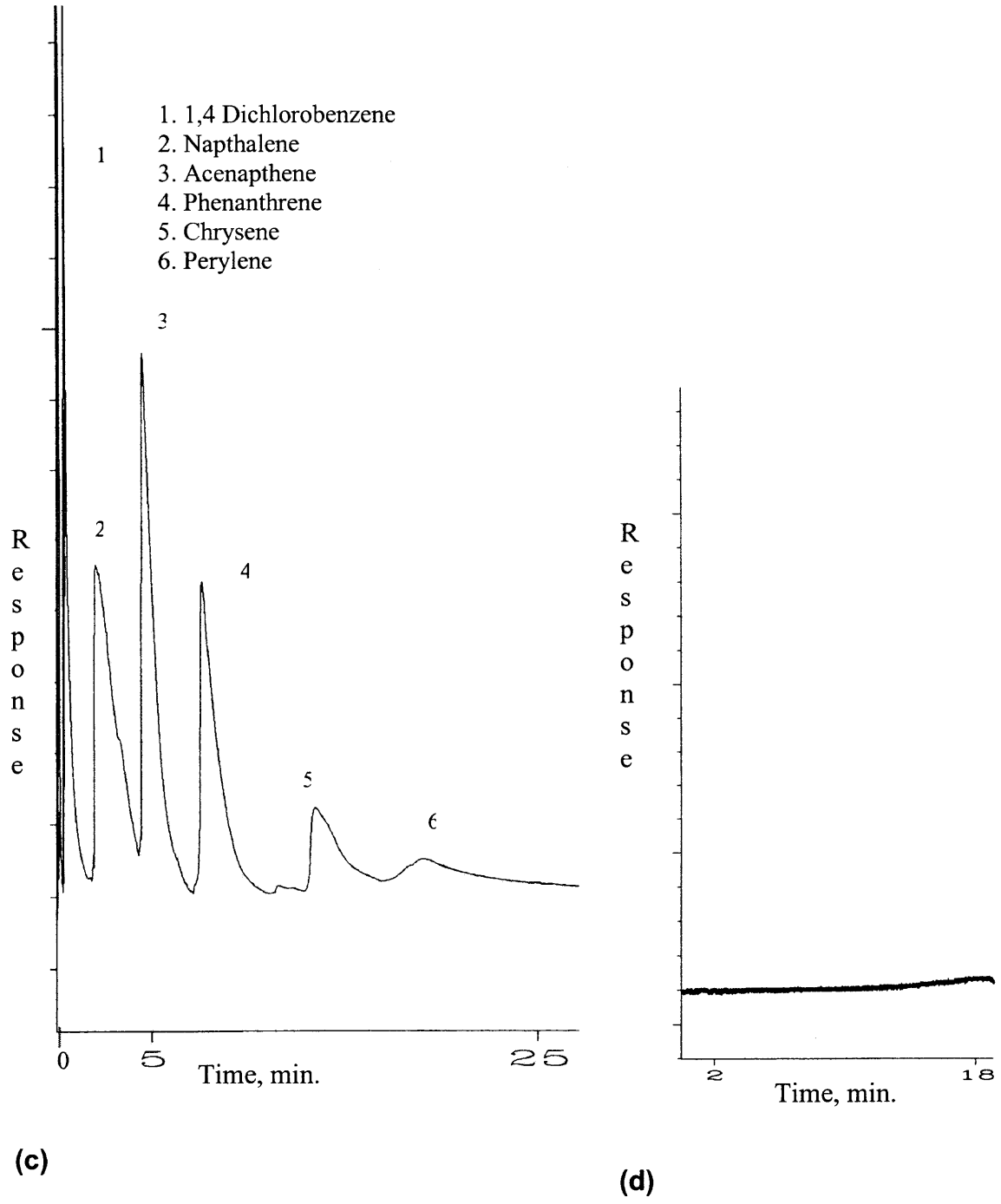

Figure 6.4 Typical chromatograms generated from the SWNT column showing the separation of c) deuterated PAH mixture, 0.6 ul, 1:20 split ratio, Oven temperature 125°C at 30°C/min. to 425°C, 10 min, 300°C injector, detector. d) Chromatogram illustrating the column bleed test. The test shows a stable baseline. Conditions: 30°C, 2 min, at 30°C / min to 425°C, 4 min. (Continued)

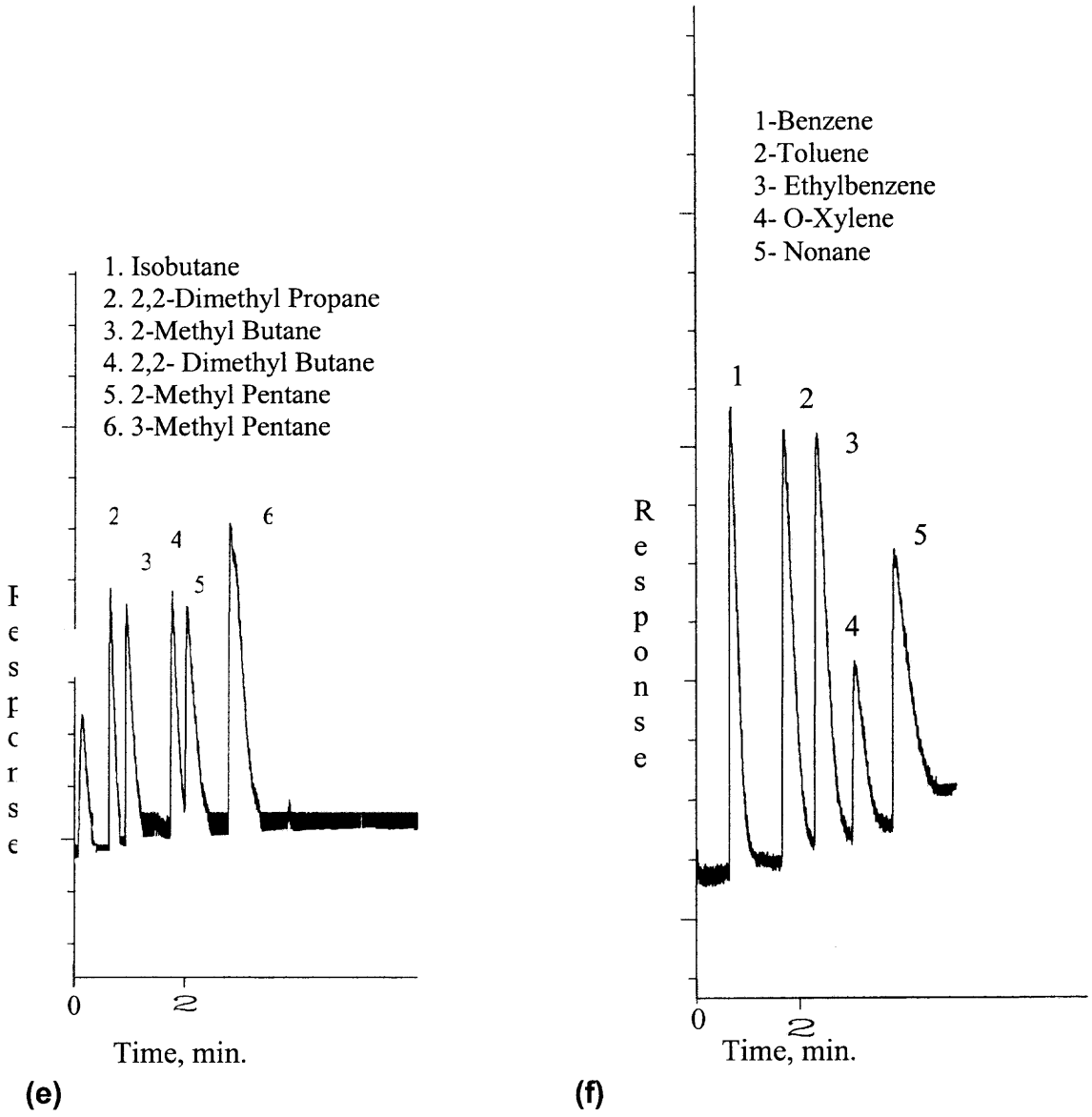

Figure 6.4 Typical chromatograms generated from the SWNT column showing the separation of e) isomers of branched hydrocarbons, ppb level standard conditions: 40°C for 0.1 mins, 40°C/min. to 200° C/min, 50 µl injection, flow rate of carrier gas was 4.0 ml/min. f) aromatics, conditions: 120° C for 0.1 mins, 45°C/min. to 300°C/min., flow rate of carrier gas was 5.7 ml/min. (Continued)

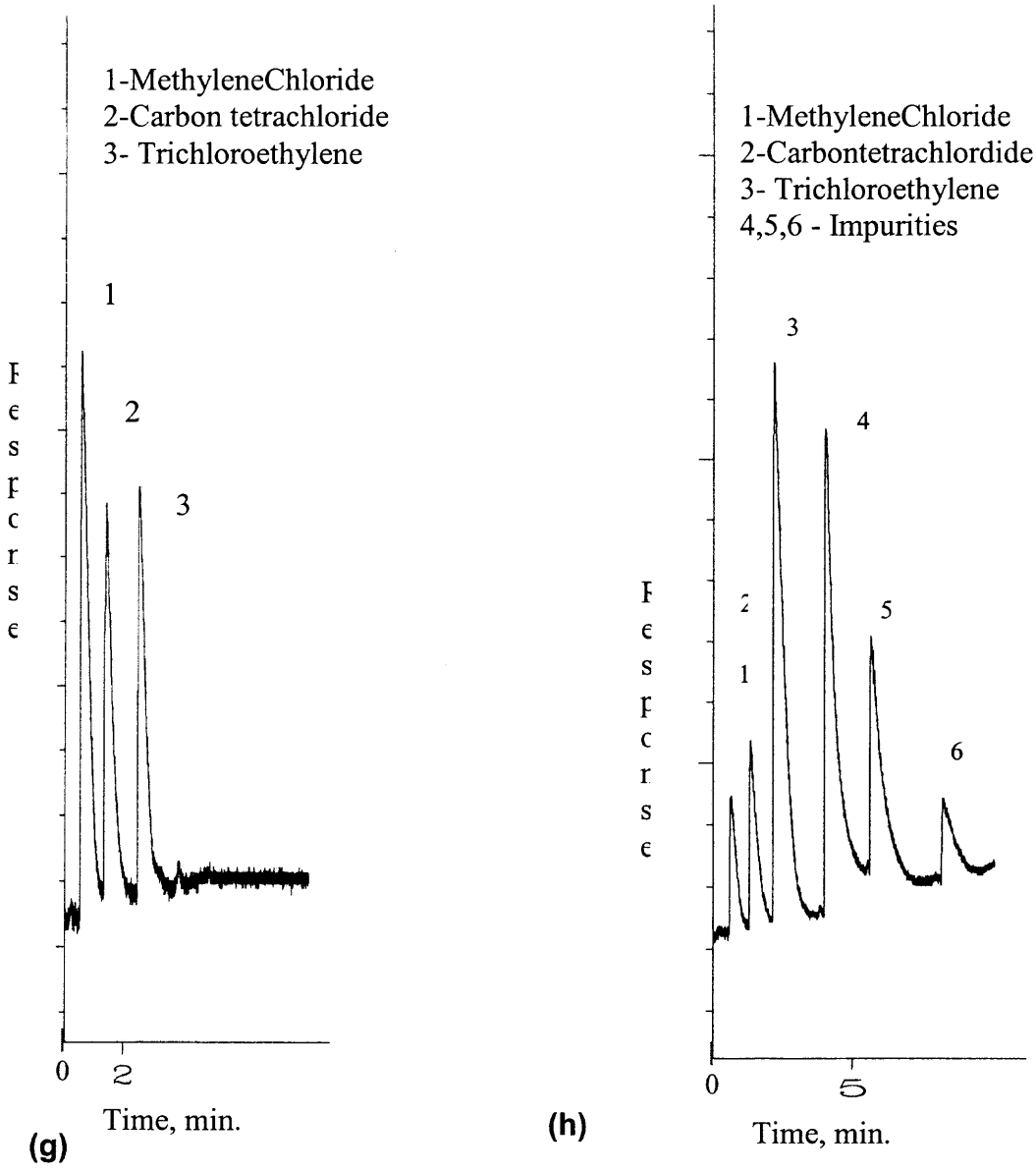

Figure 6.4 Typical chromatograms generated from the SWNT column showing the separation of g) chlorohydrocarbons, conditions: 60°C for 0.5 mins, 45° C/min. to 240°C/min, flow rate of carrier gas was 4.0 ml/min. h) chlorohydrocarbons with few impurities, conditions: 60°C for 0.5 mins, 45° C/min. to 325°C, flow rate of carrier gas was 5.0 ml/min. (Continued)

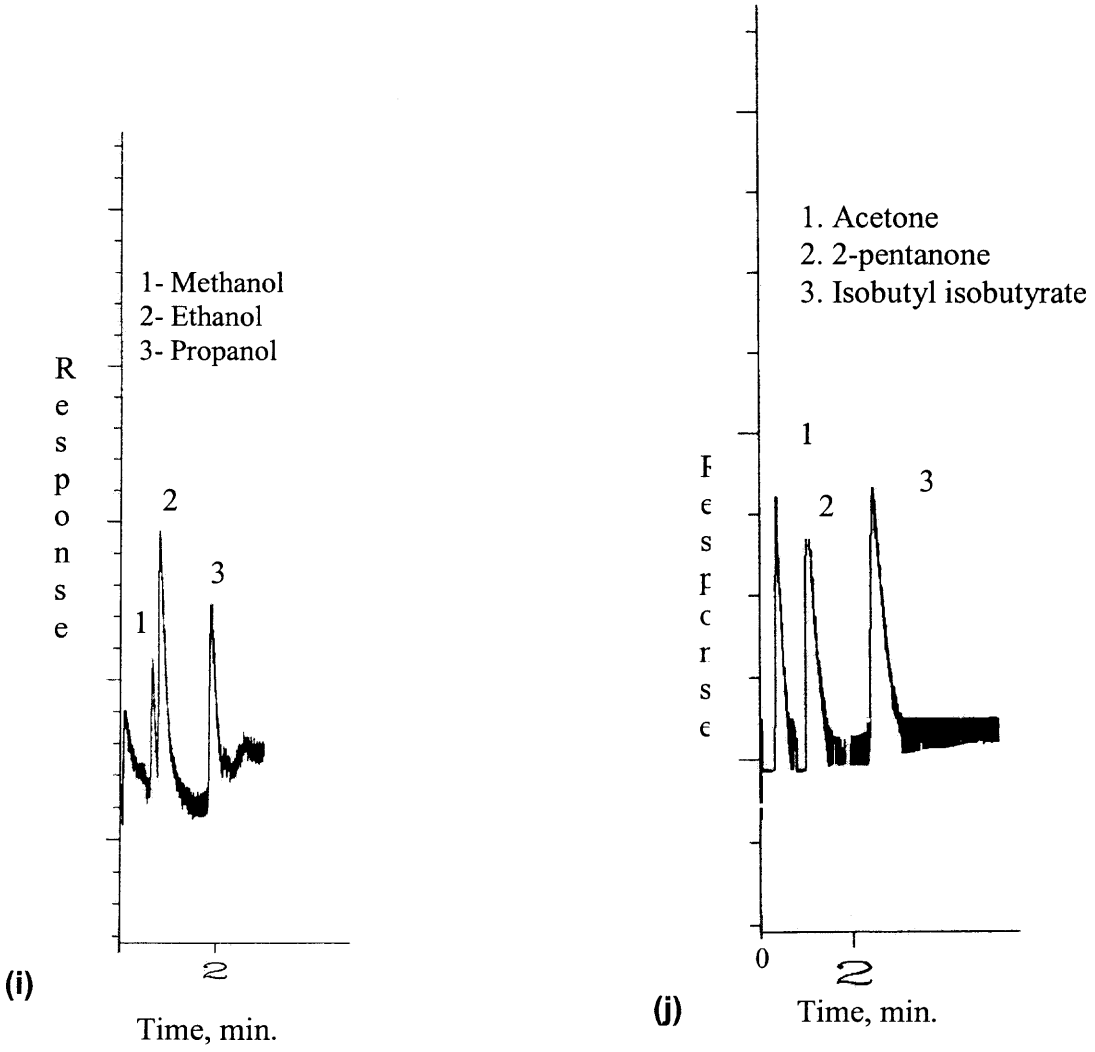

Figure 6.4 Typical chromatograms generated from the SWNT column showing the separation of i) alcohols, conditions: 120°C for 0.5mins, 40° C/min. to 250°C, flow rate of carrier gas was 5.7 ml/min .j) Polar compounds, conditions: 145° C for 0.1mins, 45° C/min. to 300°C, flow rate of carrier gas was 5.0 ml/min.

Figure 6.5 shows the Van Deemter plot for the column with ethylbenzene at 200°C. The Van deemter plot helps in the determination of the optimum flow rate required in order to minimize the band broadening. The minimum height equivalent theoretical plate (HETP) was 0.42 cm and the optimum flow rate of the carrier gas ranged between 3.5 to 4.5 ml/min, which is typical of these columns with this internal diameter. HETP or H is obtained from the following formula:

$$H = L / N \tag{6.2}$$

Where H is the height equivalent theoretical plate (HETP), L is the length of the column and N is the number of theoretical plates.

Figure 6.6 shows the Van't Hoff plot with the dependence of log k' vs. reciprocal temperature for n-hexane as well as benzene. The linear plot (with correlation coefficients of 0.99) suggests that the separation follows classical chromatographic behavior. k' is called capacity factor and it is a measure of sample retention on the column. It is obtained from the following formula:

$$k' = t_R - t_M \ / \ t_M \tag{6.3}$$

Where t_R is the retention time of the analyte and t_M is the dead time or the retention time of a non adsorbed compound on the column.

Figure 6.7 shows the plot of alkane homologous series, where the log of retention time is plotted against the carbon number. A linear plot suggests that the classical chromatography behavior is being followed.

Retention on the SWCNT film was compared to that on a column packed with a commercial carbon phase, such as, Carbopack C™ (Supelco, Bellefonte, PA). Table 6.4 presents the capacity factors of few representative analytes on SWCNT column versus

Table 6.1 Retention Time Repeatability Data (n=5) for the Separation of n-Alkanes Mixture

Solute	Avg. Retention time (min)	RSD (%)
n-Hexane	0.87	4.43
Heptane	1.92	2.54
Octane	2.75	2.71
Nonane	3.51	1.77
Decane	4.42	0.82
Undecane	5.25	0.87
Dodecane	6.57	1.47
Tetradecane	8.74	3.31

Table 6.2 Retention Time Repeatability Data for the Separation of Deuterated PAH Mixture (n=5)

Solute	Avg. Retention time (min)	RSD (%)
1,4 dichlorobenzene	0.35	2.02
Napthalene	1.96	0.63
Acenapthene	3.88	1.79
Phenanthrene	6.39	1.34
Chrysene	10.84	2.15
Perylene	13.58	2.25

Table 6.3 Column Efficiency Data

Solute	Column efficiency (N)	Capacity Factor (k')	Temp. (°C)
Pentane	759	3.270	130
Dichloromethane	745	4.486	50
Toluene	785	7.283	200
O-Xylene	793	10.962	240
Ethylbenzene	689	6.216	230
Nonane	625	13.915	270

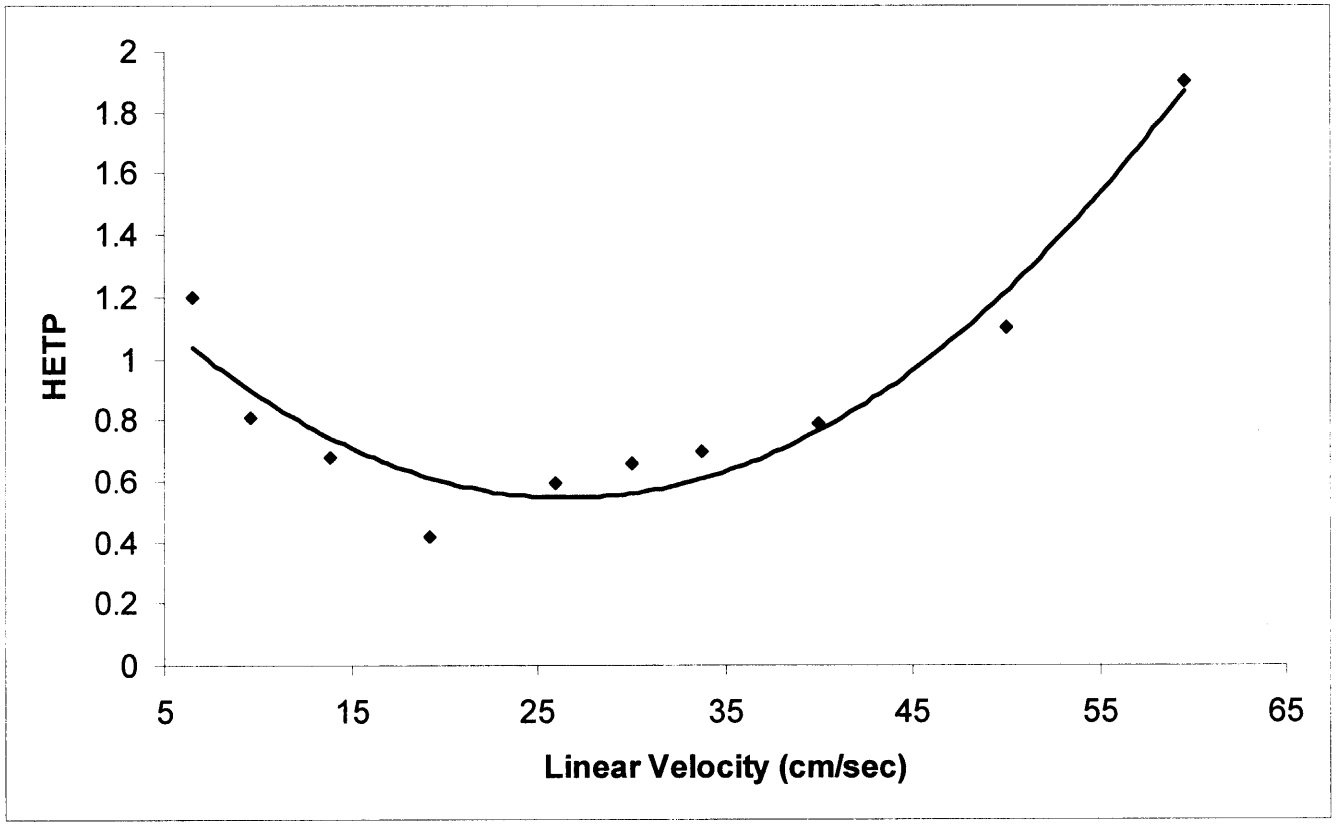

Figure 6.5 Van Deemter plot for ethylbenzene. (Hmin: 0.42 cm at 3.5 ml/min).

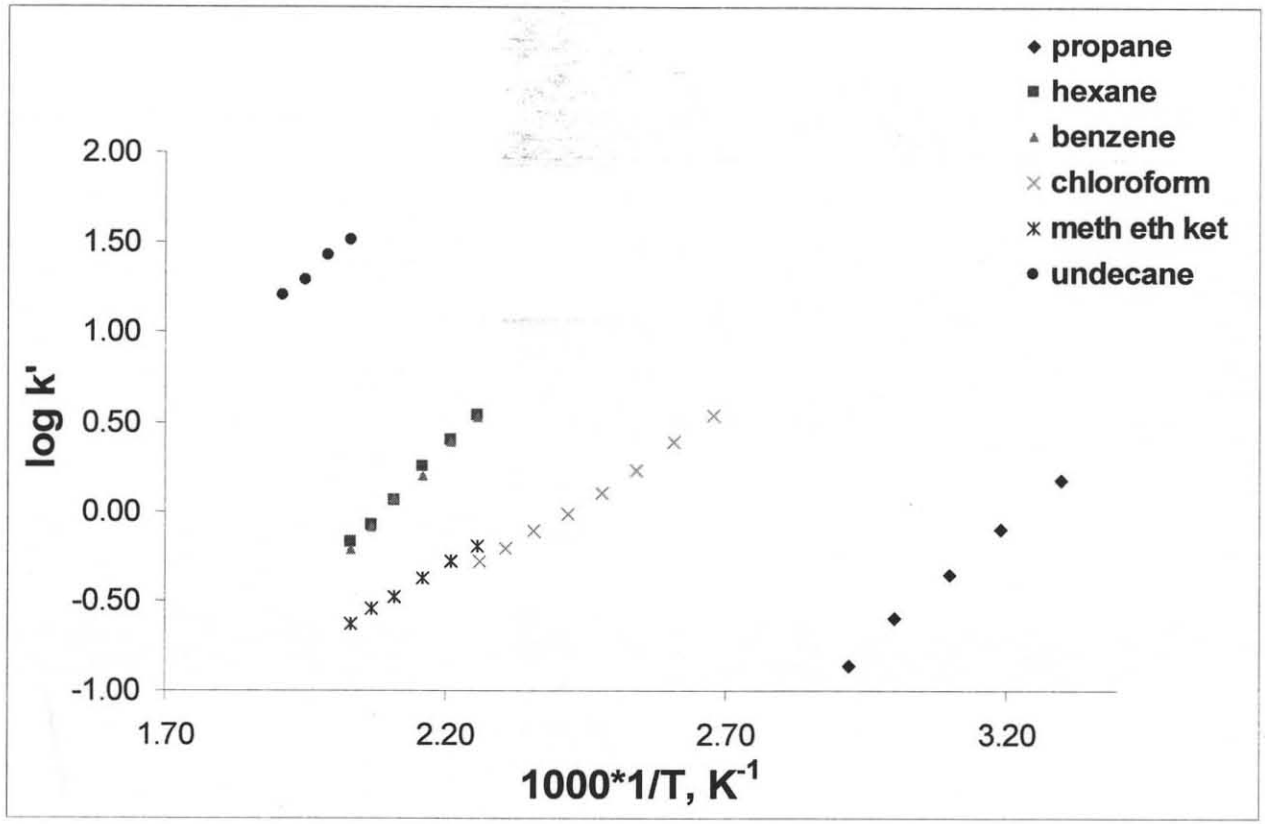

Figure 6.6 Van't Hoff plots (Variation in capacity factor with temperature) for various analytes.

the in-house packed Carbopack C^{TM} column. The capacity factors are usually proportional to the mass and the surface areas of the sorbent material used and are a measure of the retention of the analyte on the sorbent material. They were obtained from Equation 6.3. The table suggests that the capacity factors obtained on the 200 - 300 nm thick SWCNT phase were comparable to a packed column containing 0.352 gm of the sorbent material. The specific surface area of the Carbopack C^{TM} was about 10 m^2/g [168]. The high capacity factor on such a thin film reflects the high surface area of the SWCNT phase.

Table 6.4 Comparison of Capacity Factors (k') on SWCNT Column and Packed Carbopack C^{TM} Column

Sample	SWNT-k'	Carbopack-k'	Temp.
Hexane	3.390	4.005	180
Benzene	3.125	2.562	180
Methylethylketone	0.531	1.500	180
Chloroform	3.450	3.048	100
Propane	1.508	1.625	30

Table 6.5 Isosteric Heats of Adsorption (ΔH_s) on SWCNT Column and Packed Carbopack C^{TM} Column

Sample	SWNT-ΔH_s ($kJ.mol^{-1}$)	Carbopack-C- ΔH_s ($kJ.mol^{-1}$)
Hexane	59.53	19.18
Benzene	55.88	16.0
Methyl ethyl ketone	39.12	14.88

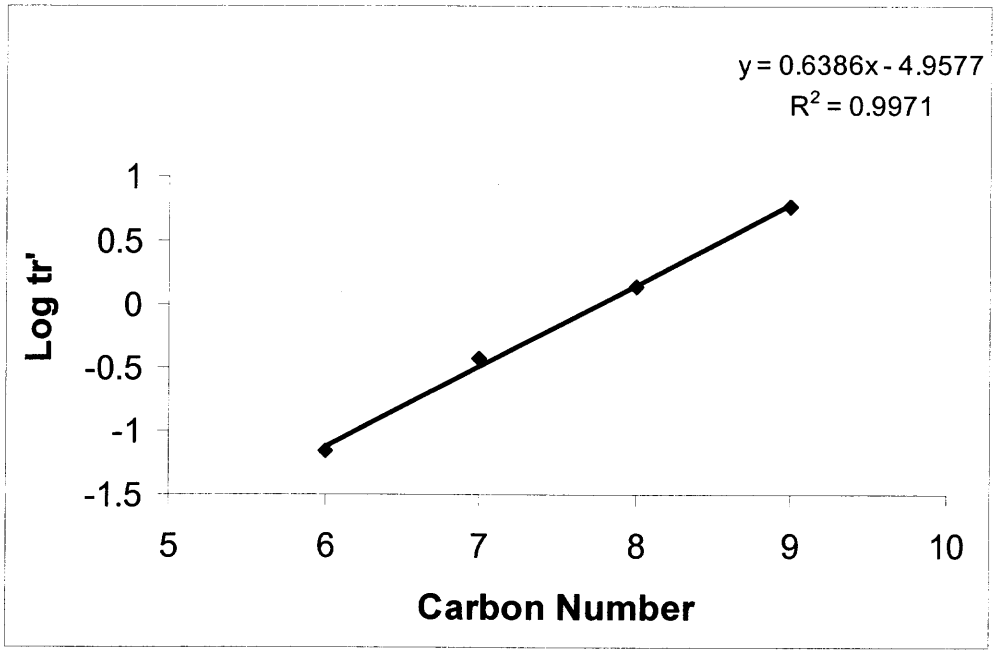

Figure 6.7 Plot of n-alkane homologous series. A mixture of n-hexane, heptane, octane and nonane were injected at 110^0C.

Table 6.5 presents the isosteric heats of adsorption (ΔH_s) in the infinite dilution region for selected analytes on the SWNT column and on the packed Carbopack C™ column over a temperature range of 443 – 493 K. The ΔH_s values for the adsorption of organic vapors were calculated from the retention volumes (plot of $\ln(V_N) / T$ against $1 / T$, where the slope is $-\Delta H_s / R$ as described in the next paragraph below based on the work of Bilgic et al. [169]. The regression coefficients were about 0.99 for all the plots. The isosteric heats of adsorption characterizes the activation energy for sorption, and consequently is a measure of sorbate-sorbent interaction. The data suggests stronger interaction of organic vapors with the SWCNT sorbent, relative to the Carbopack C™. The trend of ΔH_s of adsorption for the SWCNT phase was hexane > benzene > Methyl ethyl ketone (MEK), opposite to that of their dipole moments and capacity factors (k'). This trend was similar to that observed by Agnihotri et al. [170] in their estimation of ΔH_s for these organic vapors from a gravimetric approach.

Although retention time is the variable that is directly observed in gas chromatography it is not used to characterize a system, since it is affected by many variables (such as the length of the column and its internal diameter, the amount of stationary phase present, and the flow rate of the carrier gas). Therefore a variable called retention volume is used to characterize a system. The retention volume of a retained solute is given by

$$F^* t_{R'} = V_R \tag{6.4}$$

Where F is the flow-rate of the carrier gas and $t_{R'}$ is the adjusted probe retention time obtained after substracting the dead time (t_m). Similarly the retention volume of an unretained solute is given by

$$F^* t_M = V_M \quad (6.5)$$

t_m is the dead time (retention time of a non adsorbed compound) and V_M is the column gas holdup or column dead volume. The dead volume of the column can be subtracted from the retention volume to obtain the adjusted retention volume, V'_R

$$V'_R = V_R - V_M \quad (6.6)$$

In order to correct the retention volumes for the fact that the mobile gas phase is compressible, the pressure gradient factor, j, is applied to V'_R to give V_N, the net retention volume:

$$V_N = j\, V'_R \quad (6.7)$$

Where j is the James-Martin pressure correction factor and can be calculated from the equation:

$$J = 3((P_i/P)^2-1) / 2((P_i/P)^2-1) \quad (6.8)$$

where P_i is the initial pressure on the column and P is the outlet pressure which is atmospheric pressure. The net retention volume V_N can be re written from the above equations 1-4 as follows

$$V_N = (t_R - t_m) * F * T/T_f * j \quad (6.9)$$

Where T is the column temperature and T_f is the temperature of the flow meter, i.e., ambient temperature.

The capacity factor, k' which is defined as the ratio of the amount (mass) of solute dissolved in the stationary phase to the amount dissolved in the mobile gaseous phase is related to the retention volumes by

$$k' = V_N / V_M \quad (6.10)$$

The net retention volume, V_N can be expressed in terms of changes in thermodynamic functions, like enthalpy and entropy of adsorption

$$\ln V_N = \ln(RTn_S) + \Delta S/R - \Delta H/R*1/T \quad (6.11)$$

Where n_S (mol) is the total amount of adsorbate in the adsorbed state. Since all the experiments were performed in the infinite dilution region the first term can be neglected.

By determining V_N at various temperatures, ΔH (isosteric heat of adsorption) and ΔS can be calculated from slope and intercept of the plot of ln V_N versus 1/T, provided that the range of T is narrow enough for ΔH and ΔS to be regarded as temperature independent.

The polarity of the SWCNT stationary phase was evaluated by calculating the McReynolds constants (ΔI) at 120°C [171-172]. It is described in detail in the paragraph below. The data presented in Table 6.6 suggests that the SWCNT phase was non-polar. Benzene showed a negative ΔI value, which implies hexane adsorbed more strongly than benzene. This was also observed from the ΔH_s of adsorption and the capacity factors. This property of the CNTs has been reported previously by Bittner et al. [173] during their study on the characterization of the surfaces of SWCNTs by pulse adsorption technique. They observed that hexane was the most strongly held among other organic compounds such as benzene, ethanol and iso-propanol. Therefore with respect to benzene, the SWNT phase is more non-polar than squalane. The elution sequences of the McReynolds probes were benzene, 1-butanol, 2-pentanone and pyridine respectively.

The McReynolds constant for a particular solute on a given stationary phase is defined as the difference between its retention index (I^P) on that particular phase and its retention index on a non polar reference phase (I^{NP}) usually taken as squalane (C_{30})

hydrocarbon. Since a solute's retention index on squalane is primarily reflective of its partial pressure with respect to the n-alkanes, a difference in its retention index on some other column material will be indicative of some specific solute interaction with that stationary phase.

$$\Delta I_x = I^P - I^{NP} \qquad (6.12)$$

The retention index, I, is defined by

$$I = 100 [\log t'_{r\,x} - \log t'_{r\,n} / \log t'_{r\,n+1} - \log t'_{r\,n}] + 100n \qquad (6.13)$$

Where $t'_{r\,x}$ is the adjusted retention time for the sample; $t'_{r\,n}$ and $t'_{r\,n+1}$ are the adjusted retention times for the n-alkanes eluting just before, and just after the sample, respectively; and n is the number of carbon atoms in the n-alkane eluting at $t'_{r\,n}$.

To aid in an assessment of the various interactions McReynolds has selected several reference compounds, which are representative of specific classes of interactions, thus permitting empirical determination of the extent of such an interaction with a particular stationary phase.

In order to evaluate the column-to-column reproducibility, three SWCNT columns were prepared under identical conditions and the capacity factors were obtained for selected solutes (Table 6.7). The low %RSD values bear testimony to the fact that the CVD process used for the SWNT deposition was a reliable technique and reproducible.

Table 6.6 McReynolds Constants for SWCNT Column

Probe	**benzene**	**1-butanol**	**2-pentanone**	**1-nitropropane**	**pyridine**
Interaction Type	Inductive	H-bonding	Dipolar	Dipolar	H+Acceptor
I for swnt	589.7	689.5	752.2	-	874.9
I for squalane	653	590	627	652	699
ΔI	-63 (x')	100 (y')	125 (z')	(u')	176 (s')

Table 6.7 Evaluation of Capacity Factors for Column - Column Reproducibility

Column	Ethylbenzene Capacity Factor (k')	Nonane Capacity Factor (k')
1	10.423	8.690
2	10.269	8.653
3	10.216	8.480
	RSD (%) 1.04	RSD (%) 1.3

6.4 Conclusions

SWCNT based open tubular GC stationary phase was fabricated via catalytic CVD inside silica lined steel capillary columns. SWCNTs demonstrated good separation efficiency, classical chromatography behavior, and high-resolution separations. The high surface area of the SWCNT phase allowed separations of gases, and at the same time, its high thermal stability permitted separations of higher molecular weights at higher temperatures, thus extending the range of conventional chromatography on the same column. SWCNTs therefore have the potential to be the high-performance separation media through nanoscale interactions.

REFERENCES

1. Ramsey, W., *Proc. Roy. Soc.* **1905**, A76, 111-113.

2. Tswett, M., Ber. Deutsch. *Botan. Ges.* **1906** 24, 316-384.

3. Martin. A. J. P., and Synge, R.L.M., *Biochem. J.* **1941,** 35, 1358-1368.

4. James, A. T., and Martin, A. J. P., *Biochem. J.* **1952**, 50, 679-690.

5. Golay, M. J. E., *Gas Chromatography*; Butterworth Scientific Publications, London,1958. p. 36-55.

6. Skoog, D. A.; Holler, F. J.; Niemann, T. A. *Principles of Instrumental Analysis*; Saunders College Publishing: Philadelphia, PA, 1998. 5th edn, p.713.

7. Matisoda, E.; SkrabBkova, S. *J. Chromatogra. A* **1995**, *707*, 145-179.

8. Mattson, J. S.; H.B. Mark, J. *Activated Carbon*; M. Dekker: New York, 1971, p.1.

9. Kiselev, A. V.; Yashin, J. P. *Gas Adsorption Chromatography*; Plenum Publishing: New York, 1969.

10. Dewulf, J.; Langenhove, H. V. *J. Chromatogra. A* **1999**, *843*, 163-177.

11. Bernal, J.D. *Proc. Roy. Soc. London Ser. A*, **1924** 100 749-750.

12. Lipson, H.; Stokes, A.R. *Proc. Roy. Soc. London Ser. A* **1942**, 181, 93-96.

13. Hiroshi Tabataa; Fujiib, M.; Hayashi, S. *Carbon* **2006**, *44*, 522-529.

14. Kartsova, L. A.; Makarov, A. A. *Russian Journal of Applied Chemistry* **2002**, *75*, 1725-1731.

15. Schutzenberger, P.; Schutzenberger, L. *C.R. Acad. Sci* **1890**, *111*, 774-778.

16. Baker, R. T. K.; Harris, P. S. In *Chemistry and Physics of Carbon*; Jr., P. L. W., Thrower, P. A., Eds.; Dekker: New York, 1978; Vol. 14, pp 83-165.

17. Ijima, S. *Natrure* **1991**, *354*, 56-58.

18. Ijima, S.; Ichihashi, T. *Nature* **1993**, *363*, 603-605.

19. Bethune, D. S.; Kiang, C. H.; deVries, M. S.; Gorman, G.; Savoy, R.; Vazquez, J.; Bayers, R. *Natrure* **1993**, *363*, 605-607.

20. Dresselhaus, M. S.; Dresselhaus, G.; Eklund, P. C. In *Science of Fullerenes and Carbon Nanotubes*; Academic Press: San Diego, 1996, p. 985.

21. Dai, H. *Acc. Chem. Res.* **2002**, *35*, 1035-1044.

22. Bhushan, B. *Handbook of NanoTechnology*; Springer-Verlag: Berlin, 2004.

23. Maser, W. K.; Munoz, E.; Benito, A. M.; Martýnez, M. T.; Fuente, G. F. d. l.; Maniette, Y.; Anglaret, E.; Sauvajol, J.-L. *Chem. Phys. Lett.* **1998**, *292*, 587-593.

24. Niyogi, S.; Hamon, M. A.; Hu, H.; Zhao, B.; Bhowmik, P.; Sen, R.; Itkis, M. E.; Haddon, R. C. *Acc. Chem. Res.* **2002**, *35*, 1105 - 1113.

25. Damnjanovic, M.; Milosevic, I.; Vukovic, T.; Sredanovic, R. *Physical Review B* **1999**, *60*, 2728-2739.

26. Yang, Q. H.; Hou, P. X.; Bai, S.; Wang, M. Z.; Cheng, H. M. *Chem. Phys. Lett.* **2001**, *345*, 18-24.

27. Eswaramoorthy, M.; Sen, R.; Rao, C. N. R. *Chem. Phys. Lett.* **1999**, *304*, 207-210.

28. Peigney, A.; Laurent, C.; Flahaut, E.; Bacsa, R. R.; Rousset, A. *Carbon* **2001**, *39*, 507-514.

29. Frackowiak, E.; Delpeux, S.; Jurewicz, K.; Szostak, S.; Cazorla-Amoros, D.; Beguin, F. *Chem. Phys. Lett.* **2002**, *361*, 35-41.

30. Muris, M.; Dupont-Pavlosky, N.; Bienfait, M.; Zepenfeld, P. *Surf. Sci.* **2001**, *492*, 67-74.

31. Fujiwara, A.; Ishii, K.; Suematsu, H.; Kataura, H.; Maniwa, Y.; Suzuki, S.; Achiba, Y. *Chem. Phys. Lett.* **2001**, *336*, 205-211.

32. Zhao, J.; Buldum, A.; Han, J.; Lu, J. P. *Nanotechnology* **2002**, *13*, 195-200.

33. Chambers, A.; Park, C.; Baker, R. T. K.; Rodriguez, N. *J. Phys. Chem. B.* **1998**, *102*, 4253-4256.

34. Hilding, J.; Grulke, E. A.; Sinnott, S. B.; Qian, D.; Andrews, R.; Jagtoyen, M. *Langmuir* **2001**, *17*, 7540-7544.

35. Masenelli-Varlot, K.; McRae, E.; Dupont-Pavlosky, N. *Appl. Surf. Sci.* **2002**, *196*, 209-215.

36. Froudakis, G. E. *Nanolett.* **2001**, *1*, 531-533.

37. Ulbricht, H.; Moos, G.; Hertel, T. *Phys. Rev. B* **2002**, *66*, 075404-075401-075404-075407.

38. Arepalli, S.; Nikolaev, P.; Gorelik, O.; G.Hadjiev, V.; Holmes, W.; Files, B.; Yowell, L. *Carbon* **2004**, *42*, 1783-1791.

39. Itkis, M. E.; Perea, D. E.; Jung, R.; Niyogi, S.; Haddon, R. C. *J. Am. Chem. Soc.* **2005**, *127*, 3439-3448.

40. Itkis, M. E.; Perea, D.; Niyogi, S.; Love, J.; Tang, J.; Yu, A.; Kang, C.; Jung, R.; Haddon, R. C. *J. Phys. Chem. B* **2004**, *108*, 12770-12775.

41. Ajayan, P. M.; Terrones, M.; Gaurdia, A. d. l.; Huc, V.; Grobert, N.; Wei, B. Q.; Lezec, H.; Ramanath, G.; Ebbesenl, T. W. *Science* **2002**, *296*, 705.

42. Bom, D.; Andrews, R.; Jacques, D.; Anthony, J.; Chen, B.; Meier, M. S.; Selegue, J. P. *Nano Lett.* **2002**, *2*, 615-619.

43. Saridara, C.; Brukh, R.; Iqbal, Z.; Mitra, S. *Anal. Chem.* **2005**, 77, 1183-1187.

44. Li, Q.-L.; Yuan, D.-X.; Lin, Q.-M. *J. Chromatogr. A* **2004**, *1026*, 283-288.

45. Long, R. Q.; Yang, R. T. *J. Am. Chem. Soc.* **2001**, *123*, 2058-2059.

46. Cai, Y.; Jiang, G.; Liu, J.; Zhou, Q. *Anal. Chem.* **2003**, *75*, 2517-2521.

47. Cai, Y.-Q.; Jiang, G.-B.; Liu, J.-F.; Zhou, Q.-X. *Anal. Chim. Acta* **2003**, *494*, 149-156.

48. Peng, X.; Li, Y.; Luan, Z.; Di, Z.; Wang, H.; Tian, B.; Jia, Z. *Chem. Phys. Lett.* **2003**, *376*, 154-158.

49. Li, Y.-H.; Wang, S.; Cao, A.; Zhao, D.; Zhang, X.; Xu, C.; Luan, Z.; Ruan, D.; Liang, J.; Wu, D.; Wei, B. *Chem. Phys. Lett.* **2001**, *350*, 412-416.

50. Li, Y.-H.; Wang, S.; Wei, J.; Zhang, X.; Xu, C.; Luan, Z.; Wu, D.; Wei, B. *Chem. Phy. Lett.* **2002**, *357*, 263-266.

51. Liang, P.; Liu, Y.; Guo, L.; Zeng, J.; Lu, H. *J. Anal. At. Spectrom.* **2004**, *19*, 1489-1492.

52. Fugetsu, B.; Satoh, S.; Shiba, T.; et al., *Environ. Sci. Technol.* **2004**, *38*, 6890-6896.

53. Munoz, J.; Gallego, M.; Valcarcel, M. *Anal. Chem.* **2005**, *77*, 5389-5395.

54. Li, Q.; Yuan, D. *J. Chromatogr. A* **2003**, *1003*, 203-209.

55. Saridara, C.; Mitra, S. *Anal. Chem.* **2005**, 77, 7094-7097.

56. Collins, P. G.; Bradley, K.; Ishigami, M.; Zettl, A. *Science* **2000**, *287*, 1801-1804.

57. Kong, J.; Franklin, N. R.; Zhou, C.; Chapline, M. G.; Peng, S.; Cho, K.; Dai, H. *Science* **2000**, *287*, 622-625.

58. Lu, Y.; Li, J.; Han, J.; Ng, H.-T.; Binder, C.; Partridge, C.; Meyyappan, M. *Chem. Phys. Lett.* **2004**, *391*, 344-348.

59. Li, J.; Lu, Y.; Ye, Q.; Cinke, M.; Han, J.; Meyyappan, M. *Nano Lett.* **2003**, *3*, 929-933.

60. Novak, J. P.; Snow, E. S.; Houser, E. J.; Park, D.; Stepnowski, J. L.; McGill, R. A. *Appl. Phys. Lett.* **2003**, *83*, 4026-4028.

61. Santhanam, K. S. V.; Sangoi, R.; Fuller, L. *Sens. Actuators, B* **2005**, *106*, 766-771.

62. Lee, C. Y.; Strano, M. S. *Langmuir* **2005**, *21*, 5192-5196.

63. Saito, R.; Dresselhaus, G.; Dresselhaus, M. S. *Physical Properties of Carbon Nanotubes*; Imperial College Press: London, 1998.

64. Adu, C. K. W.; Sumanasekera, G. U.; Pradhan, B. K.; Romero, H. E.; Eklund, P. C. *Chem. Phys. Lett.* **2001**, *337*, 31-35.

65. Qi, P.; Vermesh, O.; Grecu, M.; Javey, A.; Wang, Q.; Dai, H.; Peng, S.; Cho, K. J. *Nano Lett.* **2003**, *3*, 347-351.

66. Bekyarova, E.; Davis, M.; Burch, T.; Itkis, M. E.; Zhao, B.; Sunshine, S.; Haddon, R. C. *J. Phys. Chem. B* **2004**, *108*, 19717-19720.

67. Wong, Y. M.; Kang, W. P.; Davidson, J. L.; Wisitsora-at, A.; Soh, K. L. *Sens. Actuators, B* **2003**, *93*, 327-332.

68. Wei, B.-Y.; Hsu, M.-C.; Su, P.-G.; Lin, H.-M.; Wu, R.-J.; Lai, H.-J. *Sens. Actuators, B* **2004**, *101*, 81-89.

69. Peng, S.; Cho, K. *Nano Lett.* **2003**, *4*, 513-517.

70. Chopra, S.; Pham, A.; Gaillard, J.; Parker, A.; Rao, A. M. *Appl. Phys. Lett.* **2002**, *80*, 4632-4634.

71. Penza, M.; Antolini, F.; Vittori-Antisari, M.; Zhao, B. *Thin Solid Films* **2005**, *472*, 246-252.

72. Sotiropoulou, S.; Chaniotakis, N. A. *Anal. Bioanal. Chem.* **2003**, *375*, 103-105.

73. Xin Yua; Chattopadhyay, D.; Galeskab, I.; Papadimitrakopoulos, F.; Rusling, J. F. *Electrochem. Comm.* **2003**, *5*, 408-411.

74. Wang, J.; Li, M.; Shi, Z.; Li, N.; Gu, Z. *Anal. Chem.* **2002**, *74*, 1993-1997.

75. Wang, Z.; Liu, J.; Liang, Q.; Wang, Y.; Luo, G. *Analyst* **2002**, *127*, 653-658.

76. Wang, J.; Kawde, A.-N.; Musameh, M. *Analyst* **2003**, *128*, 912-916.

77. Munge, B.; Liu, G.; Collins, G.; Wang, J. *Anal. Chem.* **2005**, *77*, 4662-4666.

78. Zhang, M.; Smith, A.; Gorski, W. *Anal. Chem* **2004**, *76*, 5045-5050.

79. Wang, J.; Deo, R. P.; Poulin, P.; Mangey, M. *J. Am. Chem. Soc.* **2003**, *125*, 14706-14707.

80. Wang, J.; Musameh, M.; Lin, Y. *J. Am. Chem. Soc.* **2003**, *125*, 2408-2409.

81. Zhang, M.; Gorski, W. *Anal. Chem.* **2005**, *77*, 3960-3965.

82. Zhao, Q.; Gan, Z.; Zhuang, Q. *Electroanalysis* **2002,** 14, 1609-1613.

83. Chen, J.; Hamon, M. A.; Hu, H.; Chen, Y.; Rao, A. M.; Eklund, P. C.; Haddon, R. C. *Science* **1998**, *282*, 95-98.

84. O'Connell, M. J.; Poul, P.; Ericson, L.; Huffman, C.; Wang, Y.; Haroz, E.; Kuper, C.; Tour, J.; Ausman, D.; Smalley, R. E. *Chem. Phys. Lett.* **2001**, *342*, 265-271.

85. Chen, J.; Hamon, M. A.; Hu, H.; Chen, Y.; Rao, A. M.; Ehlund, P. C.; Haddon, R. C. *Science* **1998**, *282*, 95-98.

86. Poul, P. J.; Liu, J.; Mickelson, E. T.; Huffman, C. B.; Ericson, L. M.; Chiang, I. W.; Smith, K. A.; Colbert, D. T.; Hauge, R. H.; Margrave, J. L.; Smalley, R. E. *Chem. Phys. Lett.* **1999**, *310*, 367-372.

87. Wang, Y.; Iqbal, Z.; Mitra, S. *J. Am. Chem. Soc.* **2005**.

88. Dai, H.; Hafner, J. H.; Rinzler, A. G.; Colbert, D. T.; Smalley, R. E. *Nature* **1996**, *384*, 147-150.

89. Nguyen, C. V.; Stevens, R. M. D.; Barber, J.; Han, J.; Meyyappan, M.; Sanchez, M. I.; Larson, C.; Hinsberg, W. D. *Appl. Phys. Let.* **2002**, *81*, 901-903.

90. Nguyen, C. V.; Chao, K.-J.; Stevens, R. M. D.; Delzeit, L.; Cassell, A.; Han, J.; Meyyappan, M. *Nanotechnology* **2001**, *12*, 363-367.

91. Nguyen, C. V.; So, C.; Stevens, R. M.; Li, Y.; Delziet, L.; Sarrazin, P.; Meyyappan, M. *J. Phys. Chem. B.* **2004**, 108, 2816-2821.

92. Wong, S. S.; Joselevich, E.; Woolley, A. T.; Cheung, C. L.; Lieber, C. M. *Nature* **1998**, *394*, 52-55.

93. Wong, S.S.; Woolley, A.T.; Odom, T.W.; Huang, J.L.; Kim, P.; Vezenov, D.V.; Lieber, C.M.; *Appl.Phys.Lett* .**1998**, 73 ,3465.

94. Wong, S.S. Harper, J. D. Lansbury, P.T. Lieber, C.M. *J.Am. Chem.Soc.* **1998** , 120, 603.

95. Li, Y.; Chen, Y.; Xiang, R.; Ciuparu, D.; Pfefferle, L. D.; Horva´th, C.; Wilkins, J. A. *Anal. Chem* **2005**, *77*, 1398-1406.

96. Xu, S.; Li, Y.; Zou, H.; Qiu, J.; Guo, Z.; Guo, B. *Anal. Chem.* **2003**, *75*, 6191-6195.

97. Ugarov, M. V.; Egan, T.; Khabashesku, D. V.; Schultz, J. A.; Peng, H.; Khabashesku, V. N.; Furutani, H.; Prather, K. S.; Wang, H.-W. J.; Jackson, S. N.; Woods, A. S. *Anal. Chem.* **2004**, *76*, 6734-6742.

98. Soneda, Y.; Makino, M. *Carbon* **2000**, 38, 475-494.

99. Lin, C-L.; Chen, C-F.; Shi, S.C. *Diamond and Related Mater.* **2004**,13, 1026-1031.

100. Park, D.; Kim, Y, H.; Lee, J.K. *Carbon* **2003,** 41, 1025-1029.

101. Yuan, L.; Saito, K.; Hu, W.; Chen, Z. *Chem. Phys. Lett.* **2001**, 346, 23-28.

102. Wal, R.L.V.; Hall, L.J. *Carbon* **2003,** 41, 659-672.

103. Pan,C.; Liu,Y.; Cao, F.; Wang, J.; Ren, Y. *Micron* **2004**, 35, 461-468.

104. Wagner, R.S.; Ellis, W.C. *Appl. Phys. lett.* **1964**, 4, 89-90.

105. Sinnott, S.B.; Andrews, R.; Qian, D.; Rao, A.M.; Mao, Z.; Dickey, E.C.; Derbyshire, F. *Chem. Phys. Lett.* **1999**, 315, 25-30.

106. Han, J.; Yoo, J-B.; Park, C.Y.; Kim, H-J.; Park, G.S.; Yang, M.; Han, I.T.; Lee, N.; Yi, W.; Yu, S.G.; Kim, J.M. *J. Appl. Phys.* **2002**, 91, 483-486.

107. Fan, S.; Chapline, M.G.; Franklin, N.R.; Tombler, T.W.; Cassell, A.M.; Dai, H. *Science* **1999,** 283, 512-514.

108. Chen, X.; Wang, R.; Xu, J.; Yu, D. *Micron* **2004,** 35, 455-460.

109. Saridara, C.; Mitra, S. *Anal. Chem.* **2005**, 77, 7094-7097.

110. Li, Q.; Yuan, D. *J. Chromatogr. A* **2003**,1003, 203-209.

111. Fujiwara, A.; Ishii, K.; Suematsu, H.; Kataura, H.; Maniwa, Y.; Suzuki, S.; Achiba, Y. *Chem. Phys. Lett.* **2001**,336, 205-211.

112. Bittner, E.W.; Smith, M.R.; Bockrath, B.C. *Carbon* **2003**, 41, 1231–1239.

113. Cai, Y.; Jiang, G.; Liu, J.; Zhou, O. *Anal. Chem.* **2003**, 75, 2517-2521.

114. Cai, Y.; Jiang, G.; Liu, J.; Zhou, Q. X. *Anal. Chim. Acta.* **2003**, 494, 149-156.

115. Johnson, D. F.; Craft, B. J.; Jaffe, S.M. *J. Nanoparticle Res.* **2001**, 3, 63-71.

116. Speck, J. S.; Endo, M.; Dresselhaus, M. S. *J. Cryst. Growth* **1989**, 94, 834-848.

117. Ivanov, V.; Nagy, J. B.; Lambin, P.; Lucas, A.; Zhang, X.B.; Zhang, X.F.; Bernaerts, D.; Tendeloo, G. V.; Amelinckx, S.; Landuyt, J.V. *Chem. Phys. Lett.* **1994**, 223, 329-335.

118. Rodriguez, N. M.; Chambers, A.; Baker, R.T. K. *Langmuir* **1995**,11, 3862-3866.

119. Park, Y. S.; Choi, Y. C.; Kim, K.S.; Chung, D-C.; Bae, D. J.; An, K. H.; Lim, S. C.; Zhu, X. Y.; Lee, Y. H. *Carbon* **2001**, 39, 655–661.

120. Colomera, J. F.; Piedigrossoa, P.; Fonsecaa, A.; Nagya, J. B. *Synthetic Metals* **1999**, 103, 2482-2483.

121. Ward, J.W.; Wei, B.Q.; Ajayan, P.M. *Chem. Phys. Lett.* **2003**, 376, 717-725.

122. Ajayan, P.M.; Zhou, O. *Applications of carbon nanotubes*, in Carbon Nanotubes: Synthesis, Structure, Properties, and Applications (Topics in Applied Physics, 80), Dresselhaus, M.S.; Dresselhaus, G.; and Avouris, P. Editors. Springer-Verlag: Heidelberg, 2000.

123. Peigney, A. *Nature Mater* **2003,** 2, 15-16.

124. Kong, J.; Franklin, N.R.; Zhou, C.; Chapline, M.G.; Peng, S.; Cho, K.; Dai, H. *Science* **2000**, 287, 1801-1804.

125. Journet, C.; Maser, W. K.; Bernier, P.; Loiseau, A.; Lamy de la Chapelle, M.; Lefrant, S.; Deniard, P.; Lee, R.; Fisher, J. E. *Nature*, **1997**, 388, 756-758.

126. Guo, T.; Nikolaev, P.; Thess, A.; Colbert, D.T.; Smalley, R.E. *Chem. Phys. Lett.* **1995**, 243, 49-54.

127. Deck, C.P.; Vecchio, K. *Carbon* **2005**, 43, 2608-2617.

128. Dupuis, A-C. *Progress in Mater. Sci.* **2005**, 50, 929-961.

129. Saridara, C.; Brukh, R.; Iqbal, Z.; Mitra, S. *Anal. Chem.* **2005**, 77, 1183-1187.

130. Karwa, M.; Mitra, S.; Iqbal, Z. *Carbon* **2006,** 44, 1235-1242.

131. Cheung, C.L.; Kurtz, A.; Park, H.; Lieber, C.M. *J. Phys. Chem. B.* **2002,** 106, 2429-2433.

132. Maruyama, S.; Kojima, R.; Miyauchi, Y.; Chiashi, S.; Kohno, M. *Chem. Phys. Lett.* **2002,** 360, 229-234.

133. Ward, J.W.; Wei, B.Q.; Ajayan, P.M. *Chem. Phys. Lett.* **2003**, 376, 717-725.

134. Franklin, N.R.; Li, Y.; Chen, R.J.; Javey, A.; Dai, H. *App. Phys. Lett.* **2001,** 79, 4571-4573.

135. Murakami, Y.; Miyauchi, Y.; Chiashi, S.; Maruyama, S. *Chem. Phys. Lett.* **2003**, 377, 49-54.

136. Delzeit, L.; Chen, B.; Cassell, A.; Stevens, R.; Nguyen, C.; Meyyappan, M. *Chem. Phys. Lett.* **2001**, 348, 368.

137. Méhn, D.; Fonseca, A.; Bister, G.; Nagy, J.B. *Chem. Phys. Lett.* **2004**, 393, 378-384.

138. Ago, H.; Ohshima, S.; Tsukuagoshi, K.; Tsuji, M.; Yumura, M. *Current App. Phys.* **2005,** 5, 128-132.

139. Bai, S.; Li, F.; Yang, Q.; Cheng, H.M.; Bai, J. *Chem. Phys. Lett.* **2003**, 376, 83-89.

140. Bonard, J.M.; Kind, H.; Stockli, T.; Nilsson, L.A. *Solid-State Electr.* **2001,** 45, 893-914.

141. Wong, S.S.; Joselevich, E.; Woodley, A.T.; Cheung, C.L.; Lieber, C.M. *Nature* **1998**, 394, 52-55.

142. Li, J.; Lu, Y.; Ye, Q.; Cinke, M.; Han, J.; and Meyyappan, M. *NanoLett.* **2003**, 3, 929.

143. Wal, R.L.V.; Hall, L.J. *Carbon* **2003**, 41, 659-672.

144. Saridara, C.; Mitra, S.; *Anal. Chem.* **2005**, 77, 7094-7097.

145. Zhou, W.; Ooi, Y.H.; Russo, R.; Papanek, P.; Luzzi, D.E.; Fischer, J.E.; Bronikowski, M.J.; Willis, P.A.; and Smalley, R.E. *Chem. Phys. Lett.* **2001**, 350, 6-14.

146. Bandow, S.; Asaka, S.; Saito, Y.; Rao, A.M.; Grigorian, L.; Richter, E.; Eklund, P.C. *Phys. Rev. Lett.* **1998,** 80, 3779-3782.

147. Jorio, A.; Saito, R.; Hafner, J.H.; Lieber, C.M.; Hunter, M.; McClure, T.; Dresselhaus, G.; Dresselhaus, M.S. *Phys. Rev. Lett.* **2001,** 86, 1118-1121.

148. Dai, H. *Acc. Chem. Res.* **2002**, *35*, 1035-1044.

149. Guaya, P.; Stansfielda, B. L.; Rochefort, A. *Carbon* **2004**, *42*, 2187-2193.

150. Saridara, C.; Brukh, R.; Iqbal, Z.; Mitra, S. *Anal. Chem.* **2005**, *77*, 1183-1187.

151. Cai, Y.; Jiang, G.; Liu, J.; Zhou, Q. *Anal. Chem.* **2003**, *75*, 2517-2521.

152. Saridara, C.; Mitra, S. *Anal. Chem.* **2005**, *77*, 7094-7097.

153. Fujiwara, A.; ishii, K.; suematsu, H.; Kataura, H.; Maniwa, Y.; Suzuki, S.; Achiba, Y. *Chem. Phys. Lett.* **2001**, *336*, 205-211.

154. Li, Q.; Yuan, D. *J. Chromatogr. A* **2003**, *1003*, 203-209.

155. Saito, R.; Dresselhaus, G.; Dresselhaus, M.S. *Physical Properties of Carbon Nanotubes*; Imperial College Press: London, 1998.

156. Thess, A.; Lee, R.; Nikolaev, P.; Dai, H.; Petit, P.; Robert, J.; Xu, C.; Lee, Y. H.; Smalley, R. E. *Science* **1996**, *273*, 483-487.

157. Journet, C.; Matser, W. K.; Bernier, P.; Laiseau, L.; Lefrant, S.; Deniard, P.; Lee, R.; Fischer, J. E. *Nature* **1997**, *388*, 756-758.

158. Makris, T. D.; Giorgi, L.; Giorgi, R.; Lisi, N.; Salernitano, E. *Diamond Relat. Mater.* **2005**, *14*, 815-819.

159. Nasibulin, A. G.; Moisala, A.; Brown, D. P.; Jiang, H.; Kauppinen, E. I. *Chem. Phys. Lett.* **2005**, *402*, 227-232.

160. Flahaut, E.; Laurent, C.; Peigney, A. *Carbon* **2005**, *43*, 375-383.

161. Karwa, M.; Iqbal, Z.; Mitra, S. *Carbon* **2006** 44, 1235-1242.

162. Ward, J. W.; Wei, B. Q.; Ajayan, P. M. *Chem. Phys. Lett.* **2003**, *376*, 717-725.

163. Karwa, M.; Iqbal, Z.; Mitra, S. *J. Mat. Res.* Submitted.

164. Dupuis, A.-C. *Progress Mater Sci* **2005**, *50*, 929-961.

165. Cheung, C. L.; Kurtz, A.; Park, H.; Lieber, C. M. *J. Phy. Chem. B* **2002**, *106*, 2429-2433.

166. Bandow, S.; Asaka, S.; Saito, Y.; Rao, A.M.; Grigorian, L.; Richter, E.; Eklund, P.C. *Phy. Rev. Lett.* **1998**, *80*, 2779.

167. Skoog, D. A.; Holler, F. J.; Niemann, T. A. *Principles of Instrumental Analysis*; Saunders College Publishing: Philadelphia, PA, 1998.

168. Catalog, *Chromatography Products for Analysis and Purification*, Supelco, Bellefonte, PA 2005.

169. Bilgic, C.; Askin, A. *J. Chromatogra. A* **2003**, *1006*, 281-286.

170. Agnihotri, S.; J.Rood, M.; Rostam-Abadi, M. *Carbon* **2005**, *43*, 2379-2388.

171. McReynolds, W. O. *J. Chromatogra. Sci.* **1970**, 8, 685-691.

172. Rotzsche, H. *Stationary Phases in Gas Chromatography*, Elsevier Science B.V.; Amsterdam, 1991, 81-94.

173. Bittner, E. W.; Smith, M. R.; Bockrath, B. C. *Carbon* **2003**, *41*, 1231-1239.